

RICE UNIVERSITY

C₆₀ in Water: Aggregation Characterization, Reactivity and Behavior

by

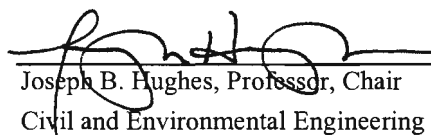
John Dyer Fortner




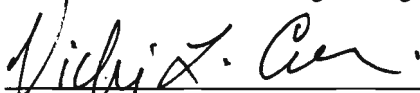
A Thesis submitted
In Partial Fulfillment of the
Requirements for the Degree

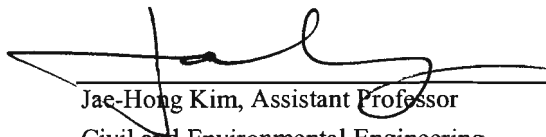
Doctor of Philosophy

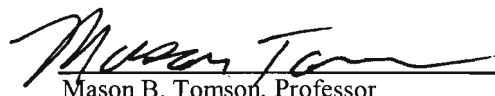
Approved, Thesis Committee:


Joseph B. Hughes, Professor, Chair
Civil and Environmental Engineering
Georgia Institute of Technology


Pedro J. Alvarez, George R. Brown Chair, Director
Civil and Environmental Engineering


Vicki L. Colvin, Professor
Chemistry


Jae-Hong Kim, Assistant Professor
Civil and Environmental Engineering
Georgia Institute of Technology


Mason B. Tomson, Professor
Civil and Environmental Engineering

Thesis
C.E.
2007
Fortner

Houston, Texas

October 2006

2123954

ABSTRACT

C₆₀ in Water: Aggregation Characterization, Reactivity and Behavior

by

John D. Fortner

Industrial scale production, coupled with unique material properties, underpin rising concerns of nano-scale materials inadvertently impacting the health and function of natural systems. Fullerenes, C₆₀ in particular, have been proposed for a variety of applications and are soon expected to be produced in multi-ton quantities. Understanding how these materials behave in natural matrixes, specifically aqueous systems, is needed for accurate risk assessment and to manage waste disposal practices appropriately.

Research presented here addresses outstanding questions and expands upon current knowledge regarding C₆₀ nano-scale aggregation in water (nano-C₆₀). Four areas of focus are: 1.) Aggregate formation, composition, and stability 2.) Reactivity with a dissolved reactant (ozone) 3.) Association with mineral surfaces and 4.) Interaction with selected biological systems. Results indicate that aggregates are crystalline in order and remain as underivatized C₆₀ throughout the formation/stabilization process. The aggregate suspensions readily react with dissolved ozone resulting in a molecularly soluble, highly oxidized fullerene. Furthermore, nano-C₆₀ associates with mineral surfaces as a function of surface charge and is observed to accumulate at the cell wall of a fungal culture. Taken together, results indicate that nano-scale, fullerene aggregates must be considered appropriately, as they deviate from predictions based on bulk and molecular property estimates.

Acknowledgements

My family has been a constant source of encouragement, perspective and love. They have provided a foundation of solid rock that has given me the rare chance to hope and dream. For that, I am eternally grateful. Thank you Mom, Dad and Ike.

All my friends, both new and old, have made being poor, discouraged and stressed actually quite bearable. In fact, it has been a great time. Thank you. I'm looking forward to the good times to come. I would like to especially thank Marisa for putting up with me and being there for me during the past few years.

I would like to thank my committee members; it has been a wonderful experience working with each of them. Their time and efforts are valued more than they know. Such guidance and example will serve as reference over the course of my career.

I would like to express my deep gratitude toward my advisor, Joe Hughes, for all that he has done for me. Joe has been a shining example of a scientist, educator and mentor. I am only here because he gave me a chance and believed in me.

Finally, I would like to thank the funding agencies and various institutions for their generous support including: The Center for Biological and Environmental Nanotechnology (CBEN) at Rice University; School of Civil and Environmental Engineering at the Georgia Institute of Technology; Institute of Geotechnical Engineering (IGT) at the Swiss Federal Institute of Technology, Zurich (ETHZ); Air Force Research Laboratory (AFRL) and the United States Environmental Protection Agency (US-EPA) among others.

Preface

An excerpt from *The American Scholar*, an oration delivered by Ralph Waldo Emerson before the Phi Beta Kappa Society, at Cambridge, August 31, 1837:

The first in time and the first in importance of the influences upon the mind is that of nature. Every day, the sun; and, after sunset, night and her stars. Ever the winds blow; ever the grass grows. Every day, men and women, conversing, beholding and beholden. The scholar is he of all men whom this spectacle most engages. He must settle its value in his mind. What is nature to him? There is never a beginning, there is never an end, to the inexplicable continuity of this web of God, but always circular power returning into itself. Therein it resembles his own spirit, whose beginning, whose ending, he never can find, — so entire, so boundless. Far, too, as her splendors shine, system on system shooting like rays, upward, downward, without centre, without circumference, — in the mass and in the particle, nature hastens to render account of herself to the mind. Classification begins. To the young mind, every thing is individual, stands by itself. By and by, it finds how to join two things, and see in them one nature; then three, then three thousand; and so, tyrannized over by its own unifying instinct, it goes on tying things together, diminishing anomalies, discovering roots running under ground, whereby contrary and remote things cohere, and flower out from one stem. It presently learns, that, since the dawn of history, there has been a constant accumulation and classifying of facts. But what is classification but the perceiving that these objects are not chaotic, and are not foreign, but have a law which is also a law of the human mind? The astronomer discovers that geometry, a pure abstraction of the human mind, is the measure of planetary motion. The chemist finds proportions and intelligible method throughout matter; and science is nothing but the finding of analogy, identity, in the most remote parts. The ambitious soul sits down before each refractory fact; one after another, reduces all strange constitutions, all new powers, to their class and their law, and goes on for ever to animate the last fiber of organization, the outskirts of nature, by insight.

“Only a life lived for others is a life worth while.” – Albert Einstein

Table of Contents

Abstract	ii
Acknowledgements	iii
Preface	iv
Chapter 1: Introduction	1
Chapter 2: Literature Review	5
Historical Perspective	5
Overview.....	11
Fullerene Formation and Production	12
C ₆₀ Properties	15
Structure.....	15
Solid C ₆₀	17
C ₆₀ in solvents.....	18
Spectroscopy.....	19
Aromaticity	21
Reactivity	28
Electrochemistry	28
Nucleophilic Additions.....	30
Hydrogenation.....	31
Halogenation.....	31
Electrophilic Additions and Oxidation	32
Photophysical Reactivity	33
Other Chemistries	32
Fullerenes in Water	34
Water Stable C ₆₀ Aggregates	35
Figures.....	42
Tables	45
Literature Cited.....	48

Chapter 3.A: C₆₀ in water: Nanocrystal Formation and Microbial Response	61
Introduction.....	63
Materials and Methods.....	65
Chemicals.....	65
Nano-C ₆₀ Preparation.....	65
Particle Stability.....	66
Concentration Determination.....	67
Characterization.....	68
Microbial Assays.....	69
Results.....	70
Discussion.....	75
Acknowledgements.....	79
Literature Cited.....	80
Figures.....	85
Tables.....	92
3.B: Supplemental Characterization	93
Materials and Methods.....	93
Chemicals.....	93
Nano-C ₆₀ preparation.....	93
Destabilization, Extraction and HPLC Concentration Determination.....	94
Carbon Measurements.....	95
Gravimetric Concentration Determination.....	95
X-Ray Diffractometry.....	96
NMR.....	97
Mass Spectroscopy.....	97
Results and Discussion.....	98
Figures.....	100
Tables.....	105
Chapter 4: Ozonation of C₆₀ in Water	106
Introduction.....	106

Materials and Methods.....	109
Nano-C ₆₀	109
Ozone Reactions	110
Characterization	111
Results and Discussion	112
Semi-Batch Reactions.....	112
Batch Stoichiometry Results.....	114
Product Analyses	115
Acknowledgements.....	119
Figures.....	120
Literature Cited	128
Chapter 5: Association of Nano-C₆₀ with Clay Minerals	133
Introduction.....	133
Materials and Methods.....	134
Nano-C ₆₀	134
Clay Minerals.....	135
Association Studies	136
Microscopy	136
X-Ray Diffractometry	137
Column Studies.....	137
Results and Discussion	138
Acknowledgements.....	141
Figures.....	143
Literature Cited	152
Chapter 6: Biological Interactions with Nano-C₆₀.....	156
Introduction.....	156
Materials and Methods.....	157
Nano-C ₆₀	157
<i>In vitro</i> Enzymatic Studies.....	158
<i>In vivo</i> Studies.....	158

Results and Discussion	161
Figures.....	165
Literature Cited	174
Chapter 7: Conclusions	176
Characterization	176
Reactivity	177
Mineral Surface Interactions.....	178
Biological System Interaction.....	178
Chapter 8: Engineering Significance	180
Chapter 9: Future Work Recommendations.....	181
Reduction Reactions in Water	181
Surface Charge Source.....	181
Fungal Interactions.....	182
Literature Cited	183

Chapter 1

Introduction

Rapid industrial scale production, coupled with unique material properties, underpin rising concerns of nano-scale materials inadvertently impacting the health and function of natural systems. Carbon based nano-scale materials such as fullerenes and nanotubes in particular, have been widely proposed for a variety of applications and soon expected to become widely available (*e.g.* Frontier Carbon expects to produce multi-ton quantities in 2007). An understanding of how these materials behave in natural matrixes, specifically aqueous systems, is needed for accurate risk assessments and to manage waste disposal practices appropriately.

Research presented and discussed herein considers fullerenes in aqueous based systems primarily as suspended aggregates, building on what is currently understood in the following areas:

- 1.) Material characterization including formation dynamics and stability
- 2.) Aggregate reactivity with dissolved ozone
- 3.) Specific aggregate interactions with subsurface, clay mineral constituents
- 4.) Biological processes capable of changing aggregate properties

Guiding hypotheses along with brief research summaries within these focus areas are provided below, serving as a road map to this document. Full text and figures are included in Chapters 3-6 respectively, with Chapter 2 providing a pertinent literature review. Later chapters summarize research findings (Chapter 7), discuss engineering

significance (Chapter 8) and outline future studies (Chapter 9). Results from these studies contribute to the current understanding of said material and provide useful information to the ongoing dialog concerning engineered carbon nanomaterials in natural systems.

1.) Characterization

Hypotheses were designed to provide chemical/physical information about C₆₀, the most common and well studied fullerene, as a nano-scale aggregate suspension (20-300 nm aggregate diameter; termed here nano-C₆₀). Primary hypotheses include: 1.) C₆₀ in water, as a suspended aggregate, remains underivatized and crystalline in orientation. 2.) That aggregate size is a function of mixing conditions and water chemistry, particularly pH.

Findings

Results support the overarching hypotheses, indicating nano-C₆₀ is an ordered, crystalline structure comprised of underivatized C₆₀. Furthermore, the size and stability of these materials are affected by conditions of formation which include the rate of water addition and solution pH, and the stability varies, depending on the solution ionic strength. These findings have been reported in *Environmental Science and Technology* (2005, 39, 11).

2.) Reactivity

Considering the olefin like reactivity of C₆₀, it is reasonable to hypothesize that individual C₆₀ molecules located at the surface of nano-C₆₀ aggregates will be reactive towards ozone, resulting in: 1.) Products with increased aqueous solubility due to addition of hydrophilic moieties, such as hydroxyl groups. 2.) Size reduction and structural destabilization of the aggregate due to the water soluble nature of the reaction products.

Findings

Results support the primary hypotheses, indicating that an aqueous based ozonation reaction with nano-C₆₀ proceeds over a range of pH values (5-9) and reaction products are water soluble, molecular fullerene oxides (C₆₀(O)_y(OH)_x, y + x ~29). Nano-C₆₀ aggregate size was found to be a function of ozone contact time with final products <5 nm.

3.) Clay Mineral Interactions

Based on the availability of applicable surface chemistries of clay minerals, it was hypothesized that: 1.) Available surface area will be a factor in association of nano-C₆₀ with clay minerals (*i.e.* more surface area available will result in higher association capacities). 2.) Preferential nano-C₆₀ association (as electrostatic interaction) will occur at positively charged points on the mineral surface and/or edge. 3.) Incorporation of nano-C₆₀ into/within mineral interlayers can be part of the overall association process.

Findings

Experiments have been completed examining nano-C₆₀ association with three clay minerals via batch studies, transmission electron microscopy (TEM), X-ray diffraction (XRD) analyses and simple, 1-D flow through column studies. Findings support the stated hypotheses, in that interactions are primarily dominated by the available surface area and edge charges of the materials in relation to the net negative surface charge of nano-C₆₀. Evidence regarding smectite intercalation is inconclusive.

4.) Biological Interactions

Primary hypotheses were designed to provide insight into interactions with nano-C₆₀ and applicable microbial process including: 1.) Nano-C₆₀ is susceptible to biochemical based transformation via non-specific, oxidizing enzymes that catalyze hydroxyl radical production *in vitro*. 2.) Based on previous reports of toxicity, nano-C₆₀ is not expected to directly associate with viable cells *in vivo*.

Findings

Cell free enzyme studies with a well characterized manganese peroxidase (MnP) did not transform C₆₀, as suspended nano-C₆₀, within our detection limits. However, fungal association of nano-C₆₀ *in vivo* was observed and delineated via UV-Vis, TEM and NMR analyses. In addition, respirometry studies coupled with TOC measurements suggest that C₆₀ (as nano-C₆₀) is not metabolized by this fungus, nor is C₆₀(OH)₂₂₋₂₄, and that fungal growth is supported by residual THF oxide.

Chapter 2

Literature Review

Historical Prospective

A closed, carbon cage molecule consisting of 60 carbon atom vertices arranged through 12 hexagons and 20 pentagons was first hypothesized in 1970 by Eiji Osawa a Japanese researcher who was investigating large PAH stability as a function of shape and size (1). His hypothesis was independently suggested by others and empirically confirmed some 20 years later, establishing the third allotrope of carbon along with diamond and graphite. A Nobel Prize in chemistry was awarded in 1996 to Robert F. Curl Jr., Harold W. Kroto and Richard E. Smalley for their seminal experiments, which eventually lead to direct confirmation of such a structure, described in the 1985 *Nature* report titled, C-60 Buckminsterfullerene (3), which has since been cited over 5,000 times to date. The 60 carbon, caged structure was named buckminsterfullerene by the laureates after Buckminster Fuller, who was famous for his geodesic dome designs that where in many ways analogous to the discovered molecule (vertices of a repeating pattern allowing for curvature or 'bend' via pentagons arranged in an other wise flat series (2-D) of hexagons). These architectural structures were of particular fame and distinction as part of the United States pavilion during the 1967 World Fair in Montreal. The path leading to the actual observation and record of the molecule at Rice University during the mid 1980's was rapid, happening over the course of approximately 10 days. According to Prof. Kroto, who, at the time, was a visiting professor from Sussex University studying interstellar, carbon clusters (as described in his Nobel lecture (4)):

“Rick discovered that the structure started to curve into a saucer shape as soon as pentagons were included among the hexagons and finally closed as he added a twelfth pentagon. The next morning, when he revealed his paper model, I remember being ecstatic. It was beautiful and looked like the stardome (a reference to a geodesic dome of constellations he recalled as a youth) as I remembered it. It is of course a truncated icosahedron and the fact that it turned out to be a football too was most appropriate. After all, the whole discovery story is an archetypal example of team effort. I remember thinking that the molecule was so beautiful that it just had to be right – and even if it were not, everybody would surely love it, which they did eventually! My suggestion that we call the molecule Buckminsterfullerene (the –ene ending fitted perfectly) was, after some discussion, accepted and we sent the paper off to Nature – the date of the receipt was 13th of Sept. (1985) (NB – the experiments had started on 1st of Sept.)”

The Rice experiments leading to the proposition of an all carbon, truncated icosahedron (C_{60}) formation were originally based Dr. Kroto and Dr. Curl’s scientific interests, which, at the time were directed towards the electronic adsorption spectra of carbon clusters (C_n , $n=5-15$), being proposed as the source of diffuse interstellar bands (5). Streams of unusual IR emissions from red giant carbon stars were thought to be from large carbon cluster formations (6). Around that time, Professor Richard (Rick) Smalley was developing techniques and instrumentation to investigate compounds and clusters formed from refractory elements (7). To accomplish this, a laser supersonic molecular beam source (pulsed) was developed to vaporize solid sources into a tangential, inert gas stream (He). Once in the gas stream, the vaporized material was cooled and further

mixed which initiated clustering. These clusters could be varied via operational parameters such as pressure (backing); laser operation, such as pulse timing; and the length and geometry of the channel downstream from the vaporization point (5,7). After clustering, the gas pulse was expanded supersonically through a nozzle into a large vacuum chamber, which drops the temperature to a few Kelvin, which lowered the collision rate of clusters. After repeated to a “few dozen times’ in line, a jet of cold clusters, with a narrow, highly directional, velocity distribution results. The beam of clusters was then skimmed into a molecular beam (for ionization) and interrogated via mass spectroscopy (MS-TOF) (3). To look for small carbon clusters formed under high energy vaporization, similar to high energy cosmic incidents, it was proposed to use Smalley’s instrument with a carbon substrate (graphite) as it might provide insight into small carbon cluster composition, formation and spectral properties. A flat, rotating, graphite disk was vaporized by pulse laser (5 nanosecond pulse, 532 nm laser (green), 30-40 mJ energy) and analyzed via TOF-MS.

The stability of clusters was recognized by so called ‘magic numbers’, which was a term loosely applied to those carbon clusters (n = number of carbon atoms) which appeared at consistently higher intensities, indicating relatively higher levels of stabilities, when compared to other mass clusters. Among these ‘magic’ numbers, a 60 carbon mass peak was frequently identified and through variations in the experimental protocol, became a ‘super-magic number’, that is to say, the signal intensity for 60 carbon atoms was orders of magnitude above other mass signals (3). This stable cluster, which was later hypothesized and then empirically demonstrated to be a symmetrical carbon cage structure with no dangling bonds and 60 satisfied carbon valence states (3), with an

architecture following Euler's rule: that a 3-D figure with any even number of, n , of 24 or more vertices, could be constructed with 12 pentagons and $(n-20)/2$ hexagons (6).

Additional work was immediately done with variable gas composition such as NO with a similar laser graphite vaporization protocol, leading to further degradation of those clusters (odd numbered) with dangling bonds (*i.e.* open structures) which increased the ratio of 'closed', carbon structures (>40 carbon atoms). Fragmentation patterns were investigated with a photofragmentation laser with a second TOF-MS to determine fragment size (*i.e.* carbon number) (5). Results were consistent with the hypothesized closed structure, in that a sequential loss of two carbon atoms (even numbered) was observed down to C_{32}^+ , which then "jumped" to C_{20}^+ clusters(5,7). This fit the cage structure hypothesis, in that, with a loss of two carbons the cation cluster could spontaneously rearrange, regaining the thermodynamic stability of a closed structure. At 32 carbon atoms the reformation becomes unfavorable until 20 carbon atoms (another 'magic number' observed) is reached whereby a stable structures can be formed again. In line with these observations, exponentially decreasing formation energies (kJ/mol) as a function of increasing carbon number was calculated, with two distinct 'dips' or lower lying derivations from the regression, indicating slightly lower than expected energy of formation (*i.e.* relative favorable formation energy), is demonstrated for 60 carbon atoms and 70 carbon atoms (C_{70}) (8), which would be the next stable, carbon cluster to be proposed and identified (5).

While these initial observations and calculations were compelling, empirical evidence of the molecular structure(s) via IR, ^{13}C -NMR, UV/Vis, among others, were necessary to identify the molecular symmetry, thus confirming the hypothesized

structure. Fullerene research during the late 1980's became focused on the production of macroscopic quantities of the material necessary for such spectral analyses. In 1990 a research team led by Wolfgang Krätschmer, at the Max Planck Institute for Nuclear Physics in Heidelberg, Germany and Donald Huffman at the University of Arizona published in *Nature* the first report describing the production of macroscopic quantities of the material (9), which to date has been cited over 4,300 times. Within this report, distinct IR and UV/Vis spectra were demonstrated which, in fact, matched previous predicted values and along with crystal patterns matching those expected of solid C₆₀ (9,10). To achieve macroscopic quantities of the material, a rather simple protocol was devised (resistive heating of pure graphite) which at the time was found to produce over 1% C₆₀ (w/w) which was found to be extractable via organic solvent such as toluene thus purified via chromatography (9). Since the seminal Kratchmer *et al.* paper, a number of other production protocols production have been established (8), by which fullerenes are now widely available at purities upwards of >99.9% which can accomplished by double or even triple chromatographic purification and sublimation techniques (MER Corp. Tucson AZ; personal correspondence). Furthermore, it is now understood that fullerenes have been produced, albeit unknown, in many cases, including high carbon soot formations, which apply to a number of basic combustion scenarios, such as basic coal fire power plants as recently observed by Utsunomiya *et al.* (11,12).

After the breakthrough in production, research on fullerenes, primarily as C₆₀ and C₇₀, expanded quickly in both depth and breadth. For example, a simple topic search for "fullerene*" on the Web of Knowledge, an online citation database, currently produces some 17,300 hits (articles) as of August 2006. Within this body of research, other, large

stable carbon caged structures C_{76} , C_{84} , C_{90} , C_{94} and higher have been identified, albeit in much smaller mass ratios and/or frequency than C_{60} and C_{70} (13). This entire family of carbon, the third allotrope, consisting of caged structures has simply come to be known as ‘fullerenes’.

Fullerene properties have been widely researched and observed to be quite unique in many areas giving rise to application potential for a range of diverse fields including: hydrogen fuel cell development, pharmaceuticals, antimicrobial properties, superconducting capacity (K, Rb - doped), unique catalyst, and nonlinear optical devices among others (14-28). Unique photochemical properties (29,30) have given C_{60} priority as possible applications in photodynamic therapy (31,32), oxidative synthetic reaction (33), and electron shuttling action in dye-sensitized solar cells (34).

Furthermore, as an important side note, in 1991 a report by Prof. Iijima, observed elongated ‘fullerenes’ – like carbon structures with large length to width aspect ratios (> 20) termed simply, carbon nanotubes (35). Carbon nanotubes (CNT) are pure carbon cylindrical, macromolecules consisting of seamless walls arranged in organized, hexagonal arrays, capped by fullerene-like ends (*i.e.* curved) which are made possible through pentagon ring(s) inclusion (6). CNT architecture is variable with diameters in the nanometer range (1 to 100 nm) with much longer cylindrical wall lengths ranging from nanometers to microns. Based on their structure, CNT are categorized into two main species; single wall nanotubes (SWNT) and multiwall nanotubes (MWNT) which result from a co-axial assembly of the multiple SWNT (36).

Generally speaking, CNT’s are widely considered to have significant application potential due to their desirable mechanical, electro-optical, and thermal properties

(37,38). Such properties and application include: High tensile strength materials(39); electronic conductance (39-41); hydrogen adsorption capacity (storage) (42,43); electronic sensitivity in different chemical environments allowing for novel sensors (44-47); among others, including nanofiltration devices (48,49), thermal management materials (50) and solar cells (51). With increasing commercial interests and industrial scale production facilities currently being constructed (52), both fullerene and CNT supply and demand, by all accounts, are expected to grow rapidly over the next decade (22,53,54).

In summary, many view the time at which and even the discovery of C₆₀ (having an effective molecular diameter of approximately 1 nm) as a seemingly logical starting point for much of the nano-sciences as they are known today. This is of note, as it has been estimated that by 2015, the economic impact of nano-scale research, production and application will globally reach upwards of a 1 trillion dollars annually (55).

Overview

Fullerenes have been studied extensively over the past 20 years. Regardless of which aspect of fullerene research, or any research topic for that matter, is being considered, previous peer reviewed observations are absolutely critical as reference points in terms standardizing methodologies and organizing observations, thus revealing questions outstanding. The purpose of this particular literature review is to organize relevant portions of the fullerene literature, from which readers are presented with pertinent fullerene chemistries, physical properties and (potential) behavior of C₆₀ in natural systems. To begin, fundamental fullerene properties and chemistries are presented and

discussed but due to the large number of published literature on fullerenes can not be considered an exhaustive review. Numerous books and published review articles are widely available and specifically address and describe detailed chemical and physical fullerene properties (6,28,34,56-59). Particularly, the recent reference text, *Fullerenes: Chemistry and Reactions* by Andreas Hirsch and Michael Brettreich, is a currently comprehensive report.

Fullerene Formation and Production

As mentioned, fullerenes are available *en masse* and with industrial scale production facilities beginning soon (9,22). Since the macro-scale production (*i.e.* gram quantities) of fullerenes was first accomplished by Kratshmer *et al.* (9), fullerene synthesis has been developed and improved through a number of protocols which share several common factors. Generally, high energy fullerene formation includes a high carbon content source (such as graphite), an O₂ free or extremely lean atmosphere, and a source of energy to effectively vaporize the carbon atoms which allows for reformation (or ‘clustering’ as often described). Fullerenes were first found to be efficiently produced through resistive heating of pure graphite (9). Briefly, this method simply maintains contact of two graphite rods, which are kept in constant contact by a spring mechanism, allowing for an electrical current applied across the two rods. At the contact point, one rod is sharpened as to minimize the contact area, thus increase the heat from resistance at that point (Ohmic power heating). As the temperature reaches upwards of 3x10³ °C, a sooty “smoke” begins to develop and is collected at cooler surfaces, such as a vacuum tube surface (9). The soot is then collected and fullerenes extracted (upwards of 8 %, w/w

soot) with an organic solvent (often toluene) and then chromatographically separated (60). For this method, C_{60} to C_{70} ratios were usually *ca.* 85:15 with higher fullerenes at < 1%. This basic design has since been streamlined to lower costs and improving efficiencies (60,61). Two graphite rods can also be used to produce fullerenes via an arc discharge process (8). This technique, while similar in theory to process described previously, relies on energy from electric dissipation via arc discharge across two closely aligned, but not touching graphite tips. While such an arc plasma at the graphite surface gives rise to sufficient energy for carbon vaporization and clustering for fullerene production (upwards of 15% w/w soot in some cases), intense UV radiation is produced, reducing formation of fullerenes, as unstable radical species are readily formed (62). Variations of this basic method include variable atmosphere compositions, graphite with “light” elements imbedded such as Al, B and Si, and pulse discharge inputs have been described (62). The discovery of fullerenes in sooty flames was the next production breakthrough and is the current choice for pilot and industrial scale fullerene production (22,63,64). Sooty flame production fundamentally differs from the resistant and arc heating of graphitic carbon in that PAH monomers, such as benzene, are the initial carbon source. Howard *et al.* first describe a benzene-argon-oxygen flame setup to produce appreciable amounts of fullerenes (0.003-9.0% soot mass) depending on mixture ratios, pressure and flame temperature (optimal mixture at carbon:oxygen at 0.995, 10% argon) (63). Under these conditions, it was hypothesized that fullerene formation resulted from both carbon atom vaporization/clustering and through the polymerization of PAH monomers, which the authors correlate to the variable C_{60} : C_{70} ratios observed, (*i.e.* C_{60} : C_{70} ratios could be varied depending on the synthesis conditions; in some cases

greatly decreased, thus producing more C_{70} than C_{60} (12,63). Since these initial findings, other methodologies of fullerene production have been developed, varying the classic graphitic vaporization and clustering and pyrolysis techniques with a variety of hydrocarbon sources (6,62).

While fullerenes, especially C_{60} and C_{70} , seem to readily form during carbon vaporization events in inert atmospheres, understanding the formation kinetics and thermodynamic is complex and remains ongoing. Specifically, when comparing fullerene structural stabilities to other carbon isotopes (*i.e.* graphite and diamond), fullerenes are thermodynamically less stable. Furthermore, within the family of fullerenes, higher numbered fullerenes are actually more stable in structure than C_{60} , which conversely, is normally the major fullerene produced. These facts, coupled with ability to alter the ratio of C_{60} to higher fullerenes (C_{70} , etc.) in sooty flame production, suggest, as Hirsch discusses, that formation of C_{60} is not dependent on structural thermodynamic stabilities alone and that kinetics of formation are critical (62). Furthermore, Hirsch gives a synopsis, consisting of three major stages, for fullerene generation by carbon vaporization: “(1) The vaporization itself and the nature of the initially formed intermediates; (2) the structures of growing clusters; (3) the annealing of fullerenes” (62). To begin, individual carbon atom or rings from a lower energy, PAH C-source are cleaved from the parent material. They reform into small linear and cyclic clusters (<10 carbon atoms) and/or larger carbon rings (> 10 carbon atoms) as observed via MS and ion chromatography (65-68). Ring and large chains can rearrange and/or anneal to form smaller fullerenes (*e.g.* C_{30}^+) which continue to anneal, forming larger fullerenes such as C_{60} (62,65-68). Such annealing, or fusing, processes of ringed

structures are hypothesized to be made possible in part through Stone-Wales rearrangements (62,69).

Recently synthesis based approaches to create fullerenes have gained attention as they allow for enhanced control and insight. Such processes would provide distinct production advantages including, but not limited to: facile endohedral fullerene synthesis, which have another atom (metal) or molecule inside the cage structure; precisely derivatized fullerenes; and high yield, low energy fullerene production. While such routes have proven difficult, they have been verified empirically. For example, Boorum *et al.* produced C₆₀ from a large symmetrical, 60 carbon PAH (C₆₀H₃₀) precursor termed PAH 6, when the molecule was exposed to a nitrogen laser (LDI), the molecule was effectively “zipped” or condensed together into C₆₀ with corresponding dehydration (70). This mechanism of formation was verified via ¹³C enrichment at known ring placement(s) and corresponding MS analysis, which fundamentally differs from a other fragment-recombination fullerene mechanisms discussed (70). Other synthesis possibilities have been discussed elsewhere (62).

C₆₀ Properties

Structure

The C₆₀ molecule (Fig 2.1) is a closed, cage structure with 60 carbon atoms arranged in the most symmetrical arrangement possible. The diameter across (nucleus to nucleus of furthest carbon atoms apart) has been measured to be 0.71 ± 0.007 nm via NMR measurements (71). The electron cloud (primarily from π bonding) has been estimated to

add an additional 0.335 nm (δ) to the diameter of the molecule giving C₆₀ an effective diameter of *ca.* 1.034 nm (6,56). Ring architecture is critical to the stability of C₆₀, as with all fullerenes. The arrangement of hexagon and pentagon rings, or the building principle as Hirsch put it, in fullerenes was correctly hypothesized to be a function of Euler's Theorem whereby each fullerene contains 2(10 + M) carbon atoms corresponding to exactly 12 pentagons and M hexagons (62). As a repeating hexagonal sheet will remain flat as observed for pure graphite, which can even be "rolled" as observed for nanotubes walls, pentagon ring inclusion in all fullerenes is obligatory for cage curvature (*i.e.* rounding) (72,73). Similarly, both single wall and multi-wall nanotubes require pentagon inclusion in round end formations (6,7). Furthermore, the 'more' isolated each pentagon is from each other results in increased cage stability as discussed elsewhere for the "isolated pentagon rule" (IPR) (73,74). The isolated pentagon rule (IPR) is based on the fact that adjacent pentagon rings will be thermodynamically unfavorable due to steric constraints, resulting in excess curvature (strain) as discussed by Kroto *et al.* and 8 π -electron systems which would lead to resonance destabilization as discussed by Hirsch (62,73). Out of *ca.* 15,000 possible isomer structures for C₆₀ in particular, only one possibility can be calculated that symmetrically incorporates 12 pentagons which are each "equally" isolated by 5 hexagon ring structures (20 total) minimizing the anisotropic contributions to the strain energy (62). This stable, truncated icosahedral, 3-D structure exhibits I_h symmetry which is analogous to an American soccer ball (3). While C-C bonding environments must meet the required carbon valence needs, one double bond and two single bonds for each carbon, the lowest energy Kekulé structure was calculated, keeping the IPR, such that all double bonds should to be located between hexagon

vertices [6,6] which are tangential to each pentagon vertices [5,6] (62). These two types of bonds have been directly measured via neutron, electron and X-ray diffraction along with ^{13}C -NMR and reported to be 0.144, 0.146, 0.147 and 0.145 for [5,6] bonds (pentagon ring, single bonds) respectively and 0.139, 0.140, 0.136 and 0.137 nm for [6,6] bonds (hexagon ring, double bonds) respectively (62, 71,75-77). Differing averaged bond lengths between [5,6] and [6,6] are attributed the minimization strain energies by molecular symmetry and the π bonding environments (57). Interestingly, similar C-C bonds in larger fullerenes can be more variable as there are more C-C bonding environments to consider (*i.e.* higher degree of bond length alternation) (62). Basic C_{60} chemical-physical properties, largely underpinned by the symmetrical 3-D carbon ring structure and localized conjugated π system, including heat of formation, electron affinity, material density, ionization potentials among others have been studied extensively and summarized in a number of review papers and books (6,28,34,56-59) with selected properties and constants tabulated again here in Table 2.1.

Solid C_{60}

Physically, as a solid, pure C_{60} is crystalline, with a FCC (face centered cubic) unit cell ($a = 14.17 \text{ \AA}$) at room temperature and atmospheric pressure with a demonstrated density of 1.72 g/cm^3 . In this crystal state, C_{60} molecules rotate quite freely due to relatively weak molecular interactions (78). According to Prassides *et al.*, as the temperature is lowered (*ca.* 261 K), the crystal restructure undergoes a transition (rearrangement) to a simple cubic (SC) unit cell structure (6,79). At atmospheric pressure, sublimation occurs around $1 \times 10^3 \text{ K}$ in inert atmosphere, which varies with pressure. In theory, at high temperature ($>1 \times 10^3 \text{ K}$) and elevated pressure ($>1 \times 10^4 \text{ Torr}$) solid C_{60} can melt to a liquid state (6,8)

but has not been empirically verified. Molecular C₆₀ begins to fragment at temperatures exceeding 4x10³ K and collapse at pressures greater than 1x10⁸ Torr (6). It has been noted though, that in the presence of oxygen, UV, or a catalyst, such as TiO₂, thermal stabilities dramatically lowered as oxidative degradation occurs (8). Furthermore, a number of co-crystallates and clathrate structures with other molecules (such as benzene, CCl₄, etc.), usually as solvents, have been widely observed and described (6,80).

C₆₀ in Solvents

C₆₀ solubility has been widely studied, with an estimated 150 known values for various solvents (80). However, as Korobov and Smith explain (80), “There is still no good theory to explain or predict absolute values for fullerene solubility and changes in solubility when changing the solvent or the fullerene itself.” Nevertheless, quality empirical observations and theoretical discussions regarding specific trends exist that are of value. Ruoff *et al.* attempted to correlate C₆₀ solubility to the polarizability, polarity, molecular size and cohesive energy density of the solvent (81). In this study, no one distinctive parameter universally explained C₆₀ solubility, however, positive correlations were observed with similar solvent parameters to that of C₆₀ such as molecular size (81). Multivariate analyses employed by Murray *et al.* using 22 solvents achieved a linear coefficient of 0.95 (r²), indicating that solvent surface area was critical (82). Studies by others indicate found similar positive correlations with solvent size (expressed as molar volume) in addition to positive correlation to solvents that are a good Lewis acid and Lewis base (both) but with minimal polarity or charge (80). In addition, organic solvent electron donor capacity (Lewis base) was further identified by Talukdar *et al.* as being positively correlated with C₆₀ solubility, along with more evidence supporting that

solvent size and polarizability are critical (80). In addition, C₆₀ solubility displays an abnormal temperature dependence in a number of solvents (83), actually decreasing with increased temperature. While the solubility of C₆₀ in water has not been measured directly, it has been estimated < 10⁻⁹ mg/L by Heymann (84). Taken from Kadish and Ruoff, a list of selected solubilities at 298 K are tabulated in Table 2.2.

Spectroscopy

Unique spectral properties were critical in the initial fullerene identification and remain so for current analytical analyses. C₆₀ has been well characterized with a range of spectral analyses including mass spectroscopy (MS), UV-Vis, FTIR, Raman and NMR (9,10,62,85-89). Mass spectroscopy has been employed in fullerene identification via molecular weight(s) since the conjecture of C₆₀ by Kroto *et al.* in 1985 (72). With a molecular weight of 720 (m/z 720 @ mono-ionized) and being fairly easily ionized due HOMO LUMO molecular orbital situation, MS identification of C₆₀ has been reported throughout the literature using both positive and negative ion modes with LDI (with and without matrix assistance), FAB and EI (62,85,86). Based on inherit electronic and vibrational structures, IR and UV/Vis spectra observed and reported by Krätschmer *et al.* in 1990 confirming the molecule by matching values calculated previously for an icosahedral 60 carbon cage structure by others (9,10,28,88,90). C₆₀ vibrational structure (IR and Raman spectroscopy) was predicted to have four IR-active frequencies (T_{1u} modes, dipole) based on via four spring constants (C-C (pentagon bond), C=C (hexagon bond), C-C=C (angle) and C-C-C (angle)) and derived eigenvalues along with 10 theoretically active Raman frequencies (H_g and A_g modes) despite being 60 carbons (360 total electrons and a calculated 174 active modes) as described by Weeks and Harter

among others (28,90). Four such IR active absorption bands were empirically observed to be at 1,429; 1,183; 577 and 528 cm^{-1} indicating high molecular symmetry and confirming a free, truncated icosahedral molecule (9,88,90). In comparison, a 60 carbon graphite isomer (D_{6h} symmetry) has some 20 IR-active frequencies (88). Following IR reports, 10 empirical Raman shifts were later observed, matching vibrational predictions (albeit slightly shifted) (90) further confirming the molecule's electronic structure (91). A C_{60} UV/Vis absorption spectra was suggested as early as 1987 and then confirmed in 1990 (9,10). Larsson *et al.* calculated oscillator strengths, which correspond to the probability of orbital transitions, of the allowed transitions as a function of eV (which can be converted to wavelength), These predictions match absorbance spectra (overlaid) by Kroto *et al.* in the UV/Vis (200-700 nm) range (C_{60} as a thin film). In addition, Kroto *et al.* observe broad absorption at 450 nm which is also discussed by Larsson *et al.* and Dresselhaus *et al.* as symmetry forbidden transitions and observed by others normally for solid state C_{60} films, indicating probable solid state C_{60} - C_{60} interactions. Dissolved C_{60} UV/Vis spectra have been published extensively and can exhibit slight red or blue shifts depending on the solvent (81). Specifically, dissolved in hexanes (low background UV absorbance), C_{60} exhibits strong absorbance in the UV at 211, 256 328 nm, a lesser absorbance peak at 410, and low visible absorbance peaks centered 492, 540, 568, 591, 598, and 621 nm (86). ^{13}C NMR C_{60} spectra were reported independently by three groups almost simultaneously in 1990 (85,86,89). All three reported, as hypothesized, observed C_{60} as a single line response, ranging from 143.3 - 143.68 ppm shift from TMS reference, indicating icosahedral symmetry (*i.e.* I_h symmetry), and further confirming the exact equivalency of all carbon atoms. Such a downfield shift from the benzene or other

PAH analogues was further hypothesized to be a function of strain induced hybridization changes similar to indane (143.9 ppm) and benzocyclobutene (146.3 ppm) (89).

Aromaticity

Kroto suggested in 1985 that C_{60} could be, “the first example of a spherical aromatic molecule” (72). Since then, the question whether fullerenes are truly aromatic has been the source of many studies and is still debated (57). The problem lies in the fact that fullerenes in many ways are difficult to compare with planar aromatics by which aromaticity has been defined. Moreover, the actual definition of aromaticity has changed over time and is still even considered controversial in some regards (92). Buhl and Hirsch recently published a review article evaluating fullerene aromaticity (57) and discuss some of the problems with defining and/or characterizing fullerene aromaticity:

Compared to benzene, being the archetype of a two-dimensional aromatic molecule, the discussion of aromaticity of fullerenes must take into account the strain provided by the pyramidalization of the C atoms. The rich exohedral chemistry of fullerenes which is basically an addition to the conjugated π system, is to a large extent, driven by the reduction of strain. Analysis of the reactivity and region-chemistry of addition reactions reveals behavior reminiscent of electron-deficient olefins. However, especially the magnetic properties of fullerenes clearly reflect delocalized character of the conjugated π system, which, depending on the number of π electrons, can cause the occurrence of diamagnetic or paramagnetic ring currents within the loops of the hexagons and pentagons. Neutral C_{60} for example, containing diatropic hexagons and paratropic pentagons was labeled by others ‘ambiguously aromatic’(57).

Following the Buhl and Hirsh text, fullerene aromaticity is discussed in classic aromatic criteria, which include: structure (including count numbers), energy, reactivity, and magnetism (57). Briefly, C_{60} properties for each criterion are discussed, but should only be interpreted as a brief summary of extensive studies by others on the subject.

Structure

Ring structure, particularly with regard to bond lengths ([5,6] pentagon bonds and [6,6] hexagon bonds), and induced strain from the pyramidization are critical to fullerene aromaticity properties. As discussed before, neutral C_{60} [5,6] and [6,6] bond lengths differ, which is attributed to the filling of h_u , t_{1u} and the t_{1g} orbitals within the $I=5$ shell (π) (57). When C_{60} is neutral, the $I=5$ shell is incompletely filled, as it requires 22 π electrons, 72 total ($I=4$ shell requires 18 π electrons, 50 total). This fact actually causes higher incidence of electron *localization*, giving rise to single bond characteristics, which are physically longer, along the [5,6] and double bond characteristics along the [6,6] which are shorter and more reactive (57). Intuitively, charged fullerenes such as the theoretical C_{60}^{10+} and even C_{60}^{-n} ($n=2-12$) are considered 'more' aromatic in this regard as the $I=5$ shell is varied. C_{60}^{10+} [5,6] and [6,6] C-C bonds have been calculated to relax based on the loss of electrons from the $I=5$ shell electrons giving rise only to a completely filled $I=4$ shell which corresponds of lower the bond length difference, thus increasing delocalization. Similarly, the addition of electrons to the $I=5$ shell has also been calculated to increase aromaticity as bond lengths would also relax based on increased delocalization as the filled shell (57). However, it should be noted that electron additions above 6 is unlikely as the $I=6$ nodal plane take on electrons after C_{60}^{6-} , instead of complete $I=5$ filling (57). These bond length differences in neutral C_{60} contribute to

the weakly antiaromatic pentagons and weakly aromatic hexagons based on the HOMA indexing (harmonic oscillator model of aromaticity).

Energetics

Aromaticity can also be investigated from energetics. A number of methods have been designed to measure the molecular orbital (MO) resonance energy (RE), or the molecular stabilization of the cyclic bonding π delocalization. As Buhl and Hirsh point out however, such measurements have been classically zeroed to, or designed for well characterized planar PAH molecules such as benzene. While work has been done to normalize the caged structure for such measurements, including strain energies from pyramidilzation (*i.e.* bond angle contributions) (93), disparities exist when comparing C_{60} characteristics to the planar benzene structure, indicating that while C_{60} is aromatic, just how aromatic (compared to benzene) depends on the methodology of choice (57). For larger fullerenes, such MO - RE calculations begin to converge with aromatic values for graphite (73) as bond angles relax and the ratio of hexagons to pentagons increases. Other, more straightforward, estimates of aromaticity stabilization contributions measure the bond separation energy or heat of hydrogenation. Through the use of isodesmic equations, which maintain the number of formal single and double bonds between the carbon atoms, the energy of separating the bonds can be predicted. Such analysis was described by Fowler *et al.* and demonstrates C_{60} to be generally less aromatic when compared to benzene and based on the energy associated with the separation (2245 kJ/mol for C_{60}) (94). Similarly, the heat of hydrogenation for C_{60} , which can be taken as a measure of energetic stability (the higher the heat the less stable) has been theoretically

calculated to be *ca.* double (normalized per C) that of benzene (-206 kJ/mol), indicating that C₆₀ is to a 'lesser' degree aromatic (94,95).

Reactivity

Generally speaking classic aromatic reactivity such as substitution reactions cannot be considered as fullerenes lack boundary hydrogens, and aromatic substitution reactions are not possible, leaving only addition and redox reactions to consider (again making traditional PAH comparisons difficult). In addition, caged molecules differ from traditional planar aromatic in that bond strain can alter reactivity from what is expected (6,8,62). Traditional indexes of molecular reactivity such as chemical hardness, defined as η where $\eta = (\text{HOMO} - \text{LUMO})/2$, are based on molecular orbital energy gaps. A larger η equates, normally, to less reactive molecule. Compared to benzene, C₆₀ has an η approximately 3 times lower hardness index, indicating a higher reactivity than benzene. While there are a number of reactions to consider, Buhl and Hirsch summarized reactivity as it relates to aromaticity (57):

The reversibility of several addition reactions could be an indication of the propensity of the retention of the structural type which is considered to be a reactivity criterion of aromaticity. The regioselectivity of two-step additions, such as the addition of a nucleophile followed by the trapping of the fullerene intermediate with an electrophile, on the other hand shows that the charge is in not delocalized over the whole fullerene. This speaks against a pronounced aromatic character. Also, other reactions such as the additions of transition-metal fragments are reminiscent of olefins rather than of aromatics. In many cases an important driving force for the regioselectivity of multiple addition reactions is

the formations of the substructures that are more aromatic than the substructures of the parent fullerene.

Magnetic Properties

Electron delocalization in aromatic compounds is the source of characteristic magnetic properties and can be observed via NMR shifts and diamagnetic susceptibilities. Fullerenes were first predicted by Kroto *et al.* to have unusual magnetic properties in 1985 (72). Since then, numerous studies have been completed which evaluate fullerene magnetic properties, many of which are beyond the scope of this review. However, as they relate to aromaticity, relevant fullerene magnetic properties must be acknowledged. Ring current theories, which are based on π electrons freely and separately along a σ -bonded ring framework, allow for the computation of magnetic susceptibilities, which are difficult to observe; and NMR chemical shifts. Empirically, ring currents can be measured indirectly through proton shielding (which only applies to fullerenes upon hydrogenation). When a perpendicular magnetic field is applied to an aromatic ring, delocalized π electrons are induced to circulate around the ring producing a small local magnetic field (92). According to McMurry, this induced field opposes the applied field in the middle of the ring, but actually reinforces the applied field outside of the ring, thus effectively deshielding aromatic protons (on the ring exterior) (95), which can be observed via ^1H NMR. For example, when a strong magnetic field is applied to [18]annulene ($\text{C}_{18}\text{H}_{18}$), a cyclic conjugated polyene with 18 π electrons, the 6 interior protons are strongly shielded by the ring current (-3.0δ relative to TMS), whereas the 12 exterior (outside) protons are deshielded and observed in the typical aromatic region (9.3δ TMS) (95). Benzene as a model PAH, has demonstrates similar proton deshielding (7.2δ

TMS) consistent with a near-free π circular electron current (57,96). However, for underivatized fullerenes, deshielding measurements are not possible to observe as there are no boundary bonds thus other estimates are necessary. Proper use of derivatized fullerenes appears to be quite difficult, as it is hard to know the exact architecture of the product. Generally though, gainful employment of appropriate covalent adducts has shed insight of the shielding capacity via an applied magnetic field (57). The application of quantum chemical methods such as (Hückel-MO- based London method and Hartree-Fock ab initio calculations for current densities) can calculate localized (individual ring) aromatic, also termed diatropic, π electron ring currents and antiaromatic, also termed or paratropic, ring currents (57). Conjugated antiaromatic molecules (*e.g.* cyclobutadiene) increase in molecular energy when π electrons are delocalized in contrast to aromatic conjugated molecules which are lower in molecular energy with increased delocalization (92,95). Taken together over the whole molecule, ring current calculations indicate that C_{60} is slightly aromatic, with regard to magnetic susceptibility (97). However, individual ring current calculations indicate that the hexagon rings are diatropic, with similar values to benzene and pentagons are paratropic, which, when taken together, account for a small, *net* aromatic index (magnetic susceptibility). C_{70} on the other hand with an equatorial band of additional paratropic hexagons (same 12 pentagons as C_{60}), is calculated to be more susceptible to magnetic fields and thus more aromatic when considered as a whole (*net*) (93,97). Similarly, ‘giant’ fullerenes C_{240} , C_{540} , etc. with increasing number of hexagons and less bond angle strain, have been calculated to have π electron ring current susceptibilities that begin to approach graphite (*i.e.* higher than C_{60} and C_{70}) (57).

Count Rules

For simple, planar anulene aromatics, the Hückle count rule of aromaticity which simply states that $4n + 2 \pi$ electrons are necessary, where $n =$ succeeding energy levels (95). For such planar systems, $4n + 2 \pi$ electrons represents a closed shell system. However, this rule is general, and not applicable for more complex polycyclic systems that contain benzenoid rings joined by four or five member rings, as demonstrated for biphenylene (which still demonstrates aromatic properties) (92). Similarly, fullerene aromaticity cannot be considered by the $4n + 2$ Hückel rule. A spherical, closed shell situations is realized if the fullerene contains $2(N + 1)^2 \pi$ electrons, similar to noble gas configurations (57). For C_{60} to reach a $2(N + 1)^2 \pi$ electron configuration, it must exist as C_{60}^{10+} ($I=4$, filled) or C_{60}^{-12} ($I=5$, filled) the later of which would not likely occur as outer shell orbitals (t_{1g} , $I=6$) of C_{60} are filled before inner shells are (t_{2u} , $I=5$) (57). Theoretical calculations of ^3He (endohedral) chemical shifts (-81.4δ) in the center of C_{60}^{10+} support this, indicating extreme diamagnetic shielding (57).

In conclusion, the consideration of fullerene aromaticity is a complex subject. As Buhl and Hirsh summarize, “When π MOs on the surface of a sphere are grouped into shells according to their nodal properties, a simple model predicts that maximum aromaticity is reached when the individual shells are filled (*i.e.* $2(N + 1)^2 \pi$ electrons).....Such complete shell filling occurs less often than in cyclic anulenes, with many intermediate situations exhibiting both aromatic and antiaromatic properties (57)”. This is the case for neutral C_{60} , as it demonstrates both aromatic properties, including calculated localized ring current, diamagnetic shielding (as demonstrated by adduct additions) and increased molecular stabilization; and also anitaromatic properties

including reactivity behaviors, which is similar to electron deficient olefins, bond length alterations and paratropic ring current regions (pentagons). Based on these criteria, the term ‘ambiguously aromatic’ or as Fowler *et al.* states, “ a more or less aromatic system” seems to describe neutral C₆₀ well (97).

Reactivity

C₆₀ reactivity is a function of electronic (*e.g.* HOMO-LUMO energy gaps, incomplete $I=5$ nodal shell, paratropic / diatropic ring currents) and physical structure (*e.g.* bond strain, bond length alterations, etc.), which are irreducibly intertwined. Briefly, electrochemistries (redox), covalent additions, photophysical reactivity among others are discussed below. Figure 2.2, reproduced with permission from Kroto, Taylor and Walton, summarizes general fullerene reaction routes. Each area of fullerene reactivity has been studied and discussed extensively in the literature. Brevity, discussion of each is limited to fundamental, representative studies.

Electrochemistry

Based on degenerate low lying unoccupied molecular orbitals (LUMO t_{1u} symmetry and LUMO+1 t_{1g} symmetry), C₆₀ is predicted to be an electronegative molecule capable of accepting up to 6 electrons upon reduction. This was shown to be true via cyclic voltammetry, producing the anionic forms (fullerides) consisting of 1-6 electron additions which fill the LUMO t_{1u} (6,87,98-101). C₆₀ potentials ($E_{1/2}$) in a mixed solvent system of acetonitrile:toluene (1:5) under vacuum at -10°C with TBAPF₆ (tetra-n-butylammoniumhexafluorophosphate) as a supporting electrolyte were measured by Eschegoyen *et al.* to be -0.98, -1.37, -1.87, -2.35, -2.85 and -3.26 V vs Fc/Fc⁺ (101).

While mono- through tetra- anions have been shown to be stable on the time frame of hours to days depending on the solvent temperature, and supporting electrolyte; penta- and hexa-anions quickly reverse back to lower anions (101). Conversely, it was predicted to be difficult to oxidize C_{60} giving rise to a charged cation species.

Voltammetric studies showed a 1 electron oxidation in TCE (under vacuum) occurs at +1.26 eV vs Fc/Fc⁺ (101). The difference between the first reduction and first oxidation, which is a measure of the HOMO-LUMO energy gap, can be calculated to be 2.32 eV for C_{60} under these described conditions (80). Similar calculations for C_{70} indicated a slightly smaller HOMO-LUMO gap of 2.22V (80,101). Additionally, it has been demonstrated that the choice of solvent and supporting electrolyte can have significant effect on the potential at which fullerene ions are generated (62,87,101). Furthermore, based on electron symmetry and orbital levels filled, C_{60}^{n-} (n= 1-4) anionic forms of C_{60} take on unique spectral properties. For example adding one or more electron to the degenerate LUMO MO results in a new IR transitions, widening and red shifting of UV absorbance, change in visible color (C_{60}^{-} red-purple; C_{60}^{2-} red orange; C_{60}^{3-} dark red brown), ¹³C NMR downfield shifts (62) and unique ESR spectra. Such reductions can also be accomplished via traditional chemical reaction such as with Rb, Li (Birch reaction) and other alkali earth metals, in liquid ammonia; potassium naphthalenide; naphthalene; mercury among other donors (6,62). Furthermore, upon ionization (C_{60}^{n-}) it has been well established that fullerides readily react with a variety electrophiles to form covalently bonded adducts (6,58,62).

Nucleophilic Additions

Based on electronic structure, neutral C₆₀ undergoes a number of nucleophilic additions. Such an addition gives rise to an intermediate anion species which is then subsequently stabilized with an electrophile addition, such as H⁺ (62). Such addition(s) gives rise to many possible isomers. However, based on electron density calculations (Mulliken Charges based on AM1 calculations) after a nucleophile addition (tBuOH forming the intermediate tBuC₆₀⁻ anion), the carbon (across the double bond [6,6], see figure 2.1D) directly across the once double bond becomes the most negative (increase e⁻ density) and thus most probable electrophilic addition position (62). Simple examples of nucleophile additions include early observations of reactions with typical nucleophiles such as primary amines, as RNH₂, (where R is an aryl or alkyl group); alkyls (simple to complex); cyanide, organolithium compounds, and Grignard reagents among others (6,59,62,102). Number and cage placement of such additions depend on the reaction conditions and type of nucleophile. In addition, some nucleophiles with leaving groups (such as Br) can be electrophilic enough to undergo intra-molecular substitution at the electron dense carbon (along the fullerene [6,6] C-C) and form a cyclo adduct. Additionally, other cycloadditions can be accomplished via Diels-Alder type reactions with appropriate dienes (*e.g.* cyclopentadiene) (6,58,62,95). Such cyclo- additions can happen via a number of reactants and through a number of shared pathways (4+2, 3+2, 2+2 and 2+1 types in reference to shared π electrons) that are beyond the scope of this review.

Hydrogenation

Fullerene reduction via hydrogen addition (hydrofullerene) can be accomplished via a number of standard hydrogenation reactions. Degrees and placement of proton additions vary according to reactant types, ratios and solvents (6,58,59,62). Early reports of hydrogen addition included $C_{60}H_{18}$ and $C_{60}H_{36}$ via Birch Reduction (98) along the [6,6] C=C double bond (termed by some as a 1,2 addition). Reducing metal treatment with Zn/Cu, Mg, Ti, Al or Zn with a proton source produces a number of lower hydrofullerenes including $C_{60}H_2$, $C_{60}H_4$ and $C_{60}H_6$ (62). Additionally, C_{60} can be hydrogenated with molecular hydrogen in the presence of a solid reductant (62). Such reactions proceed with an elevated H_2 pressure under heat, pressure and a reducing environment such as supported (alumina or activated carbon) Ru, Rh, Ir, Pd, Pt, Co and Ni giving rise to $C_{60}H_{18}$ (Ru, Rh, Ir) and $C_{60}H_{36}$ (Pd, Pt, Co and Ni) isomers (103). Other, organic reactants such as a NADH analogue (BNAH under photoexcitation) can be used to accomplish lower numbered hydrofullerenes ($C_{60}H_2$) under mild conditions (104). It has also been shown that hydrofullerenes can be oxidized back to the parent fullerene via treatment with DDQ (2,3-dichloro-5,6-dicyanobenzoquinone) (62).

Halogenation

Exothermic halogenation reactions readily occur with fluorine, chlorine, bromine giving rise to final products that are limited by the size and affinity of the halogen. Fluorination (C-F), the most exothermic of the halogenation reactions, can be accomplished via fluorine gas, noble gas fluorides, halogen fluorides, metal fluorides among others (58,59,62,105). While a variety of fluorinated fullerenes have been reported, including $C_{60}F_{48}$ as observed by a number of groups, however higher

derivatives including $C_{60}F_{60}$ have been reported (105). Direct chlorination occurs in a similar manner, via chlorine gas under elevated temperatures or with liquid chlorine at lowered temperatures (-35°C) results in $C_{60}Cl_n$ ($n = 6 - 26$ depending on reaction conditions) (62,106). Bromination occurs less readily, however, can be accomplished directly with liquid bromine giving rise to $C_{60}Br_{24}$ or in benzene, giving lower derivatives such as $C_{60}Br_6$ (62,107,108). Halogen addition patterns vary by reaction conditions and halogen affinity and size as described by Taylor *et al.* (59).

Electrophilic Additions and Oxidation

While cage reduction reactions consisting of nucleophilic additions are favored for neutral fullerene species, oxidation reactions (electron withdrawing) can occur readily with appropriate electrophiles (strong). Simple epoxide adducts ($C_{60}O_n$ where $n = 1-12$) can be synthesized via a range of oxidizing agents such as oxygen (under UV), hydrogen peroxide, *m*-chloroperoxybenzoic acid (MCPBA), dimethyldioxirane, methyl(trifluoromethyl) dioxirane, among others in various solvents (8). Additionally, direct facile oxidation can be accomplished via osmylation (OsO_4) and ozonation (O_3) whereby an electron withdrawing cyclo adduct is formed, which for ozone (ozonide), quickly degrades (thermolysis) into a fullerene epoxide in organic solvents (109). Hydroxylated fullerenes (fullerols) can be synthesized similarly beginning with an electron withdrawing agent such as a nitronium ion in the presence of H_2SO_4 and KNO_3 under elevated temperatures (95°C), or with nitronium tetrafluoroborate in the presence of alkyl or aryl carboxylic acid in methylene chloride under N_2 atmosphere and subsequently hydrolyzed in basic water (via $NaOH$) (110-112). Similarly, polysulfonated fullerene intermediates, which can be synthesized via neat fuming sulfuric acid at 55°C

under N_2 , are hydrolyzed in aqueous NaOH resulting in $C_{60}(OH)_x$ (fullerols) (113). Other methods have been demonstrated, substituting halogen additions with hydroxyl groups and even a simple two phase (C_{60} dissolved in toluene-water) interface where by aqueous pH was elevated and a phase transfer agent (TBAH) employed (114,115). Depending on preparation conditions, fullerols can be composed of 8-24 hydroxyl groups, can also contain carbonyl groups, are generally hydrophilic and readily dissolve into water (8).

Photophysical Reactivity

C_{60} has been reported to exhibit chemical reactivity toward various radical, producing stable multiple radical adducts species (116,117). Especially, the photo-induced excitation of C_{60} can facilitate electron transfer from electron donors to acceptors, and mediate energy transfer to oxygen with high quantum yield, leading to the formation of singlet oxygen. These photochemical properties (29,30) have given C_{60} priority as possible applications in photodynamic therapy (31,32), oxidative synthetic reaction (33), and electron shuttling action in dye-sensitized solar cell (34). Singlet oxygen (118) and superoxide radical (31,119,120) generated in C_{60} suspension can trigger DNA damage and cellular structural destruction, (31,118-122). While pristine C_{60} in hydrocarbon solvent has been known as an efficient singlet oxygen precursor under the UV irradiation (30), there have been some controversial reports about photoactivity of C_{60} suspended in aqueous phase; Beeby *et al.* (123) demonstrated photochemical generation of singlet oxygen was efficiently performed on C_{60} solubilized into aqueous solution of Triton X100 (non-ionic surfactant, TX) applied above critical micelle concentration. On the other hand, Yamakoshi *et al.* (31,120) suggested that based on ESR (Electron Spin Resonance) analysis, C_{60} solvated into water with PVP (polyvinylpyrrolidone, PVP)

generated superoxide and $\cdot\text{OH}$ radical in the presence of electron donor (ED), with no detectable singlet oxygen produced.

Other Chemistries

Fullerene chemistry is a broad topic. In addition to the aforementioned chemistries, a number of articles (including review articles) and books have been published demonstrating similar reaction pathways albeit with higher fullerenes (*i.e.* C_{70}) and other more complex chemistries, including, but not limited to: fullerene polymer synthesis; derivatized fullerene parent materials; endohedral fullerene parent materials; radical chemistries (117); among others. Again, thorough fullerene chemistry reports by fullerene chemists including Buhl and Hirsch (62), Taylor (8), Dresselhaus et al. (124), Kadish and Ruoff (80), are widely available and provide an excellent starting point for many cases.

Fullerenes in Water

Incidentally, the behavior of C_{60} , in the aqueous phase, can differ from what is expected as C_{60} and other pristine, neutral fullerenes are virtually non-wettable (estimated solubility of $\text{C}_{60} < 10^{-9}$ mg/L) (81,125,126). The unfavorable free-energy of remaining in water should drive hydrophobic C_{60} to adsorb onto / or within (absorption) matrixes which corresponds to large octanol-water and organic carbon - water partition coefficient estimates (Table 2.2). Based on classic estimation parameters, the aqueous behavior is expected to be similar to other large, non-polar hydrophobic molecules (for example polyaromatic hydrocarbons), which tend to associate strongly with organic carbon (OC)

and in natural systems. However, apparent solubility or availability of C_{60} in water can be significantly altered by the following three pathways. First, C_{60} can be chemically modified to include hydrophilic functionalities such as hydroxyl groups which have been shown to substantially increase its aqueous solubility (110,127,128). Numerous other water soluble fullerene derivatives (*e.g.* fullerols) have been described and include organic acids (129,130) and electrophilic additions (112) as discussed above. Second, C_{60} can be rendered available in water by surfactants, polymers (*i.e.* polyvinyl pyrrolidone (PVP)) and even natural macromolecules including, γ -cyclodextrin, sucrose, and dextran (40 kDa) which can effectively to shield the hydrophobic surface of the C_{60} molecules from water (131-133). Third, C_{60} in polar solvents, including water, can form stable aggregate suspensions at the micro- to nano-scales (134-138). Compared to hydrophobic sorption alone, C_{60} rendered 'available' in water by any of these methods will be subject to dispersive processes, increasing the potential volume of media exposed.

Water Stable C_{60} Aggregates

Recent reports have demonstrated aggregation phenomenon of C_{60} in water (case 3 above) occurring in relatively simple systems such as solid C_{60} powder (>99.9 purity, MER Corp.) was mixed in water at high shear rates for an extended period of time (days to weeks) (138). C_{60} aggregate suspensions have been reported via a number of methods and have demonstrated dimensions at, or near, the nano-scale diameters, *ca.* 5-500 nm, with a net negative surface charge thus allowing for stable, ppm concentrations (134-137,139,140). A typical suspension prepared by this lab is shown in figure 2.5 (prepared by the modified Deguchi method as described by Fortner *et al.*) (137,141). These aggregates allow for concentrations up to *ca.* 150 mg/L, which is ~11 orders of

magnitude more than the estimated molecular solubility (81,84,142). Though this material has been the subject of some study over the past decade, questions concerning the formation, composition and stability remain unresolved/ambiguous (134,136,137,139,143). Water stable C₆₀ aggregates properties are summarized here; being organized by formation pathways and properties along a brief summary of the current surface charge (source) hypotheses:

Formation and Properties

First described by Scrivens *et al.* in 1994, water stable C₆₀ aggregates were observed via a solvent exchange protocol beginning with toluene containing dissolved C₆₀, which was diluted into THF then diluted further into acetone and finally into water where by a fine mustard colored suspension was formed (135). UV/Vis spectra of the suspension showed characteristic C₆₀ peaks at 227, 280 and 360 nm (red shifted, broadened) and an average size of approximately 300 nm (SEM). In addition, radio labeled (¹²C:¹⁴C = 200:1) water stable C₆₀ aggregates were synthesized with this method for *in vitro* uptake studies with human keratinocytes (135). To date, this is the only literature report of successfully synthesizing ¹⁴C labeled C₆₀. A year later, in 1995, a Ukrainian group led by Grigoriy Andrieysky observed a similar aqueous suspension after sonicating a C₆₀ laden toluene suspension overlaying water (134). A similar broad UV/Vis spectrum characteristic of C₆₀ was observed, with aggregates reported below 200 nm (134). Starting with fullerene anions, Wei *et al.* reports a similar aqueous suspension (referred to as a sol in their work) after exposing the C₆₀⁻ and C₆₀²⁻ to undegassed water (oxygen present) (140). To begin, C₆₀ was reduced to the fulleride in THF via Al-Ni alloy, tin, zinc powder or sodium hydrosulfite in the presence of NaOH. Fulleride

presence was confirmed through NIR, cyclic voltammetry, EPR and NMR (which shifts dramatically downfield to 188.2 ppm). Fulleride/THF solutions were then added drop wise into stirring water at ambient temperatures, quickly forming a dark red-brown aqueous suspension at relatively high concentrations (1 mg/ml) (140). A change in color was reported by varying concentration: 0.33 mg/ml, brown-red; 0.11 mg/ml, pale red; and 0.04 mg/ml, pale yellow. Suspensions demonstrated characteristic IR spectrum (KBr pellet) of underivatized, neutral C₆₀ (1428, 1183, 573 and 527 cm⁻¹ reported).

Interestingly when degassed water was added to THF fulleride solution, voltammetry results suggest that water alone cannot oxidize the fulleride, nor was it susceptible to proton donation from water, thus leading the authors to conclude that a fullerene anion (C₆₀⁻) is stable in oxygen free, pure water (140). Furthermore, this method reports much smaller aggregate size(s) (average aggregate size to be *ca.* 10 nm.) via TEM analysis.

Other groups have since reported similar aggregate suspensions, prepared through solvent transfers, including Deguchi *et al.* in 2001, who reported the simple method of saturating a THF solution with C₆₀ and adding it to water (1:1 volume) whereby a yellow suspension was formed (dilute). THF was then removed via rotary distillation, leaving an aqueous C₆₀ suspension (*ca.* 3-5 mg/L C₆₀) that could then be concentrated. As described, this method produced aggregates on the order of 60 nm, with similar spectral properties of other C₆₀ aggregate systems. Furthermore, C₇₀ clusters were produced using similar manner (THF/water) (137). Similarly, aggregates have been produced in other polar solvents according to Alargova *et al.*, including acetone, acetonitrile and ethanol via similar pathways (*i.e.* starting with a dissolved C₆₀ solution in toluene or benzene, which is added sequentially to more polar solvents) (136). This study also was the first to

observe aggregate size as a variable that was a function of initial C_{60} concentration, leading to an insightful conceptual model for C_{60} aggregation in polar systems (136). By lowering initial C_{60} concentrations, smaller the aggregates were formed (136). Perhaps most interesting though, is the recent observation by Cheng *et al.*, that by simply adding C_{60} to D.I. water at ambient temperatures and pressure, under a high shear rate (rapidly stirred), can form an orange-yellow suspension of water stable C_{60} aggregates (138). While producing a broader size range of aggregates (25 - 300+ nm, polydispersed) than other methods and taking longer to aggregate (weeks), these suspensions demonstrated similar, chemical and physical properties as observed by others (16,138).

Surface Chemistry

The surface chemistry of these aggregate species is of interest as it is this interface where hydrophobic fullerenes are in some way rendered hydrophilic. In fact these aggregates as noted by a number of studies, do not readily appreciate back into a polar solvent (0.8 – 3.6 %) (135,141,144). Our lab and others confirmed that the surfaces of these materials are charged by performing electrophoretic mobility studies (ζ potential ranging from *ca.* -9 mV to -40 mV) (137,141,145). A number of possible explanations (sources) have been proposed for the surface charge: It may be that upon contact with water, pristine fullerenes undergo a chemical reaction to create a small population of partially oxidized, and hence more polar, amphiphilic fullerenes which are able to stabilize the hydrophobic, underivatized core (135). C_{60} is a relatively reactive species; its degradation by light and oxygen has been noted (146,147). In particular, one inefficient method to form partially hydroxylated fullerenes relies on the introduction of THF/ C_{60} solutions to water at high pH values (>12) (148). Such a reaction may also

proceed, albeit at lower yields, when THF/C₆₀ solutions are introduced in neutral water. Alternatively, C₆₀ is an excellent electron acceptor. Both Andrievsky *et al.* and Deguchi *et al.*, along with our own findings, suggest that water itself (or another polar solvent) may form a donor-acceptor complex with C₆₀ leading to a weakly charged colloid (134,137,143). Other mechanisms proposed include hydroxyl ion adsorption to the surface of the aggregate, which seems improbable as Deguchi *et al.* points out, citing the fact that similar aggregates are formed in polar solvents without hydroxyl ions (ethanol, acetone, ACN) (136,137). Moreover, Avdeev *et al.* along with Andrievsky *et al.* discuss possible molecular C₆₀ hydration, which they term [(C₆₀@{H₂O})_n]_m, suggesting each C₆₀ molecule being hydrated by 20-24 organized water molecules, as it may relate aggregate stabilities (143,149). A number of identifying names have been assigned to the water stable C₆₀ suspensions based on preparation methods and author's discrepancies. Such names include: nC₆₀, aqu/nC₆₀, SON/nC₆₀, THF/nC₆₀, TTA/nC₆₀ (144,150); C₆₀ dispersions (136,137); C₆₀ hydrosol, C₆₀ FWS (134,139,143); and nano-C₆₀ (119,141). For consistency, the term nano-C₆₀ is used throughout the remainder of this thesis.

Based on a net negative surface charge, as measured via zeta potential (ζ) of the C₆₀ aggregate, studies have been conducted with variable ionic strengths and types (divalent and mono-valent) to better understand the surface chemistry (137,141,151). In particular, a recent study by Brant *et al.* is almost completely focused on this topic (151). Comparing C₆₀ aggregate solutions formed through a THF intermediate (Deguchi method) and by simply adding C₆₀ to water and stirring over time (Cheng method), a range of ionic strengths and types was investigated. Results indicated that as ionic strength was increased from 0 to 0.1 M, ζ potential values increased (less negative) until

aggregates settled out of solutions $\geq 0.1 I$. Furthermore, it was interestingly noted, that with divalent cations such as calcium, and within a pH range of 5-8, aggregates could actually take on a net positive surface charge. Furthermore, as pH was adjusted for suspensions with mono-valent ions (NaCl, 0.001 to 0.1 I), the ζ potential values generally decreased (less negative) for the aggregates consistent with classic electrostatic theory. Our lab observed similar results in terms of aggregate stability range as a function of ionic strength (THF prepared) noting macro-scale C_{60} aggregate settling above 0.5 I (mono-valent NaCl, pH 5) (141).

The early interest in aggregate forms of fullerenes, particularly C_{60} , was motivated by their applications in technologies, particularly those which require fullerenes in water (134,136,152). Aqueous stable C_{60} suspensions have shown little promise in this regard, as typical concentrations (< 100 ppm) are far below the 10,000 to 100,000 ppm levels that are achievable when the carbon cage is intentionally altered to include polar functionalities (113,114,127,153-155). Still, such aggregate generation through unintentional exposure of fullerenes to water is possible, and the amounts generated may be significant for ecological effects (≤ 100 ppm). Other lipophilic organic molecules, which might be analogous to C_{60} , have significant ecological impact in aqueous systems at concentrations of 1-10 ppm (156). Once available in water, these materials may be transported and react readily with both abiotic and biological processes/receptors. For instance, a recent study by Lecoanet *et al.* on the mobility of suspended nano-materials in porous media showed that both functionalized and C_{60} aggregates were capable of migrating through a well defined porous medium (157). Such water available fullerenes have been reported to cause varying biological responses upon exposure (118,158-161).

Specifically, previous reports by this lab and others have demonstrated that fullerenes, as suspended C₆₀ in aggregate form, can elicit a biological response at relatively low concentrations (<1 ppm) (119,150,162). Considering these facts, fullerenes stable in water, including those in nano-scale aggregate forms, should be well understood in terms of both chemical and physical properties for appropriate consideration during risk and lifecycle assessments of the material.

Figure 2.1

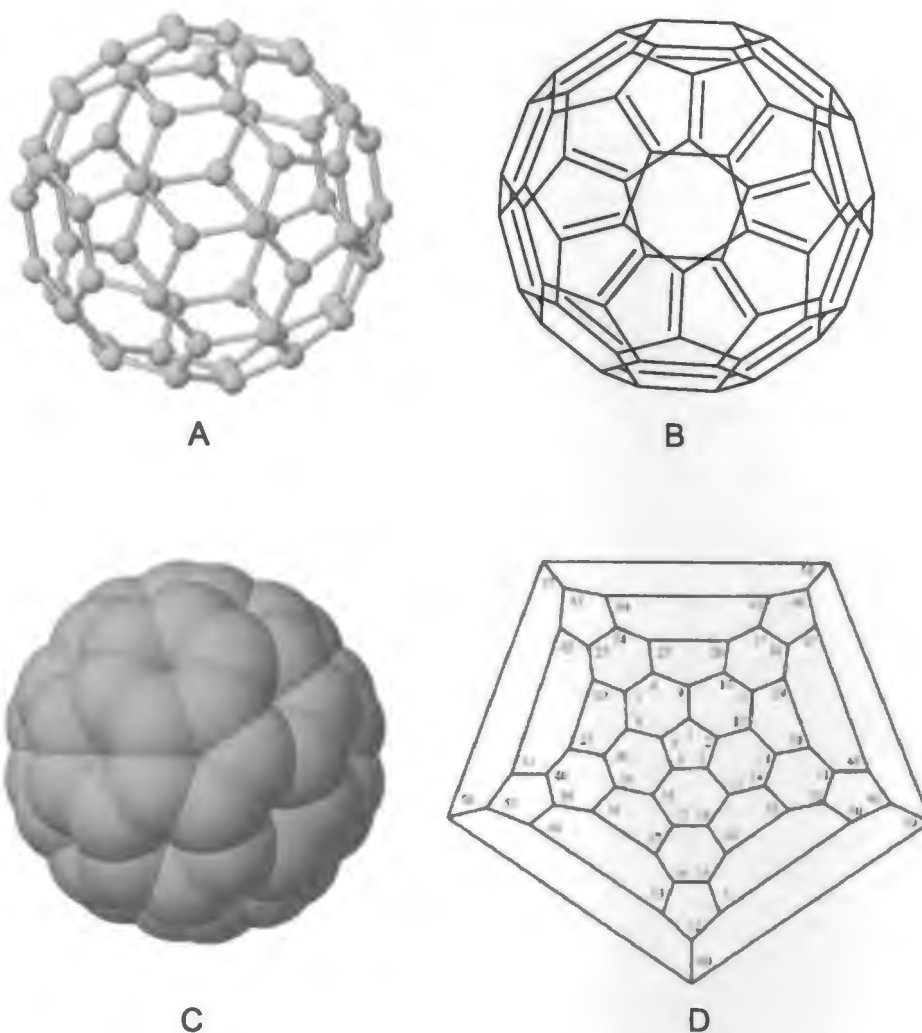


Figure 2.1. C_{60} structures: (A) Ball and Stick Model (B) Bonding Arrangement Model (C) Space Filling Model (D) Schlegel Diagram (2) (image used with Dr. Powell's and IUPAC's permission)

*Note: Images A-C were provided by ChemSketch software available through the Advanced Chemistry Department Inc., Toronto Canada, www.acdlabs.com.

Figure 2.2

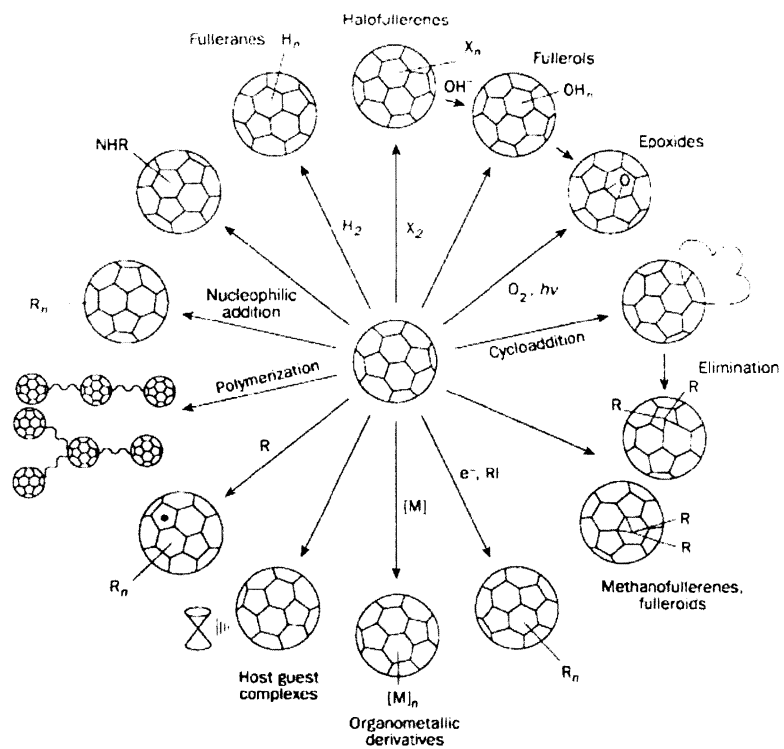


Figure 2.2. Generalize C₆₀ reaction routes. Used with permission from Taylor and Walton (58)

Figure 2.3

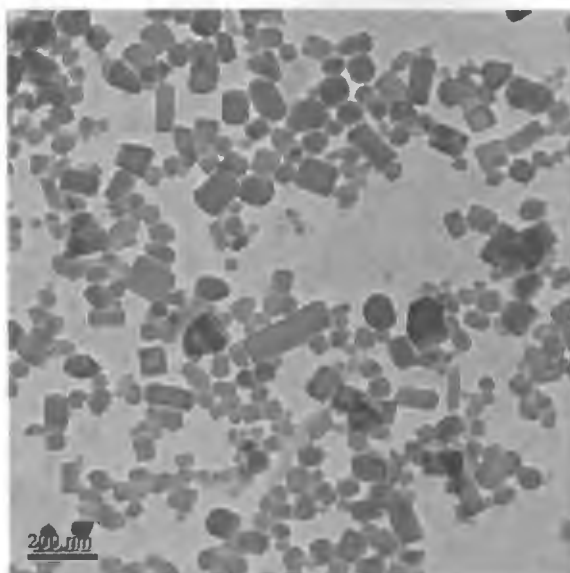


Figure 2.3 Transmission electron micrograph of nano-C₆₀ produced by our lab (Deguchi, THF method)

Table 2.1

Selected Solid State C ₆₀ Properties	
Density	1.65 g/cm ³
Graphite Density*	2.3 g/cm ³
Diamond Density*	3.5 g/cm ³
Crystal Structure (>255 K)	Face-Centered Cubic (FCC)
Crystal Structure (<255 K)	Simple Cubic (SC)
Nearest Neighbor Distance	10.04 Å (FCC)
Cage Diameter	7.1 Å
Lattice Constant	14.198 Å (FCC)
Electrical Conductivity	Nonconductor (neutral state)
Index of Refraction (RI)	2.2 at 630 nm λ

Constants summarized by Huffman (56)
*Allotrope Comparison
All values are at standard temperature and pressure unless otherwise noted

Table 2.2

Solubility of C ₆₀ in Various Solvents	
Solvent	[C ₆₀] mg/mL
Benzene	1.7
Toluene	2.8
Cyclohexane	0.036
TCE	1.2
Chloroform	0.16
Ethanol	0.001
Acetone	0.001
Pyridine	0.89
Carbon Disulfide	7.9
<i>n</i> -decane	0.071

Values taken from Kadish and Ruoff (80)

Table 2.3

Selected C ₆₀ Properties* and Partitioning Estimations [†]	
*Molecular Weight (g/mol)	720 g/mol
*Aqueous Solubility (g/L)	< 10 ⁻¹² g/L calculated by Heymann <i>et al.</i> 1996
*Vapor Pressure (atm)	6.6 x 10 ⁻⁹ atm
†Henry's Law Constant (atm. m ³ /L)	Estimated: 10⁻¹¹ based on: structural unit contributions Schwarzenbach <i>et al.</i> 1993
†Octanol-Water Partition Coefficient (K _{ow})	Estimated: 10^{14.7} – 10^{16.7} based on: Log K _{ow} = -log C _w ^{sat} (1,L) – log γ _o - log V _o Schwarzenbach <i>et al.</i> 1993
†Organic Carbon – Water Partition Coefficient (K _{oc})	Estimated at 10^{14.2} – 10^{16.2} based on: Log K _{om} = 1.01*LogK _{ow} – 0.72 (suggested for Aromatic hydrocarbons) Schwarzenbach <i>et al.</i> 1993

Literature Cited

1. Osawa, E. *Kagaku* 1970, 25, 854.
2. Powell, W. H.; Cozzi, F.; Moss, G. P.; Thilgen, C.; Hwu, R. J.-R.; Yerin, A. Nomenclature for the C₆₀-I_h and C₇₀ D_{5h(6)} Fullerenes. *Pure Appl. Chem.* 2002, 74, 629-695.
3. Kroto, H. W.; Heath, J. R.; O'Brien, S. C.; Curl, R. F.; Smalley, R. E. C₆₀: Buckminsterfullerene. *Nature* 1985, 318, 162.
4. Kroto, H. W. In *Nobel Lectures, Chemistry 1996-2000*; Grenthe, I., Ed.; World Scientific Publishing Co., Singapore, 1996.
5. Curl Jr., R. F. In *Nobel Lectures, Chemistry 1996-2000*; Grenthe, I., Ed.; World Scientific Publishing Co.: Singapore, 1996.
6. Dresselhaus, M. S.; Dresselhaus, G.; Eklund, P. C. *Science of Fullerenes and Carbon Nanotubes*; Academic Press: San Diego, 1996.
7. Smalley, R. E. In *Nobel Lectures, Chemistry 1996-2000*; Grenthe, I., Ed.; World Scientific Publishing Co., Singapore, 1996.
8. Taylor, R., Ed. *The Chemistry of Fullerenes*; World Scientific Publishing Co. Pte. Ltd., Singapore, 1995; Vol. 4.
9. Kratschmer, W.; Lamb, L. D.; Fostiropoulos, K.; Huffman, D. R. Solid C-60 - a New Form of Carbon. *Nature* 1990, 347, 354-358.
10. Larsson, S.; Volosov, A.; Rosen, A. Optical-Spectrum of the Icosahedral C₆₀ - Follene-60. *Chem. Phys. Lett.* 1987, 137, 501-504.
11. Utsunomiya, S.; Jensen, K. A.; Keeler, G. J.; Ewing, R. C. Uraninite and Fullerene in Atmospheric Particles. *Environ. Sci. Tech.* 2002, 36, 4943-4947.
12. Howard, J. B.; Lafleur, A. L.; Makarovskiy, Y.; Mitra, S.; Pope, C. J.; Yadav, T. K. Fullerenes synthesis in Combustion. *Carbon* 1992, 30, 1183-1201.
13. Diederich, F.; Ettl, R.; Rubin, Y.; Whetten, R. L.; Beck, R.; Alvarez, M.; Anz, S.; Sensharma, D.; Wudl, F.; Khemani, K. C.; Koch, A. The Higher Fullerenes - Isolation and Characterization of C₇₆, C₈₄, C₉₀, C₉₄, and C_{70o}, an Oxide of D_{5h}-C₇₀. *Science* 1991, 252, 548-551.

14. Nakamura, E.; Tokuyama, H.; Yamago, S.; Shiraki, T.; Sugiura, Y. Biological activity of water-soluble fullerenes. Structural dependence of DNA cleavage, cytotoxicity, and enzyme inhibitory activities including HIV-protease inhibition. *B Chem. Soc. Jpn.* 1996, *69*, 2143-2151.
15. Mashino, T.; Nishikawa, D.; Takahashi, K.; Usui, N.; Yamori, T.; Seki, M.; Endo, T.; Mochizuki, M. Antibacterial and Antiproliferative Activity of Cationic Fullerene Derivatives. *Bioorg. Med.l Chem. Lett.* 2003.
16. Lyon, D. Y.; Adams, L. K.; Falkner, J. C.; Alvarez, P. J. J. Antibacterial activity of fullerene water suspensions: Effects of preparation method and particle size. *L. Environ. Sci. Tech.* 2006, *40*, 4360-4366.
17. Chen, C. C.; Lieber, C. M. Isotope Effect and Superconductivity in Metal-Doped C60. *Science* 1993, *259*, 655-658.
18. Haddon, R. C.; Hebard, A. F.; Rosseinsky, M. J.; Murphy, D. W.; Duclos, S. J.; Lyons, K. B.; Miller, B.; Rosamilia, J. M.; Fleming, R. M.; Kortan, A. R.; Glarum, S. H.; Makhija, A. V.; Muller, A. J.; Eick, R. H.; Zahurak, S. M.; Tycko, R.; Dabbagh, G.; Thiel, F. A. Conducting Films of C60 and C70 by Alkali-Metal Doping. *Nature* 1991, *350*, 320-322.
19. Regueiro, M. N.; Monceau, P.; Hodeau, J. L. Crushing C60 to Diamond at Room-Temperature. *Nature* 1992, *355*, 237-239.
20. Bocquillon, G.; Bogicevic, C.; Fabre, C.; Rassat, A. C60 Fullerene as Carbon Source for Diamond Synthesis. *J. Phys. Chem.-Us.* 1993, *97*, 12924-12927.
21. Mort, J.; Okumura, K.; Machonkin, M.; Ziolo, R.; Huffman, D. R.; Ferguson, M. I. Photoconductivity in Solid Films of C60/70. *Chem. Phys. Lett.* 1991, *186*, 281-283.
22. Tremblay, J. Mitsubishi Aims at a Breakthrough. *Chem. Eng. News* 2002, *80*, 16-17.
23. Wharton, T.; Kini, V. U.; Mortis, R. A.; Wilson, L. J. New non-ionic, highly water-soluble derivatives of C-60 designed for biological compatibility. *Tetrahedron Lett.* 2001, *42*, 5159-5162.
24. Iqbal, Z.; Baughman, R. H.; Ramakrishna, B. L.; Khare, S.; Murthy, N. S.; Bornemann, H. J.; Morris, D. E. Superconductivity at 45-K in Rb/Tl Codoped C60 and C60/C70 Mixtures. *Science* 1991, *254*, 826-829.
25. Kelty, S. P.; Chen, C. C.; Lieber, C. M. Superconductivity at 30-K in Cesium-Doped C60. *Nature* 1991, *352*, 223-225.

26. Gupta, B. K.; Bhushan, B.; Capp, C.; Coe, J. V. Materials Characterization and Effect of Purity and Ion Implantation on the friction wear of Sublimed Fullerene Films. *J. Mat. Res.* 1994, 9, 2823.
27. Wang, Y. Photoconductivity of Fullerene Doped Polymers. *Nature* 1992, 356, 585-587.
28. Koruga, D.; Hameroff, S.; Withers, J.; Loufty, R.; Sundareshan, M. *Fullerene C60: History, Physics, Nanobiology, Nanotechnology*; Elsevier Science Publishers: Amsterdam, 1993.
29. Arbogast, J. W.; Foote, C. S.; Kao, M. Electron-Transfer to Triplet C-60. *J. Am. Chem Soc.* 1992, 114, 2277-2279.
30. Arbogast, J. W.; Darmany, A. P.; Foote, C. S.; Rubin, Y.; Diederich, F. N.; Alvarez, M. M.; Anz, S. J.; Whetten, R. L. Photophysical Properties of C60. *J. Phys. Chem.-Us.* 1991, 95, 11-12.
31. Yamakoshi, Y.; Umezawa, N.; Ryu, A.; Arakane, K.; Miyata, N.; Goda, Y.; Masumizu, T.; Nagano, T. Active Oxygen Species Generated from Photoexcited Fullerene (C60) as Potential Medicines: O₂- versus 1O₂. *J. Am. Chem. Soc.* 2003, 125, 12803-12809.
32. Jensen, A. W.; S. R. Wilson; Schuster, D. I. Biological applications of fullerenes. *Bioorg. Med. Chem.* 1996, 767-779.
33. Jensen, A. W.; Daniels, C. Fullerene-coated beads as reusable catalysts. *J. Org. Chem.* 2003, 207-210.
34. Kamat, P. V.; Haria, M.; Hotchandani, S. C60 Cluster as an Electron Shuttle in a Ru(II)-polypyridyl Sensitizer-Based Photochemical Solar Cell. *J. Phys. Chem. B* 2004, 108, 5166-5170.
35. Iijima, S. Helical Microtubules of Graphitic Carbon. *Nature* 1991, 354, 56-58.
36. Cowley, J. M.; Liu, M. Q. The Structure of Carbon Nanotubes Impregnated with Yttrium. *Micron.* 1994, 25, 53-61.
37. Dreher, K. L. Health and Environmental Impact of Nanotechnology: Toxicological Assessment of Manufactured Nanoparticles. *Toxicol. Sci.* 2004, 77, 3-5.
38. Ajayan, P. M.; Charlier, J. C.; Rinzler, A. G. Carbon Nanotubes: From Macromolecules to Nanotechnology. *Proceedings of the National Academy of Sciences of the United States of America* 1999, 96, 14199-14200.

39. Ajayan, P. M.; Zhou, O. Z. Applications of carbon nanotubes. *Carbon Nano.* 2001, 80, 391-425.
40. Dai, H.; Wong, E. W.; Liebert, C. M. Probing Electrical Transport in Nanomaterials: Conductivity of Individual Carbon Nanotubes. *Science* 1996, 272, 523-526.
41. Rueckes, T.; Kim, K.; Joselevich, E.; Tseng, G. Y.; Cheung, C.-L.; Lieber, C. Carbon Nanotube-Based Nonvolatile Random Access Memory for Molecular Computing. *Science* 2000, 289, 94-97.
42. Dillon, A. C.; Jones, K. M.; Bekkedahl, T. A.; Kiang, C. H.; Bethune, D. S.; Heben, M. J. Storage of hydrogen in single-walled carbon nanotubes. *Nature* 1997, 386, 377-379.
43. Cheng, H. M.; Yang, Q. H.; Liu, C. Hydrogen storage in carbon nanotubes. *Carbon* 2001, 39, 1447-1454.
44. Kong, J.; Franklin, N. R.; Zhou, C.; Chapline, M. G.; Peng, S.; Cho, K.; Dai, H. Nanotube Molecular Wires as Chemical Sensors. *Science* 2000, 287, 622-625.
45. Collins, P. G.; Bradley, K.; Ishigami, M.; Zettl, A. Extreme oxygen sensitivity of electronic properties of carbon nanotubes. *Science* 2000, 287, 1801-1804.
46. Chopra, S.; McGuire, K.; Gothard, N.; Rao, A. M.; Pham, A. Selective gas detection using a carbon nanotube sensor. *Appl. Phys. Lett.* 2003, 83, 2280-2282.
47. Chopra, S.; Pham, A.; Gaillard, J.; Parker, A.; Rao, A. M. Carbon-nanotube-based resonant-circuit sensor for ammonia. *Appl. Phys. Lett.* 2002, 80, 4632-4634.
48. Miller, S. A.; Young, V. Y.; Martin, C. R. Electroosmotic flow in template-prepared carbon nanotube membranes. *J. Am. Chem. Soc.* 2001, 123, 12335-12342.
49. Casavant, M. J.; Walters, D. A.; Schmidt, J. J.; Smalley, R. E. Neat macroscopic membranes of aligned carbon nanotubes. *J. Appl. Phys.* 2003, 93, 2153-2156.
50. Biercuk, M. J.; Llaguno, M. C.; Radosavljevic, M.; Hyun, J. K.; Johnson, A. T.; Fischer, J. E. Carbon nanotube composites for thermal management. *Appl. Phys. Lett.* 2002, 80, 2767-2769.
51. Biswas, S.; Vajtai, R.; Wei, B.; Meng, G.; Schowalter, L.; Ajayan, P. Vertically aligned conductive carbon nanotube junctions and arrays for device applications. *Appl. Phys. Lett.* 2004, 84, 2889-2891.
52. Colvin, V. The Environmental Impact of Engineered Nanomaterials. *Nature Biotech.* 2004.

53. Lee, B. I.; Qi, L.; Copeland, T. Nanoparticles for materials design: present & future. *J. Ceramic Proc. Res.* 2005, 6, 31-40.
54. Ball, P. Roll up for the revolution. *Nature* 2001, 414, 142-144.
55. Murdock, S. A, Disruptive Technology with the Potential to Create New Winners and Redefine Industry Boundaries, Presentation. *AtomWorks* 2002.
56. Huffman, D. R. Solid C₆₀. *Physics Today* 1991, 22-29.
57. Buhl, M.; Hirsch, A. Spherical Aromaticity of Fullerenes. *Chem. Rev.* 2001, 1153.
58. Taylor, R.; Walton, R. M. The Chemistry of Fullerenes. *Nature* 1993, 363, 685-693.
59. Taylor, R. The Pattern of Additions to Fullerenes. *PHILOSOPHICAL TRANSACTIONS OF THE ROYAL SOCIETY OF LONDON SERIES A-MATHEMATICAL PHYSICAL AND ENGINEERING SCIENCES* 1993 343, 87-101.
60. Ajie, H.; Alvarez, M. M.; Anz, S. J.; Beck, R. D.; Diederich, F.; Fostiropoulos, K.; Huffman, D. R.; Kraetschmer, W.; Rubin, Y.; Shriver, K. E.; Sensharma, D.; Whetten, R. L. Characterization of the soluble all-carbon molecules C₆₀ and C₇₀. *J. Phys. Chem. A.* 1990, 94, 8630-8633.
61. Koch, A. S.; Khemani, K. C.; Wudl, F. Preparation of fullerenes with a simple benchtop reactor. *J. Org. Chem.* 1991, 56.
62. Hirsch, A.; Brettreich, M. *Fullerenes: Chemistry and Reactions*; Wiley-VCH Verlag GmbH & Co.: Weinheim, 2005.
63. Howard, J. B.; Mckinnon, J. T.; Makarovsky, Y.; Lafleur, A. L.; Johnson, M. E. Fullerenes C₆₀ and C₇₀ in Flames. *Nature* 1991, 352, 139-141.
64. Anacleto, J. F.; Perreault, H.; Boyd, R. K.; Pleasance, S.; Quilliam, M. A.; Sim, P. G.; Howard, J. B.; Makarovsky, Y.; Lafleur, A. L. C₆₀ and C₇₀ fullerene isomers generated in flames. Detection and verification by liquid chromatography/mass spectrometry analyses. *R. Comm. Mass Spec.* 1992, 6, 214-220.
65. Helden, G. v.; Kemper, P. R.; Gotts, N. G.; Bowers, M. T. Isomers of Small Carbon Clusters Anions: Linear Chains with up to 20 Atoms. *Science* 1993, 259, 1300-1302.
66. Helden, G. v.; Hsu, M.-T.; Gotts, N.; Bowers, M. T. Carbon Cluster with up to 84 Atoms: Structures, Formation Mechanism, and Reactivity *J. Phys. Chem.* 1993, 97, 8182-8192.

67. Helden, G. v.; Gotts, N. G.; Bowers, M. T. Experimental Evidence for the formation of fullerenes by heating of carbon rings in the gas phase. *Nature* 1993, *363*, 60-63.
68. Helden, G. v.; Gotts, N. G.; Bowers, M. T. Annealing of Carbon Cations: Rings to Rings and Rings to Fullerenes. *J. Am. Chem. Soc.* 1993, *115*, 4363-4364.
69. Stone, A. J.; Wales, D. J. Theoretical-Studies of Icosahedral C₆₀ and Some Related Species. *Chem. Phys. Lett.* 1986, *128*, 501-503.
70. Boonchan, S.; Britz, M. L.; Stanley, G. A. Degradation and Mineralization of High-Molecular Weight Polycyclic Aromatic Hydrocarbons by Defined Fungal-Bacterial Cocultures. *Appl. Environ. Micro.* 2000, *66*, 1007-1019.
71. Yannoni, C. S.; Bernier, P. P.; Bethune, D. S.; Meijer, G.; Salem, J. R. Nmr Determination of the Bond Lengths in C₆₀. *J. Am. Chem. Soc.* 1991, *113*, 3190-3192.
72. Kroto, H. W.; Heath, J. R.; O'Brien, S. C.; Curl, R. F.; Smalley, R. E. C-60 - Buckminsterfullerene. *Nature* 1985, *318*, 162-163.
73. Kroto, H. W. The stability of the fullerenes C_n, with $n = 24, 28, 32, 50, 60$ and 70. *Nature* 1987, *329*, 529.
74. Schmalz, T. G.; Seitz, W. A.; Klein, D. J.; Hite, G. E. *Chem. Phys. Lett.* 1986, *130*, 203.
75. Liu, S. Z.; Lu, Y. J.; Kappes, M. M.; Ibers, J. A. The Structure of the C₆₀ Molecule - X-Ray Crystal-Structure Determination of a Twin at 110-K. *Science* 1991, *254*, 408-410.
76. Hedberg, K.; Hedberg, L.; Bethune, D. S.; Brown, C. A.; Dorn, H. C.; Johnson, R. D.; Devries, M. Bond Lengths in Free Molecules of Buckminsterfullerene, C₆₀, from Gas-Phase Electron-Diffraction. *Science* 1991, *254*, 410-412.
77. David, W. I. F.; Ibberson, R. M.; Matthewman, J. C.; Prassides, K.; Dennis, T. J. S.; Hare, J. P.; Kroto, H. W.; Taylor, R.; Walton, D. R. M. Crystal-Structure and Bonding of Ordered C₆₀. *Nature* 1991, *353*, 147-149.
78. Yannoni, C. S.; Johnson, R. D.; Meijer, G.; Bethune, D. S.; Salem, J. R. C-13 Nmr-Study of the C₆₀ Cluster in the Solid-State - Molecular-Motion and Carbon Chemical-Shift Anisotropy. *J. Phys. Chem.-Us.* 1991, *95*, 9-10.
79. Prassides, K.; Kroto, H. W.; Taylor, R.; Walton, D. R. M.; David, W. I. F.; Tomkinson, J.; Haddon, R. C.; Rosseinsky, M. J.; Murphy, D. W. Fullerenes and Fullerides in the Solid-State - Neutron-Scattering Studies. *Carbon* 1992, *30*, 1277-1286.

80. Kadish, K. M.; Ruoff, R. S., Eds. *Fullerenes: Chemistry, Physics, and Technology*; Wiley-Interscience: New York, 2000.
81. Ruoff, R. S.; Tse, D. S.; Malhotra, R.; Lorents, D. C. Solubility of C-60 in a Variety of Solvents. *J. Phys. Chem.-Us.* 1993, *97*, 3379-3383.
82. Murray, J. S.; Gargarin, S. G.; Polititzer, P. Representation of C60 Solubilities in Terms of Computed Molecular Surface Electrostatic Potentials and Areas. *J. Phys. Chem.* 1995, *99*, 12081-12083.
83. Ruoff, R. S.; Malhotra, R.; Huestis, D. L.; Tse, D. S.; Lorents, D. C. Anomalous Solubility Behavior of C60. *Nature* 1993, *362*, 140-141.
84. Heymann, D. Solubility of C60 and C70 in seven normal alcohols and their deduced solubility in water. *Fullerene Sci. Tech.* 1996, *4*, 509-515.
85. Taylor, R.; Hare, J. P.; Abdul-Sada, A. a. K.; Kroto, H. Isolation, Separation and Characterisation of the Fullerenes C60 and C70: The Third Form of Carbon. *J. Chem. Soc., Chem. Commun.* 1990, 1423-1425.
86. Ajie, H.; Alvarez, M. M.; Anz, S. J.; Beck, R. D.; Diederich, F.; Fostiropoulos, K.; Huffman, D. R.; Kratschmer, W.; Rubin, Y.; Schriver, K. E.; Sensharma, D.; Whetten, R. L. Characterization of the Soluble All-Carbon Molecules C60 and C70. *J. Phys. Chem.-Us* 1990, *94*, 8630-8633.
87. Cox, D. M.; Behal, S.; Disko, M.; Gorun, S. M.; Greaney, M.; Hsu, C. S.; Kollin, E. B.; Millar, J.; Robbins, J.; Robbins, W.; Sherwood, R. D.; Tindall, P. Characterization of C60 and C70 Clusters. *J. Am. Chem. Soc.* 1991, *113*, 2940-2944.
88. Stanton, R. E.; Newton, M. D. Normal vibrational modes of buckminsterfullerene. *J. Phys. Chem. A* 1988, *92*, 2141-2145.
89. Johnson, R. D.; Meijer, G.; Bethune, D. S. C60 has icosahedral symmetry. *J. Am. Chem. Soc.* 1990, *112*, 8983-8984.
90. Weeks, D. E.; Harter, W. G. Vibrational Frequencies and Normal Modes of Buckminsterfullerene. *Chem. Phys. Lett.* 1988, *144*, 372.
91. Bethune, D. S.; Meijer, G.; Tang, W. C.; Rosen, H. J.; Golden, W. G.; Seki, H.; Brown, C. A.; Devries, M. S. Vibrational Raman and Infrared-Spectra of Chromatographically Separated C60 and C70 Fullerene Clusters. *Chem. Phys. Lett.* 1991, *179*, 181-186.
92. Schleyer, P. v. R. Introduction: Aromaticity. *Chem. Rev.* 2001, *101*, 1115-1118.

93. Haddon, R. C. Chemistry of the Fullerenes: The Manifestation of Strain in a Class of Continuous Aromatic Molecules. *Science* 1993, *261*, 1545-1550.
94. Fowler, P. W.; Collins, D. J.; Austin, S. J. Is aromaticity a useful concept for fullerene (C₆₀) and its derivatives? Aromatization of C₆₀ by regioselective addition. *J. Chem. Soc., Perkin Trans. 2: Phys. Org. Chem.* 1993, 275-277.
95. McMurray, J. *Organic Chemistry*; 4th ed.; Brooks/Cole Publishing Company: Pacific Grove, CA, 1996.
96. Silverstein, R. M.; Bassler, G. C.; Morrill, T. C. *Spectrometric Identification of Organic Compounds*; John Wiley & Sons: New York, 1981; Vol. 4.
97. Fowler, P. W.; Lazzeretti, P.; Malagoli, M.; Zanasi, R. Magnetic-Properties of C₆₀ and C₇₀. *Chem. Phys. Lett.* 1991, *179*, 174-180.
98. Haufler, R. E.; Conceicao, J.; Chibante, L. P. F.; Chai, Y.; Byrne, N. E.; Flanagan, S.; Haley, M. M.; O'Brien, S. C.; Pan, C.; Xiao, Z.; Billups, W. E.; Ciufolini, M. A.; Hauge, R. H.; Margrave, J. L.; Wilson, L. J.; Curl, R. F.; Smalley, R. E. Efficient Production of C₆₀ (Buckminsterfullerene), C₆₀H₃₆, and the Solvated Buckide Ion. *J. Phys. Chem.-Us.* 1990, *94*, 8634-8636.
99. Dubois, D.; Kadish, K. M.; Flanagan, S.; Haufler, R. E.; Chibante, L. P. F.; Wilson, L. J. Spectroelectrochemical Study of the C₆₀ and C₇₀ Fullerenes and Their Monoanions, Dianions, Trianions, and Tetraanions. *J. Am. Chem. Soc.* 1991, *113*, 4364-4366.
100. Allemand, P.-M.; Koch, A.; Wudl, F.; Rubin, Y.; Diederich, F.; Alvarez, M. M.; Anz, S. J.; Whetten, R. L. Two Different Fullerenes Have the Same Cyclic Voltammetry. *J. Am. Chem. Soc.* 1991, *113*, 1050-1051.
101. Echegoyen, L.; Echegoyen, L. E. Electrochemistry of Fullerenes and Their Derivatives. *Acc. Chem. Res.* 1998, *31*, 593-601.
102. Klos, H.; Rystau, I.; Schutz, W.; Gotschy, B.; Skiebe, A.; Hirsch, A. doping of C₆₀ with Tertiary Amines -TDAE, DBU, DBN, A Comparative Study. *Chem. Phys. Lett.* 1994, *224*, 333-337.
103. Song, H.; Lee, C. H.; Lee, K.; Park, J. T. Ligand-Induced Conversion of to C₆₀-Metal Cluster Complexes: Full Characterization of the 3-1:2:1-C₆₀ Bonding Mode. *Organomet.* 2002, *21*, 2514 - 2520.
104. Fukuzumi, S.; Suenobu, T.; Patz, M.; Hirasaka, T.; Itoh, S.; Fujitsuka, M.; Ito, O. Selective One-Electron and Two-Electron Reduction of C₆₀ with NADH and

- NAD Dimer Analogues via Photoinduced Electron Transfer. *J. Am. Chem. Soc.* 1998, *120*, 8060-8068.
105. Holloway, J. H.; Hope, E. G.; Taylor, R.; Langley, G. J.; Avent, A. G.; Dennis, T. J.; Hare, J. P.; Kroto, H. W.; Walton, D. R. M. Fluorination of Buckminsterfullerene. *J. Chem. Soc., Chem. Commun.* 1991, 966-969.
 106. Olah, G. A.; Bucsi, I.; Lambert, C.; Aniszfeld, R.; Trivedi, N. J.; Sensharma, D. K.; Prakash, G. K. S. Considered Polycarbon Supercage Chemistry .3. Polyarenefullerenes, C₆₀(H-Ar)_N, Obtained by Acid-Catalyzed Fullerenation of Aromatics. *J. Am. Chem. Soc.* 1991, *113*, 9387-9388.
 107. Tebbe, F. N.; Harlow, R. L.; Chase, D. B.; Thorn, D. L.; G. Creston Campbell, J.; Calabrese, J. C.; Herron, N.; Robert J. Young, J.; Wasserman, E. Synthesis and Single-Crystal X-ray Structure of a Highly Symmetrical C₆₀ Derivative, C₆₀Br₂₄. *Science* 1991, *256*, 822-825.
 108. Birkett, P. R.; Hitchcock, P. B.; Kroto, H. W.; Taylor, R.; Walton, D. R. M. Preparation and characterization of C₆₀Br₆ and C₆₀Br₈. *Nature* 1992, 479-482.
 109. Weisman, R. B.; Heymann, D.; Bachilo, S. M. Synthesis and characterization of the "missing" oxide of C-60: [5,6]-open C₆₀O. *J. Am. Chem. Soc.* 2001, *123*, 9720-9721.
 110. Chiang, L. Y.; Bhonsle, J. B.; Wang, L.; Shu, S. F.; Chang, T. M.; Hwu, J. R. Efficient One-Flask Synthesis of Water-Soluble [60]Fullerenols. *Tetrahedron* 1996, *52*, 4963-4972.
 111. Chiang, L. Y.; Swirczewski, J. W.; Hsu, C. S.; Chowdhury, S. K.; Cameron, S.; Creegan, K. Multi-hydroxy Additions onto C₆₀ Fullerene Molecules. *J. Chem. Soc., Chem. Commun.* 1992, *24*, 1791-1793.
 112. Chiang, L. Y.; Upasani, R. B.; Swirczewski, J. W. Versatile Nitronium Chemistry for C₆₀ Fullerene Functionalization. *J. Am. Chem. Soc.* 1992, *114*, 10154-10157.
 113. Chiang, L. Y.; Upasani, R. B.; Swirczewski, J. W.; Soled, S. Evidence of Hemiketals Incorporated in the Structure of Fullerols Derived from Aqueous Acid Chemistry. *J. Am. Chem. Soc.* 1993, *115*, 5453-5457.
 114. Schneider, N. S.; Darwish, A. D.; Kroto, H. W.; Taylor, R.; Walton, D. R. M. Formation of Fullerols via Hydroboration of Fullerene-C₆₀. *J. Chem. Soc., Chem. Commun.* 1994, *4*, 463-464.
 115. Husebo, L.; Sitharaman, B.; Furukawa, K.; Kato, T.; Wilson, L. Fullerenols Revisited as Stable Radical Anions. *J. Am. Chem. Soc.* 2004, *126*, 12055-12062.

116. McEwen, C. N.; McKay, R. G.; Larsen, B. S. C₆₀ as a radical sponge. *J. Am. Chem. Soc.* 1992, *114*, 4412-4414.
117. Krusic, P. J.; Wasserman, E.; Keizer, P. N.; Morton, J. R.; Preston, K. F. Radical Reactions of C₆₀. *Science* 1991, *254*, 1183-1185.
118. Kamat, J. P.; Devasagayam, T. P.; Priyadarsini, K. I.; Mohan, H. Reactive oxygen species mediated membrane damage induced by fullerene derivatives and its possible biological implications. *Toxicology* 2000, *155*, 55-61.
119. Sayes, C. M.; Fortner, J. D.; Guo, W.; Lyon, D.; Boyd, A. M.; Ausman, K. D.; Tao, Y. J.; Sitharaman, B.; Wilson, L. J.; Hughes, J. B.; West, J. L.; Colvin, V. L. The Differential Cytotoxicity of Water-Soluble Fullerenes. *Nanolett.* 2004, *4*, 1881-1887.
120. Yamakoshi, Y.; Sueyoshi, S.; Fukuhara, K.; Miyata, N. OH and O₂- generation in aqueous C₆₀ and C₇₀ solutions by photoirradiation: An EPR study. *J. Am. Chem. Soc.* 1998, 12363-12364.
121. Sayes, C. M.; Gobin, A. M.; Ausman, K. D.; Mendez, J.; West, J. L.; Colvin, V. L. Nano-C₆₀ cytotoxicity is due to lipid peroxidation. *Biomaterials* 2005, *26*, 7587-7595.
122. Colvin, V. L. The potential environmental impact of engineered nanomaterials (vol 21, pg 1166, 2003). *Nature Biotech.* 2004, *22*, 760-760.
123. Beeby, A.; Eastoe, J.; Heenan, R. K. Solubilization of C₆₀ in aqueous micellar solution. *J. Chem. Soc. Chem. Commun.* 1994, 173-175.
124. Dresselhaus, M. S.; Dresselhaus, G.; Eklund, P. C. *Science of Fullerenes*; Academic Press: San Diego, 1996.
125. Heymann, D. Solubility of fullerenes C-60 and C-70 in seven normal alcohols and their deduced solubility in water. *Fullerene Sci. Tech.* 1996, *4*, 509-515.
126. Heymann, D. Solubility of C-60 in alcohols and alkanes. *Carbon* 1996, *34*, 627-631.
127. Arrais, A.; Diana, E. Highly water soluble C-60 derivatives: A new synthesis. *Fullerenes Nanotubes Carbon Nanostr.* 2003, *11*, 35-46.
128. Chiang, L. Y.; Wang, L.-Y.; Swirezewski, J. W.; Soled, S.; Cameron, S. Efficient Synthesis of Polyhydroxylated Fullerene Derivatives via Hydrolysis of Polycyclosulfated Precursors. *J. Org. Chem.* 1994, *59*, 3960-3968.

129. Lamparth, I.; Hirsch, A. Water Soluble Malonic Acid Derivatives of C₆₀ with a Defined Three-Dimensional Structure. *J. Chem. Soc.; Chem. Commun.* 1994, 1727.
130. Dugan, L. L.; Turetsky, D. M.; Du, C.; Lobner, D.; Wheeler, M.; Almlı, C. R.; Shen, C. K.; Luh, T. Y.; Choi, D. W.; Lin, T. S. Carboxyfullerenes as neuroprotective agents. *Proc. Natl. Acad. Sci. USA* 1997, 94, 9434-9439.
131. Murthy, C. N.; Choi, S. J.; Geckeler, K. E. Nanoencapsulation of [60] fullerene by a novel sugar-based polymer. *J. Nanosci. Nanotechnol.* 2002, 2, 129-132.
132. Ungurenasu, C.; Airinei, A. Highly stable C₆₀/Poly(vinylpyrrolidone) Charge-Transfer Complexes Afford New Predictions for biological Applications of Underivatized Fullerenes. *J. Med. Chem.* 2000, 43, 3186-3199.
133. Litvinova, L. S.; Ivanaov, V. G.; Mokeev, M. V.; Zgonmik, V. N. Water-soluble [60]fullerene compositions with carbohydrates. *Mendeleev Commun.* 2001, 1-2.
134. Andrievsky, G. V.; Kosevich, M. V.; Vovk, O. M.; Shelkovsky, V. S.; Vashchenko, L. A. On the Production of an Aqueous Colloidal Solution of Fullerenes. *J. Chem. Soc. Chem. Comm.* 1995, 1281-1282.
135. Scrivens, W. A.; Tour, J. M. Synthesis of ¹⁴C-Labeled C₆₀, Its Suspension in Water, and Its Uptake by Human Keratinocytes. *J. Am. Chem. Soc.* 1994, 116, 4517-4518.
136. Alargova, R. G.; Deguchi, S.; Tsujii, K. Stable Colloidal Dispersions of Fullerenes in Polar Organic Solvents. *J. Am. Chem. Soc.* 2001, 123, 10460-10467.
137. Deguchi, S.; Alargova, R. G.; Tsujii, K. Stable Dispersions of Fullerenes, C₆₀ and C₇₀, in Water. Preparation and Characterization. *Langmuir* 2001, 17, 6013-6017.
138. Cheng, X. K.; Kan, A. T.; Tomson, M. B. Naphthalene adsorption and desorption from Aqueous C-60 fullerene. *J. Chem. Eng. Data* 2004, 49, 675-683.
139. Andrievsky, G. V.; Klochkov, V. K.; Karyakina, E. L.; McHedlov-Petrosyan, N. O. Studies of aqueous colloidal solutions of fullerene C-60 by electron microscopy. *Chem. Phys. Lett.* 1999, 300, 392-396.
140. Wei, X.; Wu, M.; Qi, L.; Xu, Z. Selective solution-phase generation and oxidation reaction of C₆₀⁻ (n=1,2) and formation of an aqueous colloidal solution of C₆₀. *J. Chem. Soc. Perkin Trans. 2* 1997, 1389-1393.
141. Fortner, J. D.; Lyon, D. Y.; Sayes, C. M.; Boyd, A. M.; Falkner, J. C.; Hotze, E. M.; Alemany, L. B.; Tao, Y. J.; Guo, W.; Ausman, K. D.; Colvin, V. L.; Hughes, J. B. C-60 in water: Nanocrystal formation and microbial response. *Environ Sci Technol* 2005, 39, 4307-4316.

142. Heymann, D. Solubility of C₆₀ in Alcohols and Alkanes. *Carbon* 1996, 34, 627-631.
143. Andrievsky, G. V.; Klochkov, V. K.; Bordyuh, A. B.; Dovbeshko, G. I. Comparative analysis of two aqueous-colloidal solutions of C-60 fullerene with help of FTIR reflectance and UV-Vis spectroscopy. *Chem Phys Lett* 2002, 364, 8-17.
144. Brant, J. A.; Labille, J.; Bottero, J.-Y.; Wiesner, M. R. Characterizing the Impact of Preparation Method on Fullerene Cluster Structure and Chemistry. *Langmuir* 2006, 22, 3878-3885.
145. Mchedlov-Petrosyan, N. O.; Klochkov, V. K.; Andrievsky, G. V. Colloidal Dispersions of Fullerene C₆₀ in water: Some Properties and Regularities of Coagulation by Electrolytes. *J. Chem. Soc. Faraday Trans.* 1997, 93, 4343-4346.
146. Diederich, F.; Thilgen, C. Covalent fullerene chemistry. *Science* 1996, 271, 317-323.
147. Taylor, R.; Parsons, J. P.; Avent, A. G.; Rannard, S. P.; Dennis, T. J.; Hare, J. P.; Kroto, H. W.; Walton, D. R. M. Degradation of C₆₀ by Light. *Nature* 1991, 351, 277-277.
148. Li, J.; Takeuchi, A.; Ozawa, M.; Li, X.; Saigo, K.; Kitazawa, K. C₆₀ Fullerol Formation catalysed by Quaternary Ammonium Hydroxide. *J. Am. Chem. Commun.* 1993, 1784-1786.
149. Avdeev, M. V.; Khokhryakov, A. A.; Tropin, T. V.; Andrievsky, G. V.; Klochkov, V. K.; Derevyanchenko, L. I.; Rosta, L.; Garamus, V. M.; Priezzhev, V. B.; Korobov, M. V.; Aksenov, V. L. Structure Features of Molecular-Colloidal Solutions of C₆₀ fullerenes in Water by Small Angle Neutron Scattering. *Langmuir* 2004, 20, 4363-4368.
150. Lyon, D. Y.; Fortner, J. D.; Sayes, C. M.; Colvin, V. L.; Hughes, J. B. Bacterial Cell Association and Antimicrobial Activity of a C₆₀ Water Suspension. *Environ. Tox. Chem.* 2005, 24, 2757-2762.
151. Brant, J.; Lecoanet, H.; Hotze, M.; Wiesner, M. Comparison of electrokinetic properties of colloidal fullerenes (n-C-60) formed using two procedures. *Environ. Sci. Technol.* 2005, 39, 6343-6351.
152. McHedlov-Petrosyan, N. O.; Klochkov, V. K.; Andrievsky, G. V. Colloidal dispersions of fullerene C-60 in water: some properties and regularities of coagulation by electrolytes. *J. Chem. Soc. Faraday Trans.* 1997, 93, 4343-4346.

153. Li, T. B.; Huang, K. X.; Li, X. H.; Jiang, H. Y.; Li, J.; Yan, X. Z.; Zhao, S. K. Studies on the rapid preparation of fullerenes and its formation mechanism. *Chem. J. Chinese Univ.* 1998, *19*, 858-860.
154. Cusan, C.; Da Ros, T.; Spalluto, G.; Foley, S.; Janto, J. M.; Seta, P.; Larroque, C.; Tomasini, M. C.; Antonelli, T.; Ferraro, L.; Prato, M. A new multi-charged C-60 derivative: Synthesis and biological properties. *Eur. J. Org. Chem.* 2002, 2928-2934.
155. Da Ros, T.; Prato, M. Easy Access to Water-Soluble Fullerene Derivatives via 1,3-Dipolar Cycloadditions of Azomethine Ylides to C60. *J. Org. Chem.* 1996, *61*, 9070-9072.
156. Chung, N.; Alexander, M. Effect on Sequestration and Bioavailability of Two Polycyclic Aromatic Hydrocarbons. *Environ. Sci. Technol.* 1999, *33*, 3605-3608.
157. Lecoanet, H. F.; Bottero, J. Y.; Wiesner, M. R. Laboratory assessment of the mobility of nanomaterials in porous media. *Environ. Sci. Technol.* 2004, *38*, 5164-5169.
158. Yamago, S.; Tokuyama, H.; Nakamura, E.; Kikuchi, K.; Kananishi, S.; Sueki, K.; Nakahara, H.; Enomoto, S.; Ambe, F. In vivo biological behavior of a water-miscible fullerene: ¹⁴C labeling, absorption, distribution, excretion and acute toxicity. *Chem. Biol.* 1995, *2*, 385-389.
159. Yang, A.; Cardona, D. L.; Barile, F. A. In vitro cytotoxicity testing with fluorescence-based assays in cultured human lung and dermal cells. *Cell Bio. Tox.* 2002, *18*, 97-108.
160. Yang, X. L.; Fan, C. H.; Zhu, H. S. Photo-induced cytotoxicity of malonic acid [C(60)]fullerene derivatives and its mechanism. *Toxicol. In Vitro* 2002, *16*, 41-46.
161. Takenaka, S.; Yamashita, K.; Takagi, M.; Hatta, T.; Tsuge, O. Photo-induced DNA Cleavage by Water-soluble Cationic Fullerene Derivatives. *Chem. Lett.* 1999, 321-322.
162. Oberdörster, E. Manufactured Nanomaterials (Fullerenes, C60) Induce Oxidative Stress in the Brain of Juvenile Largemouth Bass. *Environ. Health Persp.* 2004, *112*, 1058-1062.

Chapter 3.A

C₆₀ in Water: Nanocrystal Formation and Microbial Response

J. D. Fortner^{1,4}, D. Y. Lyon^{1,4}, C. M. Sayes^{2,4}, A. M. Boyd^{2,4}, J. C. Falkner², E. M. Hotze^{1,4}, L. B. Alemany², Y. J. Tao^{3,5}, W. Guo², K. D. Ausman⁴, V. L. Colvin^{2,4} and J. B. Hughes*^{4,5}

¹Department of Civil and Environmental Engineering, Rice University, Houston, TX 77005

²Department of Chemistry, Rice University, Houston, TX 77005

³Department of Biochemistry and Cell Biology, Rice University, Houston, TX 77005

⁴Center for Biological and Environmental Nanotechnology, Rice University, Houston, TX 77005

⁵School of Civil and Environmental Engineering, Georgia Institute of Technology, Atlanta, GA 30332

*Author to whom all correspondence should be addressed:

Georgia Institute of Technology
School of Civil and Environmental Engineering
790 Atlantic Dr. N.W., Atlanta, GA 30332-0355
Phone: (404) 894-2201
Fax: (404) 894-2278
Email: joseph.hughes@ce.gatech.edu

Abstract

Upon contact with water, under a variety of conditions, C₆₀ spontaneously forms a stable aggregate with nanoscale dimensions ($d = 25 - 500$ nm), termed here 'nano-C₆₀'. The color, hydrophobicity and reactivity of individual C₆₀ are substantially altered in this aggregate form. Herein, we provide conclusive lines of evidence demonstrating that in solution these aggregates are crystalline in order and remain as underivatized C₆₀ throughout the formation/stabilization process that can later be chemically reversed. Particle size can be affected by formation parameters such as rates and the pH of the water addition. Once formed, nano-C₆₀ remains stable in solution at or below ionic strengths of 0.05 *I* for months. In addition to demonstrating aggregate formation and stability over a wide range of conditions, results suggest that prokaryotic exposure to nano-C₆₀ at relatively low concentrations is inhibitory, indicated by lack of growth (≥ 0.4 ppm) and decreased aerobic respiration rates (4 ppm). This work demonstrates the fact that the environmental fate, distribution and biological risk associated with this important class of engineered nanomaterial will require a model which addresses not only the properties of bulk C₆₀, but that of the aggregate form generated in aqueous media.

Key Words: Fullerene, Buckminsterfullerene, Carbon-60, C₆₀, Nanoparticle, Nanocrystal Formation, Nanotoxicity

Introduction

Over the past 20 years carbon fullerenes have been extensively studied by researchers; their unique properties make them ideal candidates for widespread applications in areas as diverse as drug delivery and energy conversion (1-7). As industrial scale production of fullerenes approaches reality (Frontier Carbon Corporation estimates production of ~10 tons of fullerene per year, as C₆₀, by 2007), it is not surprising that little is known about the potential impact of fullerenes on natural systems (8). For example, current OSHA guidelines for handling and disposal of C₆₀ follow the MSDS of simple carbon black. Furthermore, recent studies by Sayes *et al.* and Oberdörster *et al.* have demonstrated that fullerenes, as C₆₀ in an aggregate form, can elicit a biological response at relatively low concentrations (<1 ppm) (9,10). Such findings take on additional significance as fullerenes have been found in particulate matter emitted from coal fired power plants (11). The purpose of this research is to begin assessing fullerene behavior in the natural environment. More specifically, we begin to assess C₆₀ as it comes into contact with water, observing the form(s) these materials may take and consider the ecological risk associated with exposure.

Carbon-60 (C₆₀), the prototypical carbon-based nanoparticle, is arguably the most well studied engineered nanomaterial to date. In particular, the low solubility of C₆₀ in polar solvents such as water (<10⁻⁹ mg/L) is well accepted (12-14). However, as demonstrated by this study and others, direct solubility is not the most relevant measure of the availability of fullerenes in water-based systems (15-19). Upon contact with water through several different exposure methods, C₆₀ forms a water-stable, colloidal aggregate referred to here as ‘nano-C₆₀’ to reflect that the aggregates are composed of C₆₀ with

diameters within the nanoscale range from ~5 to 500 nm (18-20). These aggregates allow for concentrations up to 100 mg/L, which is ~11 orders of magnitude more than the estimated molecular solubility (12-14). Though this material has been the subject of some study over the past decade, questions concerning the formation, composition and stability of nano-C₆₀ remain unresolved (16,18-21).

The early interest in aggregate forms of fullerenes, particularly nano-C₆₀, was motivated by their applications in technologies, particularly those which require fullerenes in water (16-18). Nano-C₆₀ has shown little promise in this regard, as typical concentrations (< 100 ppm) are far below the 10,000 to 100,000 ppm levels that are achievable when the carbon cage is intentionally altered to include polar functionalities (22-27). Still, such aggregate generation through unintentional exposure of fullerenes to water is possible, and the amounts generated may be significant for ecological effects (≤ 100 ppm). Other lipophilic organic molecules, which might be analogous to C₆₀, have significant ecological impact in aqueous systems at concentrations of 1-10 ppm (28).

Specifically, research presented herein addresses outstanding questions and expands upon what is currently known about the composition, formation, stability and potential biological effects of nano-C₆₀. We provide original information concerning the physical and chemical structure of nano-C₆₀ directly in water using ¹³C NMR, cryogenic transmission electron microscopy (cryo-TEM) and electron diffraction. These analyses demonstrate that nano-C₆₀ is an ordered crystal structure comprised of underivatized C₆₀. We found the size and stability of these materials are affected by the conditions of formation which include the rate of water addition and solution pH, and once the nano-C₆₀ aggregates are formed, the stability is variable, depending on the ionic strength of the

solution. A bacterial (Gram-positive and Gram-negative) response to these particles was studied and compared with similar concentrations of a soluble derivative as $C_{60}(OH)_{22-24}$ and a negative control lacking fullerenes. Results suggest that exposure to nano- C_{60} at relatively low concentrations is inhibitory, indicated by lack of growth and decreased aerobic respiration rates. This is, to our knowledge, the first examination of the response of bacteria to nano- C_{60} .

Materials and Methods

Chemicals: C_{60} (99.9% purified through sublimation), ^{13}C enriched C_{60} (25% of carbon labeled, 99.5% pure) and $C_{60}(OH)_{22-24}$ (prepared through a brominated intermediate (29)) were purchased from the Materials Electronics Research Corporation (Tucson, AZ). All water used was ultra purified to $> 18 \Omega$ (Millipore Synergy system).

Nano- C_{60} Preparation: As large volumes of solutions were used throughout the study, a reproducible and relatively simple preparation of nano- C_{60} was modified from Deguchi *et al.* as follows (19). Approximately 100 mg C_{60} was added to 4L of previously unopened tetrahydrofuran (THF) (Spectroanalyzed, $>99.99\%$, Fisher Scientific) and sparged with N_2 to remove oxygen. Upon resealing the THF- C_{60} mixture, the solution was left for 24 hours stirring at ambient temperature, allowing it to become saturated with soluble C_{60} (9 mg/L solubility in THF) (19). Upon saturation, the solution was then vacuum filtered through a $0.22 \mu m$ nylon membrane (Osmotics Corp.), resulting in a transparent solution with a pink hue, which was sparged with N_2 and stored in the dark for later use. The C_{60} saturated THF solution was added (250mL) to a 2L wide mouth Erlenmeyer flask and stirred rapidly. To this solution, ultra-pure water (250 mL) at pH 5 (the pH of the water

taken directly from the Milli-Q system) was added at 500 mL/min to the stirring THF. Mixing experiments were done similarly except by varying the rate of water addition (1000, 500, 250, 125, 63, 31 and 10 mL/min). The role pH in the formation processes was evaluated by carefully adjusting the pH of the water added (500mL/min) with dilute NaOH or HCl. As the water was added, the mixed solution changed from a pink to a transparent yellow solution. Using a rotary evaporator (Buchi Rotovap system) the mixed solution was gently heated (75-80°C), collecting the more volatile THF. To ensure a consistent level of THF removal from solution, a stepwise evaporating procedure was used as follows. Starting with 1L total volume (1:1, water:THF), approximately 550 mL was evaporated and collected. The remaining yellow solution was diluted with 100 mL water. The solution was then evaporated again to 450 mL and then diluted with 100 mL water. Finally, the solution was evaporated again to the final volume of 500 mL. This solution was transferred and left to cool overnight, at room temperature. The solution was then vacuum filtered (0.22 um cellulose acetate, Corning Inc.) into a 500 mL sterile container and stored in the dark. To concentrate the suspensions, a protein concentrating centrifugal cartridge was used with a 30,000 MWCO (Amicon Ultra 15, Millipore). 10 mL of suspension was added to each cartridge and centrifuged for 15 minutes at 5,000 rpm. After each time, the approximately 500 µL of concentrated solution remained in the receptacle which was diluted with 10 mL of the original suspension and centrifuged as mentioned until the desired concentration was reached.

Particle Stability: Stability of these suspensions was evaluated at different ionic strengths over time. A nano-C₆₀ suspension prepared with water at pH 5 added at 500

mL/min was subdivided and prepared at different ionic strength (I) by the addition of NaCl. A range of ionic strengths (0.7, 0.1, 0.05, 0.01, 0.001 I) from approximately sea water (0.7 I) to ground water (0.01 I) and below was investigated over time. Particle stability and size was evaluated over time with dynamic light scattering (ZetaPALs, Brookhaven Instruments Corporation, Holtsville, NY).

Concentration Determination: The concentrations of C₆₀ in THF, toluene and hexane were determined from the absorption spectrum. The concentration of C₆₀ as a nanoscale suspension in water was determined through a two step destabilization - extraction process as follows: One volume of water with suspended nano-C₆₀ particles was destabilized with 2/5 volume 0.1 M Mg(ClO₄)₂ and extracted with one volume toluene (as a separate phase), in which molecular C₆₀ is quite soluble 2.8 mg/mL (12). When compared to other oxidizing agents tested, Mg(ClO₄)₂ provided consistent destabilization of nano-C₆₀ over a range of pH values (5-9) allowing for a high extraction efficiencies (94-101%). If no destabilizing agent was used, extraction efficiencies were low ($\leq 10\%$). The two phase system was sealed, and vigorously mixed for 30 minutes. After extraction into the organic phase was complete, the water portion of the system was frozen in a dry ice bath allowing for removal of the toluene portion containing the dissolved C₆₀. HPLC analysis was performed on toluene solutions. C₆₀ eluted at 5.6 minutes (4.6×250 mm Cosmosil PYE column, 1 mL/min toluene mobile phase) with characteristic C₆₀ absorption peaks at 336, 407, 540, 595 nm observed. The 5.6 minute C₆₀ peak from the extraction consistently represented $\geq 98\%$ of the total chromatograph peak integration (30). This procedure was verified through the use of a gravimetric procedure, using a

microbalance, evaporating 2 mL of a 100 mg/L concentrated suspension determining the weight of suspended nano-C₆₀ in water.

Characterization: All reported UV/Vis absorption spectra were taken within a range of 190 – 800 nm (Varian Cary 5000 UV-Vis-NIR, at 0.5 nm intervals) at room temperature and corrected for the appropriate solvent background. A 100 mg/L nano-C₆₀ suspension prepared with ¹³C enriched C₆₀ (25%) in D₂O was analyzed using a 500 MHz NMR (Bruker Avance, Germany) with a broadband observe probe. The experiment used a 30° ¹³C pulse, 2.36-s FID with proton decoupling, and 5-s relaxation delay with proton decoupling taking 7680 scans over 15.7 hr. Proton decoupling was used to narrow and to detect any ¹³C signals from proton-containing species that might be present. The FID was processed with 5 Hz of line broadening to further increase signal to noise ratio. The chemical shift scale of this sample, dissolved in D₂O, is relative to the trimethylsilyl group defined as 0 ppm in (CH₃)₃Si-CD₂-CD₂-COONa dissolved in D₂O. Average ζ potential of the particles in solutions was measured using a ZetaPALS (Brookhaven Instruments Corporation) at room temperature. Particle size and shape were analyzed by two methods: dynamic light scattering (DLS) using a ZetaPALS and transmission electron microscopy, the latter of which provided dimensional information. Two types of transmission electron microscope images were taken. First, traditional dried images were prepared by evaporating two drops of concentrated suspension on a 400 mesh carbon coated copper grid and imaged with a JEOL FasTEM 2010 transmission electron microscope at 100 kV. The microscope camera length was calibrated using an aluminum standard. In addition flash frozen suspensions were imaged with a transmission electron

microscope outfitted with a cryogenic sample holder (JEOL FasTEM 2010). To aid in these image analyses, Image Pro© software was used.

Microbial Assays: The ability of Gram-negative *Escherichia coli* DH5 α and Gram-positive *Bacillus subtilis* CB315 (JH642 derivative; a facultative anaerobe capable of reducing nitrate under anaerobic conditions (31)) to grow in the presence of nano-C₆₀ was studied at pH 7 using both a rich (Luria Broth, LB) and minimal media (Minimal Davis media with 10% of the recommended potassium phosphate) with glucose as the carbon and electron source (1g/L) (32). For all anaerobic experiments KNO₃ was used as an electron acceptor. Cultures were incubated at a constant temperature of 37°C, with and without the presence of light while shaking (aerobic growth) or static in an anaerobic chamber (anaerobic growth) (33). In triplicate, Studies were inoculated with fresh overnight cultures of bacteria to an OD at 600 nm of 0.002. Growth was monitored similarly at 600 nm in 24 hour increments and verified with plate counts (data not shown). Different concentrations of nano-C₆₀ (0.04, 0.4 mg/L 4 mg/L) along with C₆₀(OH)₂₂₋₂₄ (5 mg/L) were compared to a negative control which lacked any fullerene. Results were reported simply as yes (+), growth occurred or no (-), growth did not occur (Table 1). Aerobic respiration of both cultures suspended in minimal Davis media (as described above) was monitored via CO₂ production rates over time with a 10-chamber respirometer (Columbus Instruments, Columbus, Ohio) at room temperature (20-22°C) (34). At mid-exponential phase, the bottles were amended with a varying concentration of nano-C₆₀, C₆₀(OH)₂₂₋₂₄, or no fullerene as a negative control. Results are presented as accumulative CO₂ production over time.

Results

When exposed to water, C₆₀ can form “hydrophilic” colloids that are stable in water (9,15-19). This form of C₆₀ does not extract appreciably back into a non-polar solvent, such as toluene, indicating that the process leading up to colloid formation fundamentally alters the properties of the fullerene. (Figure 3.1A). Ultraviolet visible analysis of these yellow suspensions finds characteristic peaks of solvated C₆₀ in solution between 330-350 nm; however, an additional broad 400 – 500 nm absorption is also apparent (Figure 3.1B) (19,21). This feature is characteristic of solid-state, crystalline C₆₀ and arises from close electronic interactions among adjacent C₆₀ molecules. Depending on the form and density of C₆₀ crystals, this absorbance has an initial appearance between 450 and 600 nm (35,36).

Molecular analysis of these crystal suspensions using high pressure liquid chromatography (HPLC), absorption spectroscopy and NMR indicates that nano-C₆₀ is comprised predominantly of underivatized C₆₀. HPLC analysis was completed after nano-C₆₀ was briefly treated with a mild oxidizing agent (*e.g.* 0.05M Mg(ClO₄)₂); destabilizing the aggregates allowing for complete extraction into an organic phase (toluene). Upon analysis, a single peak at 5.6 minutes which consistently represented ≥ 98% of the total chromatograph peak integration was observed. This peak was identical to fullerenes dissolved in toluene which had not been exposed to water (One peak at 5.6 minutes (@ 336 nm, 4.6×250 mm Cosmosil PYE column, 1ml/min toluene) with a characteristic C₆₀ absorption spectra including peaks at 336, 407, 540, 595 nm) (30,37,38) Additionally, ¹³C NMR analysis indicates that C₆₀ remains, within our ability to detect, underivatized in these aggregates. ¹³C NMR is quite sensitive to derivatization,

and fullerenes that have been chemically altered show multiple peaks, often broadened depending on the specificity of the chemistry (38-42). In the case of nano-C₆₀ in aqueous suspensions, the spectrum shows only one peak at 146 ppm (Figure 3.2), which is slightly shifted from solid state NMR of crystalline, bulk C₆₀ which reports a single peak at 143 ppm (40). Thermogravimetric analysis (TGA) and mass spectroscopy of solids recovered from the suspensions are consistent with these findings. The only non-fullerene species present are < 10% (w/w) organic molecules, found as THF (data not shown). This is not surprising as the starting powders of polycrystalline C₆₀ are known to contain organic molecules intercalated into its lattice, sometimes in relatively high amounts (~10%) (43).

The surface chemistry of these aggregate species is of great interest as it is this interface where the hydrophobic fullerenes are in some way rendered hydrophilic. We confirmed that the surfaces of these materials are charged by performing electrophoretic mobility studies. In agreement with prior studies, we find ζ potentials of -36 mV for a typical suspension produced with water at pH 5 mixed at 500 mL/min (17-19). This weakly charged surface makes these systems unstable in the presence of both weak oxidizing agents and salts.

Two possible explanations could account for the surface charge. It may be that upon contact with water, pristine fullerenes undergo a chemical reaction to create a small population of partially oxidized, and hence more polar, amphiphilic fullerenes which are able to stabilize the hydrophobic, underivatized core. C₆₀ is a relatively reactive species; its degradation by light and oxygen has been noted (44,45). In particular, one inefficient method to form partially hydroxylated fullerenes relies on the introduction of THF/C₆₀ solutions to water at high pH values (>12) (46). Such a reaction may also proceed, albeit

at lower yields, when THF/C₆₀ solutions are introduced in neutral water. Alternatively, C₆₀ is an excellent electron acceptor. Both Andrievsky *et al.* and Deguchi *et al.* suggested that water itself may form a donor-acceptor complex with C₆₀ leading to a weakly charged colloid (16,19,21). The latter seems a more reasonable explanation based on the information provided by ¹³C NMR analysis in Figure 3.2, which observes a slightly shifted, single peak at 146 ppm, indicating I_h symmetry which is reserved for underivatized C₆₀ (47). In addition, this hypothesis is strengthened by the extraction procedure, as the removal of electrons from the surface via a mild oxidizing agent is necessary to destabilize nano-C₆₀, allowing for virtually all C₆₀ to be extracted into an organic phase (toluene). The role of associated organic molecules, such as THF, in the stabilization process would seem to be minor, being that similar suspensions can be made by simply rapidly stirring solid C₆₀ in water over time with no intermediate solvent involved (48).

Another outstanding question about these aggregates has been their structure in solution. Past work has shown that both optical and microscopic analyses of the yellow suspensions indicate the presence of dense aggregates of C₆₀ (18-20), their form has been challenging to elucidate in solution. Previous reports have first evaporated solutions to form dried films, and then used transmission electron microscopy to visualize particles (19,20). Whether the same particles are present, in the same form and size, in the original solutions was not tested.

Here, we use cryogenic techniques to form flash-frozen suspensions of nano-C₆₀ for imaging. This method is widely used in biological systems and has been shown quite often that with rapid freezing the tertiary and quaternary structure of biological molecules

remain unaffected (49-51). Transmission electron micrographs of these suspensions are compared to data from dried films (Figure 3.3A), revealing identical size and morphology, as a large fraction of faceted particles are apparent in the cryogenic suspensions. Under these formation conditions (pH 5 water added at 500 mL/min), nano-C₆₀ exhibits a range of sizes, 100 nm ± 10 nm for these conditions, as well as shapes. Smaller aggregates are typically circular in cross section, intermediate and large particles are mostly rectangular, and the very largest particles often appear to be triangular (Figure 3.3B). These findings provide direct evidence of particle integrity in suspension, verifying previous studies which have relied on traditional TEM analysis of dried aggregates (18,20). The particle characteristics suggest that the aggregates are crystalline, and we confirmed this using electron diffraction. SAED on both single particles, as well as particle fields, yields strong diffraction patterns (Figure 3.3A, inset). Indexing results on a single particle diffraction pattern, taken along the (0001) axis, are most consistent with a simple hexagonal unit cell ($a=9.4 \text{ \AA}$ and $c/a=1.09$).

We have found that nano-C₆₀ can form over a wide range of mixing conditions and pH, and is quite stable at ionic strengths, at or below 0.05 *I*, for months. Andrievsky *et al.* suggested that pH was an important parameter for these colloids because of the stability of the surface charge (21). We found that for pH values between 3.75 and 10.25, nano-C₆₀ is formed and that as the pH of the water is varied, a change in the average particle size is observed. Higher pH values result in smaller nano-C₆₀ populations and lower pH values give rise to larger particle populations (Figure 3.4A, C). In addition, as the pH is increased and the average particle size is smaller, a blue shift in the UV/Vis spectrum is observed in the 330-350 nm range (Figure 3.4B).

Similarly, we also observed that formation of these particles can be affected by mixing processes involved, *i.e.* the rate of addition of the water during synthesis (Figure 3.5). By increasing or decreasing the rate of water addition, the average particle size varies as observed via DLS and TEM analysis (Figure 3.5A, C). As the rate of water addition is slowed, average particle size clearly increases. Again, as the average particle size decreases a blue shift is observed in the 330-350 range (Figure 3.5B). We note the similar findings by Alargova *et al.* based on the initial concentration of the C₆₀ in the organic phase before the colloids are formed (18).

Over a range (0.7-0.001 *I*) of ionic strengths, which includes approximately sea water (0.7) and groundwater (0.01) values, the stability of a typical suspension of nano-C₆₀ was evaluated. Results indicate that ionic strengths at 0.05 *I* and above increase the observed particle size; ionic strengths of 0.1 and 0.7 are high enough to precipitate the particles out of solution after 72 and 48 hours respectively. However, at ionic strengths of 0.001, 0.01 and 0.05 *I* a considerable fraction of the particles remain stable at concentrations up to 100 ppm for at least 15 weeks (Figure 3.6). It should be noted that these aggregation and stability experiments are not assumed to be representative of a C₆₀ release into a natural system, as they are more fundamental in approach. The matrix of variables tested does however provide a range of conditions within those found in nature.

With this information about the physical structure, chemical properties and stability in hand, we examined the biological effects of nano-C₆₀ using two common bacteria. Prokaryotic interactions with nano-C₆₀ were evaluated using the bacteria cultures: Gram-negative *Escherichia coli* and Gram-positive *Bacillus subtilis*, both common, well studied, soil species, with basic differences in cell wall composition.

Initial experiments were designed to observe the effect of bacterial exposure to nano-C₆₀ in two different types of media, one complex and one simple, under both anaerobic and aerobic conditions (Table 3.1). Results show that in the presence of nano-C₆₀ above 0.4 mg/L no growth for either culture is observed (under either anaerobic or aerobic conditions) using a minimal Davis media (defined previously). However, when a complex media such as Luria broth was used, growth was seen at nano-C₆₀ concentrations at and below 2.5 mg/L. Subsequent aerobic experiments studied carbon dioxide production during aerobic respiration by these same cultures after exposure to nano-C₆₀ during exponential growth in minimal Davis media (Figure 7). Similar studies monitoring CO₂ production have been used as a tool in assessing microbial inhibition by others (34,52). Results presented in Figure 3.7 are a representative response observed during a 10 chamber experiment (in duplicate, 4 variables and 1 negative control simultaneously monitored with average values presented). All experiments were done at least three times verifying the trends observed. These results are consistent with the initial findings, that with the addition of nano-C₆₀, at moderately low concentrations (4 mg/L), an adverse effect is observed, indicated by the differential rates of CO₂ production over time as compared to C₆₀(OH)₂₂₋₂₄ and a negative control consisting of no fullerenes.

Discussion

As shown here and elsewhere, C₆₀ upon contact with water can form negatively charged colloids, nanoscale in dimension, which are stable over time. Specific findings here present strong evidence that in solution, nano-C₆₀ is in fact crystalline in order with a simple hexagonal unit cell, and not low density amorphous aggregates, which are not

large enough to settle under gravitational force alone. Furthermore, all compositional analyses employed, particularly ^{13}C -NMR solution analysis, indicate, that within the margin of error, these colloids are comprised of underivatized C_{60} . These compositional findings, taken with the fact that an oxidizing agent efficiently destabilizes the colloid allowing for toluene extraction of underivatized C_{60} , support the hypothesis suggested by others, that a donor-acceptor complex with water may be responsible for the surface charge by which the colloids are stable (16,18,19).

It was also found that that the formation process is dynamic. Data presented here, along with a recent study by Alargova *et al.*, outline a number of variables, including initial C_{60} concentration, specific solvents involved, formation kinetics and chemistry of the water that play a role in the formation process (18). In particular, we have found that there is a distinct correlation between the rate of water addition and aggregate size, as shown in Figure 3.5. It appears that the formation of these aggregates is, in part, kinetically controlled by the solution chemistry involved; *i.e.* as the rate of water added was increased in the formation process, smaller sized particles were consistently produced. Corresponding formation under conditions of a slow water addition reveals larger average particle populations. Additionally, we found that over a range of pH values (3.75-10.25) nano- C_{60} was formed and that the pH of the water did seem to influence the process as the average particle size decreased with an increase in pH.

Investigations of particle stability at relevant ionic strengths revealed that these aggregates will not remain in solutions simulating seawater or even brackish waters with ionic strengths at or above 0.1 *I*. However, at ionic strengths below this (0.05 *I* and below) an appreciable percentage (0.05 *I*) if not all (0.01 and 0.001 *I*) of aggregates

remain stable for fifteen weeks. These results are important as potential long term stability is limited to aqueous systems at or below 0.05 *I*, which includes most freshwater environments such as typical groundwaters and surface waters. This study did not investigate other coagulating factors, such as protein, humic acids, or sorption onto or within solid matrixes such as organic matter and soil fractions, which may influence stability.

Bacterial systems employed in this study demonstrate a response to nano-C₆₀ at low concentrations. At relatively low concentrations (≥ 0.4 mg/L), nano-C₆₀ in a minimal media, does induce a response by common Gram positive and Gram negative cultures, indicated by the lack of growth in a variety of basic conditions, including aerobic or anaerobic conditions and with or without the presence of light. However, complex media (Luria Broth) seemed to negate this response by perhaps salting the fullerenes out of solution, as shown here at higher ionic strengths in Figure 6, or through coating the fullerenes with excess protein, which is a large component of this particular media (as yeast extract). Furthermore, these results were corroborated with respiration studies (Figure 3.7) showing similar response at comparable concentrations, as rates of CO₂ production decrease with the introduction of nano-C₆₀ during the exponential growth phase. In addition, for both cultures, when exposed to similar concentrations of a hydroxylated fullerene C₆₀(OH)₂₂₋₂₄ no significant response in bacterial respiration was observed, confirmed by a negative control lacking fullerenes, suggesting a relation in the surface chemistry of the fullerene molecules to the biological activity. This initial data is the first examination, of a microbial response to nano-C₆₀ and is consistent with

published data by Sayes *et al.* which demonstrated nano-C₆₀ toxicity to human dermal fibroblast (HDF) diminishing with an increase in derivatization (as hydroxylation) (9).

In aqueous systems, nano-C₆₀ behaves neither as an individual molecule nor as a bulk solid. Moreover, chemical properties of the aggregate, such as partition coefficients, are distinct from individual C₆₀ molecules. Based on the predicted widespread use of C₆₀, this becomes a particularly striking observation that deviates from that which is expected for similar materials such as hydrophobic polyaromatic hydrocarbons (PAH's). In this case, predictive molecular properties such as partition coefficients (K_{ow}) and solubility become inappropriate, with colloidal properties such as size and surface chemistry becoming useful in predicting behavior of these aggregates. Moreover, recent studies by Lecoanet *et al.* studying the mobility of suspended nanomaterials in porous media show that similar C₆₀ aggregates are capable of migrating through a well defined porous medium analogous to a sandy groundwater aquifer (53).

This work clearly illustrates the limitations of the current guidelines for the handling and disposal of C₆₀ which are based entirely on the properties of bulk carbon black. Most engineered nanomaterials, including C₆₀, are handled and disposed according to guidelines established for their bulk counterparts; these guidelines may need to be revisited. Proactive characterization of the environmental chemistry and associated ecological risk of engineered nanomaterials, before their use is widespread, ensures an environmentally sustainable and socially beneficial nanotechnology industry.

Acknowledgements

This research was funded through the Nanoscale Science and Engineering Initiative of the National Science Foundation (#EEC-0118007). Additionally, we acknowledge funding for NMR analysis through NSF #CHE-9708978.

Literature Cited

- (1) Kelty, S. P.; Chen, C. C.; Lieber, C. M. Superconductivity at 30-K in Cesium-Doped C₆₀. *Nature* 1991, 352, 223-225.
- (2) Kroto, H. W.; Heath, J. R.; O'Brien, S. C.; Curl, R. F.; Smalley, R. E. C₆₀: Buckminsterfullerene. *Nature* 1985, 318, 162.
- (3) Tsao, N.; Kanakamma, P. P.; Luh, T. Y.; Chou, C. K.; Lei, H. Y. Inhibition of Escherichia coli-induced meningitis by carboxyfullerene. *Antimicrob. Agents Chemother.* 1999, 43, 2273-2277.
- (4) Haddon, R. C.; Hebard, A. F.; Rosseinsky, M. J.; Murphy, D. W.; Duclos, S. J.; Lyons, K. B.; Miller, B.; Rosamilia, J. M.; Fleming, R. M.; Kortan, A. R.; Glarum, S. H.; Makhija, A. V.; Muller, A. J.; Eick, R. H.; Zahurak, S. M.; Tycko, R.; Dabbagh, G.; Thiel, F. A. Conducting Films of C₆₀ and C₇₀ by Alkali-Metal Doping. *Nature* 1991, 350, 320-322.
- (5) Ruoff, R. S.; Ruoff, A. L. Is C₆₀ Stiffer Than Diamond. *Nature* 1991, 350, 663-664.
- (6) Innocenzi, P.; Brusatin, G. Fullerene-Based Organic-Inorganic Nanocomposites and Their Applications. *Chem. Mater.* 2001, 13, 3126-3139.
- (7) Ungurenasu, C.; Airinei, A. Highly stable C₆₀/Poly(vinylpyrrolidone) Charge-Transfer Complexes Afford New Predictions for biological Applications of Underivatized Fullerenes. *J. Med. Chem.* 2000, 43, 3186-3199.
- (8) Tremblay, J. Mitsubishi Aims at a Breakthrough. *Chem. Eng. News* 2002, 80, 16-17.
- (9) Sayes, C. M.; Fortner, J. D.; Guo, W.; Lyon, D.; Boyd, A. M.; Ausman, K. D.; Tao, Y. J.; Sitharaman, B.; Wilson, L. J.; Hughes, J. B.; West, J. L.; Colvin, V. L. The Differential Cytotoxicity of Water-Soluble Fullerenes. *Nanolett.* 2004, 4, 1881-1887.
- (10) Oberdörster, E. Manufactured Nanomaterials (Fullerenes, C₆₀) Induce Oxidative Stress in the Brain of Juvenile Largemouth Bass. *Environmental Health Perspectives* 2004, 112, 1058-1062.
- (11) Utsunomiya, S.; Jensen, K. A.; Keeler, G. J.; Ewing, R. C. Uraninite and Fullerene in Atmospheric Particles. *Environ. Sci. Technol.* 2002, 36, 4943-4947.
- (12) Ruoff, R. S.; Tse, D. S.; Malhotra, R.; Lorents, D. C. Solubility of C₆₀ in a Variety of Solvents. *J. Phys. Chem.,-Us* 1993, 97, 3379-3383.

- (13) Heymann, D. Solubility of C₆₀ in Alcohols and Alkanes. *Carbon* 1996, 34, 627-631.
- (14) Heymann, D. Solubility of C₆₀ and C₇₀ in seven normal alcohols and their deduced solubility in water. *Fullerene Science and Technology* 1996, 4, 509-515.
- (15) Scrivens, W. A.; Tour, J. M. Synthesis of ¹⁴C-Labeled C₆₀, Its Suspension in Water, and Its Uptake by Human Keratinocytes. *J. Am. Chem. Soc.* 1994, 116, 4517-4518.
- (16) Andrievsky, G. V.; Kosevich, M. V.; Vovk, O. M.; Shelkovsky, V. S.; Vashchenko, L. A. On the Production of an Aqueous Colloidal Solution of Fullerenes. *J. Chem. Soc.-Comm.* 1995, 1281-1282.
- (17) Mchedlov-Petrosyan, N. O.; Klochkov, V. K.; Andrievsky, G. V. Colloidal dispersions of fullerene C₆₀ in water: some properties and regularities of coagulation by electrolytes. *J. Chem. Soc.-F T* 1997, 93, 4343-4346.
- (18) Alargova, R. G.; Deguchi, S.; Tsujii, K. Stable Colloidal Dispersions of Fullerenes in Polar Organic Solvents. *J. Am. Chem. Soc.* 2001, 123, 10460-10467.
- (19) Deguchi, S.; Alargova, R. G.; Tsujii, K. Stable Dispersions of Fullerenes, C₆₀ and C₇₀, in Water. Preparation and Characterization. *Langmuir* 2001, 17, 6013-6017.
- (20) Andrievsky, G. V.; Klochkov, V. K.; Karyakina, E. L.; Mchedlov-Petrosyan, N. O. Studies of aqueous colloidal solutions of fullerene C-60 by electron microscopy. *Chem. Phys. Lett.* 1999, 300, 392-396.
- (21) Andrievsky, G. V.; Klochkov, V. K.; Bordyuh, A. B.; Dovbeshko, G. I. Comparative analysis of two aqueous-colloidal solutions of C₆₀ fullerene with help of FTIR reflectance and UV-Vis spectroscopy. *Chem. Phys. Lett.* 2002, 364, 8-17.
- (22) Li, T. B.; Huang, K. X.; Li, X. H.; Jiang, H. Y.; Li, J.; Yan, X. Z.; Zhao, S. K. Studies on the rapid preparation of fullerols and its formation mechanism. *Chem. J. Chinese Universities-Chinese* 1998, 19, 858-860.
- (23) Chiang, L. Y.; Upasani, R. B.; Swirezewski, J. W.; Soled, S. Evidence of Hemiketals Incorporated in the Structure of Fullerols Derived from Aqueous Acid Chemistry. *J. Am. Chem. Soc.* 1993, 115, 5453-5457.
- (24) Schneider, N. S.; Darwish, A. D.; Kroto, H. W.; Taylor, R.; Walton, D. R. M. Formation of Fullerols via Hydroboration of Fullerene-C₆₀. *J. Chem. Soc., Chem. Comm.* 1994, 4, 463-464.

- (25) Arrais, A.; Diana, E. Highly water soluble C₆₀ derivatives: A new synthesis. *Fullerenes Nanotubes and Carbon Nanostructures* 2003, 11, 35-46.
- (26) Cusan, C.; Da Ros, T.; Spalluto, G.; Foley, S.; Janto, J. M.; Seta, P.; Larroque, C.; Tomasini, M. C.; Antonelli, T.; Ferraro, L.; Prato, M. A new multi-charged C₆₀ derivative: Synthesis and biological properties. *Eur. J. Org. Chem.* 2002, 2928-2934.
- (27) Da Ros, T.; Prato, M. Easy Access to Water- Soluble Fullerene Derivatives via 1,3-Dipolar Cycloadditions of Azomethine Ylides to C. *J. Org.Chem.* 1996, 61, 9070-9072.
- (28) Chung, N.; Alexander, M. Effect on Sequestration and Bioavailability of Two Polycyclic Aromatic Hydrocarbons. *Environ. Sci. Technol.* 1999, 33, 3605-3608.
- (29) Djordnevic, A.; Vojinovic-Milofadov, M.; Petranovic, N.; Devecerski, A.; Bogdanovic, G.; Adamov, J. Synthesis and Characterization of Water-Soluble Biologically Active C_{(60OH)₂₄}. *Archive of Oncology* 1997, 5, 139-142.
- (30) Wu, Y. Q.; Sun, Y. L.; Gu, Z. N.; Wang, Q. W.; Zhou, X. H.; Xiong, Y.; Jin, Z. X. Analysis of C₆₀ and C₇₀ Fullerenes by High-Performance Liquid-Chromatography. *J. Chromatography* 1993, 648, 491-496.
- (31) Hoffmann, T.; Frankenberg, N.; Marino, M.; Jahn, D. Ammonification in *Bacillus subtilis* utilizing dissimilatory nitrite reductase is dependent on resDE. *J. Bacteriol.* 1998, 180, 186-189.
- (32) Atlas, R. M. *Handbook of Microbiological Media*; CRC Press, Inc.: Boca Raton, 1993.
- (33) Marino, M.; Ramos, H. C.; Hoffmann, T.; Glaser, P.; Jahn, D. Modulation of anaerobic energy metabolism of *Bacillus subtilis* by arfM (ywiD). *J. Bacteriol.* 2001, 183, 6815-6821.
- (34) Fortner, J. D.; Zhang, C. L.; Spain, J. C.; Hughes, J. B. Soil column evaluation of factors controlling biodegradation of DNT in the vadose zone. *Environ. Sci. Technol.* 2003, 37, 3382-3391.
- (35) Bensasson, R. V.; Bienvenue, E.; Dellinger, M.; Leach, S.; Seta, P. C₆₀ in Model Biological-Systems - a Visible-Uv Absorption Study of Solvent-Dependent Parameters and Solute Aggregation. *J. Phys. Chem.-Us* 1994, 98, 3492-3500.
- (36) Hungerbuhler, H.; Guldi, D. M.; Asmus, K.-D. Incorporation of C₆₀ into Artificial Membranes. *J. Am. Chem Soc.* 1993, 115, 3386-3387.

- (37) Cox, D. M.; Behal, S.; Disko, M.; Gorun, S. M.; Greaney, M.; Hsu, C. S.; Kollin, E. B.; Millar, J.; Robbins, J.; Robbins, W.; Sherwood, R. D.; Tindall, P. Characterization of C₆₀ and C₇₀ Clusters. *J. Am. Chem. Soc.* 1991, *113*, 2940-2944.
- (38) Gu, Z. N.; Qian, J. X.; Zhou, X. H.; Wu, Y. Q.; Zhu, X.; Feng, S. Q.; Gan, Z. Z. Buckminsterfullerene C₆₀ - Synthesis, Spectroscopic Characterization, and Structure-Analysis. *J. Phys. Chem.-Us* 1991, *95*, 9615-9618.
- (39) Balch, A. L.; Costa, D. A.; Noll, B. C.; Olmstead, M. M. Oxidation of Buckminsterfullerene with M-Chloroperoxybenzoic Acid - Characterization of a C-S Isomer of the Diepoxide C₆₀O₂. *J. Am. Chem. Soc.* 1995, *117*, 8926-8932.
- (40) Yannoni, C. S.; Johnson, R. D.; Meijer, G.; Bethune, D. S.; Salem, J. R. C-13 NMR-Study of the C₆₀ Cluster in the Solid-State - Molecular-Motion and Carbon Chemical-Shift Anisotropy. *J. Phys. Chem.-Us* 1991, *95*, 9-10.
- (41) Johnson, R. D.; Yannoni, C. S.; Dorn, H. C.; Salem, J. R.; Bethune, D. S. C-60 Rotation in the Solid-State - Dynamics of a Faceted Spherical Top. *Science* 1992, *255*, 1235-1238.
- (42) Doome, R. J.; Fonseca, A.; Nagy, J. B.; Grell, A. S.; Masin, F.; Messari, I. NMR answer to the anomalous solubility behaviour of fullerenes. *Molecular Materials* 2000, *13*, 201-208.
- (43) Skokan, E. V.; Privalov, V. I.; Arkhangel'skii, I. V.; Davydov, V. Y.; Tamm, N. B. Solvent molecules in crystalline C₆₀. *J. Phys. Chem. B* 1999, *103*, 2050-2053.
- (44) Diederich, F.; Thilgen, C. Covalent fullerene chemistry. *Science* 1996, *271*, 317-323.
- (45) Taylor, R.; Parsons, J. P.; Avent, A. G.; Rannard, S. P.; Dennis, T. J.; Hare, J. P.; Kroto, H. W.; Walton, D. R. M. Degradation of C₆₀ by Light. *Nature* 1991, *351*, 277-277.
- (46) Li, J.; Takeuchi, A.; Ozawa, M.; Li, X.; Saigo, K.; Kitazawa, K. C₆₀ Fullerol Formation catalysed by Quaternary Ammonium Hydroxide. *J. Am. Chem. Commun.* 1993, 1784-1786.
- (47) Kratschmer, W.; Lamb, L. D.; Fostiropoulos, K.; Huffman, D. R. Solid C-60 - a New Form of Carbon. *Nature* 1990, *347*, 354-358.
- (48) Cheng, X. K.; Kan, A. T.; Tomson, M. B. Naphthalene adsorption and desorption from Aqueous C₆₀ fullerene. *J. Chem. Eng. Data* 2004, *49*, 675-683.

- (49) Adrian, M.; Dubochet, J.; Lepault, J.; McDowell, A. W. Cryo-electron microscopy of viruses. *Nature* 1984, 308, 32-36.
- (50) Conway, J. F.; Cheng, N.; Zlotnick, A.; Wingfield, P. T.; Stahl, S. J.; Steven, A. C. Visualization of a 4-helix bundle in the hepatitis B virus capsid by cryo-electron microscopy. *Nature* 1997, 386, 91-94.
- (51) Prasad, B. V.; Burns, J. W.; Marietta, E.; Estes, M. K.; Chiu, W. Localization of VP4 neutralization sites in rotavirus by three-dimensional cryo-electron microscopy. *Nature* 1990, 343, 476-479.
- (52) Georgiou, D.; Melidis, P.; Aivasidis, A. Use of a microbial sensor: inhibition effect of azo-reactive dyes on activated sludge. *Bioproc. Biosyst. Eng.* 2002, 25, 79-83.
- (53) Lecoanet, H. F.; Wiesner, M. R. Velocity Effects on Fullerene and Oxide Nanoparticle Deposition in Porous Media. *Environ. Sci. Technol.* 2004, 38, 4377-4382.

Figure 3.1

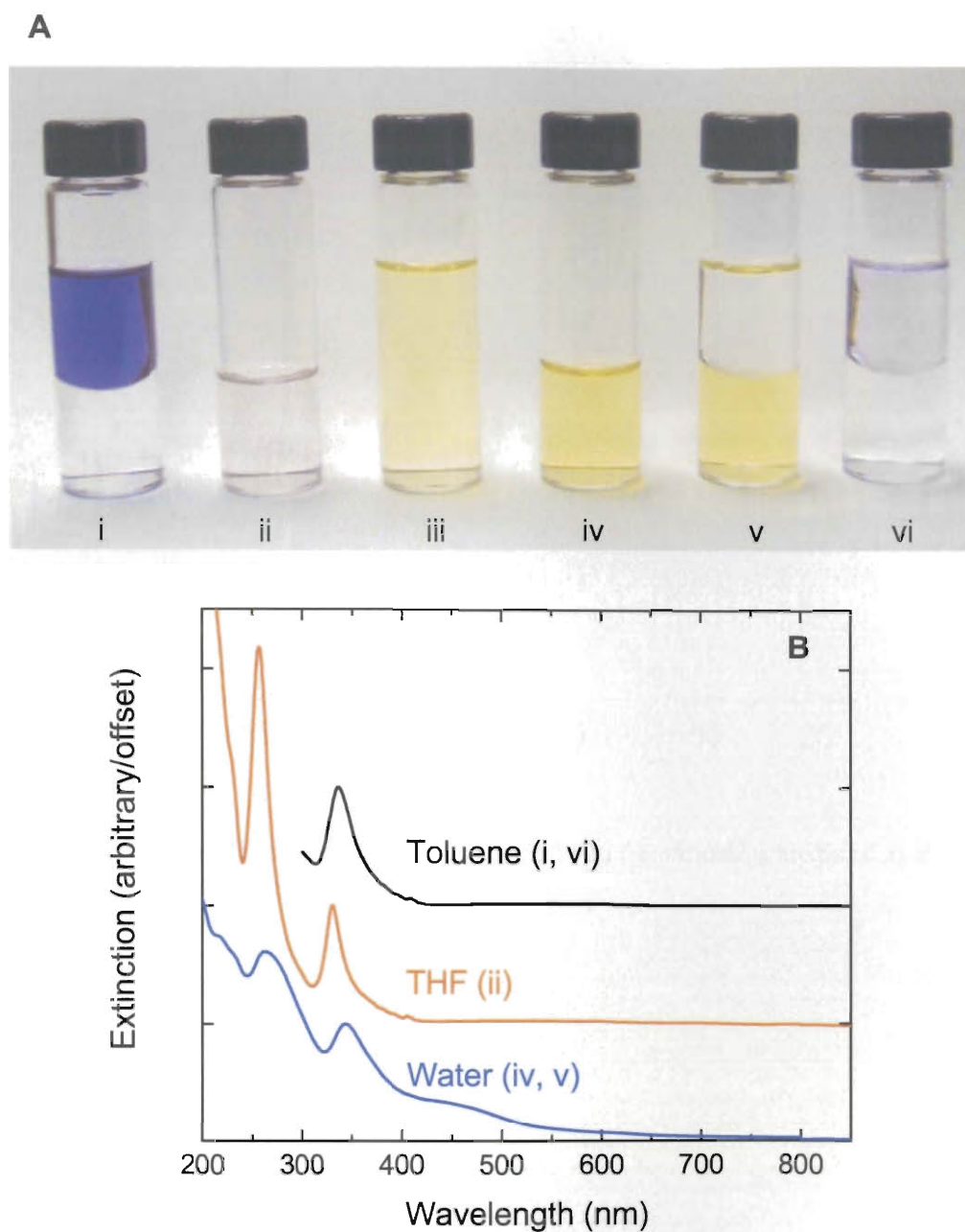


Figure 3.1 Visual and spectral analysis of C_{60} dissolved or in colloidal form in various solvents. **(A)** C_{60} dissolved in toluene (top) does not partition appreciably into water (bottom) (i). C_{60} dissolved in THF (ii). Water is added to the C_{60} /THF solution, resulting in a yellow suspension of C_{60} nano-particles (nano- C_{60}) (iii). THF can be evaporated, resulting in a water suspension of nano- C_{60} in only water (iv). The nano- C_{60} in water (bottom) only very slowly dissolves into organic solvents such as toluene (top) (v); the addition of oxidant drives the fullerenes back into the organic phase (vi). **(B)** UV/Vis analysis of C_{60} dissolved in toluene (top), THF (middle) and in colloidal form suspended in water (bottom).

Figure 3.2

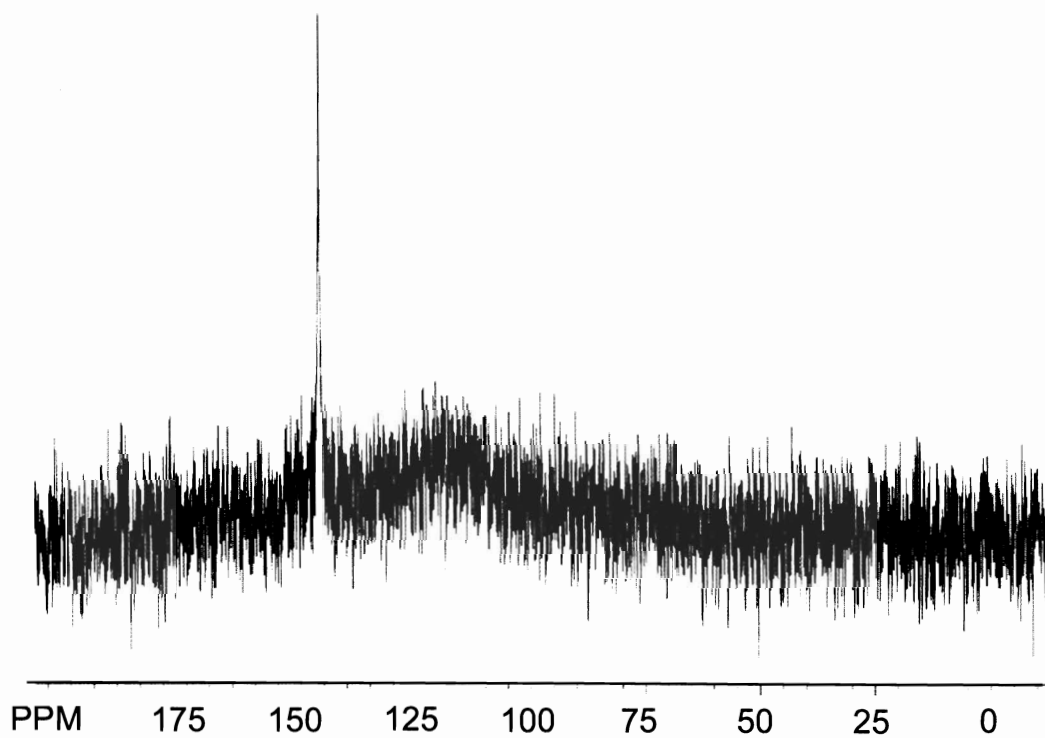


Figure 3.2 ^{13}C NMR spectrum of ^{13}C labeled (25%) nano- C_{60} suspended in D_2O . A single peak is observed at 146 ppm.

Figure 3.3

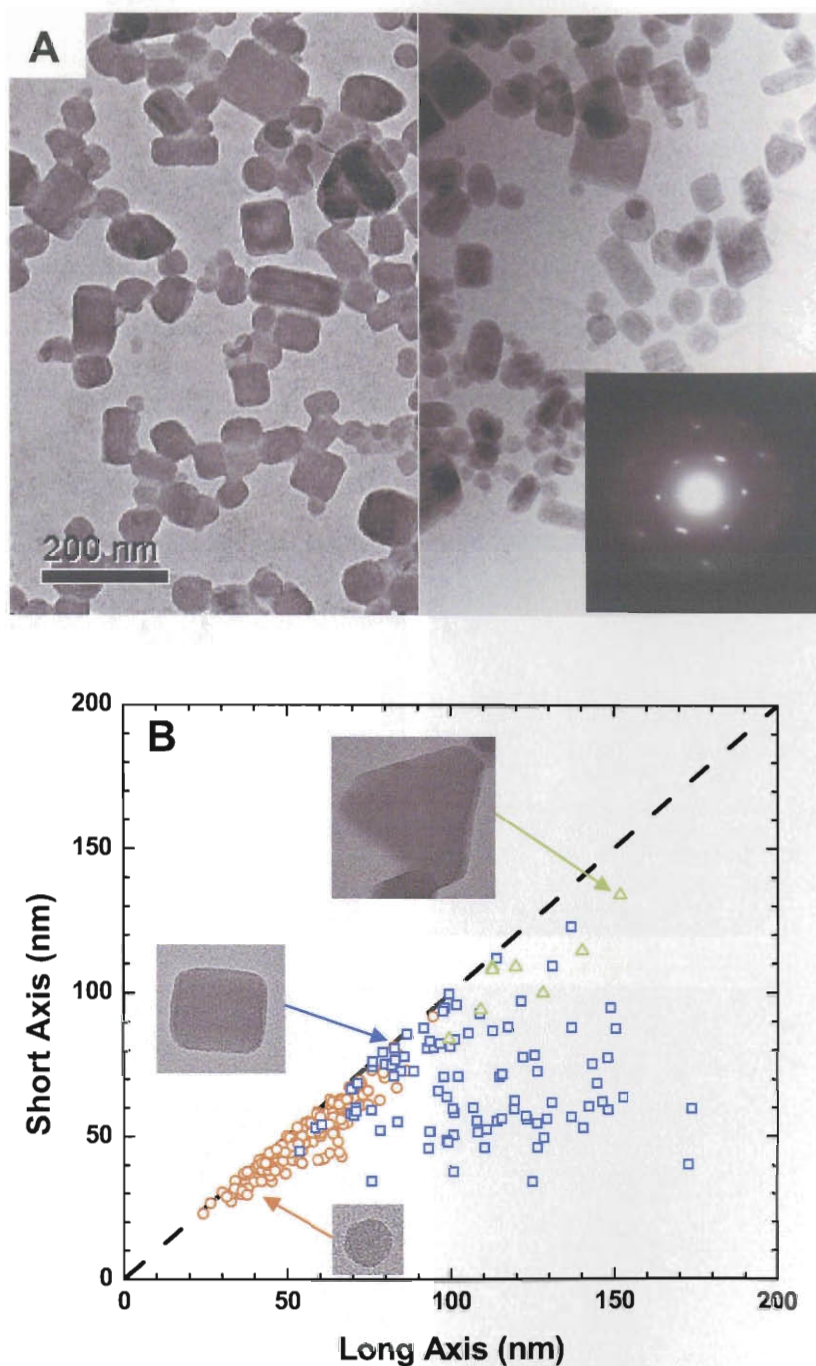


Figure 3.3 Electron microscopy and diffraction analysis of nano-C₆₀: (A) Transmission electron micrographs of dried (left) and flash-frozen (right) samples of nano-C₆₀ reveal identical morphology including a large fraction of faceted particles. Electron diffraction on individual particles (inset). (B) Particle size and shape distribution. Small aggregates are typically circular in cross section, intermediate and large ones tending to be rectangular, and with a small fraction of triangular larger particles.

Figure 3.4

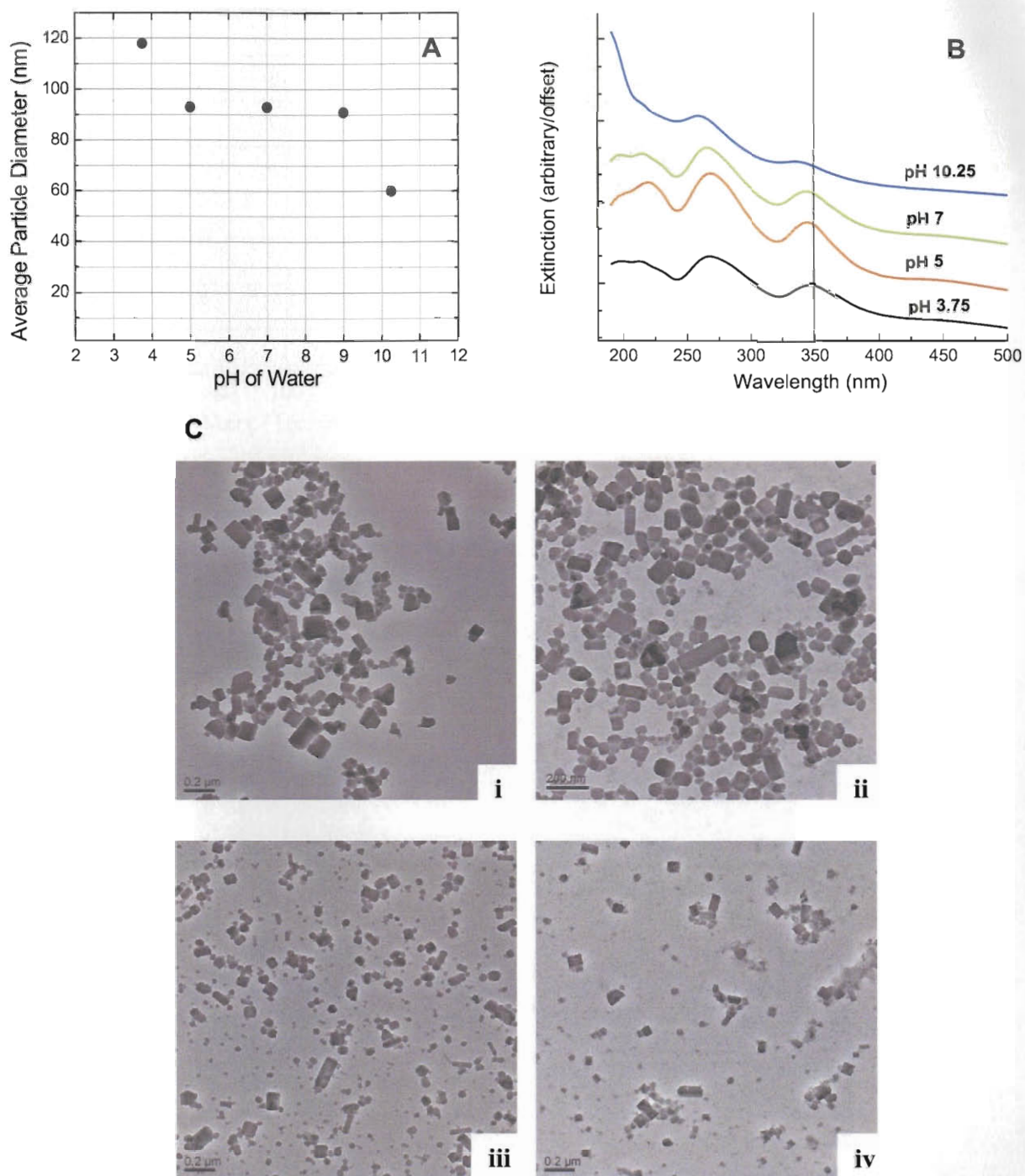


Figure 3.4 Effect of pH during the synthesis of nano-C₆₀. **(A)** DLS average particle size value as a function of the pH of the water added during formation. **(B)** UV/Vis absorption spectrums of suspensions made with pH 10.25, 7, 5, and 3.75. Note the blue shift in the 330-350 nm region as the pH is increased. All spectra are offset with arbitrary adsorption units assigned. **(C)** Dried TEM images of these nano-C₆₀ suspensions: **(i)** Prepared at pH 3.75. **(ii)** Prepared at pH 5. **(iii)** Prepared at pH 7. **(iv)** Prepared at pH 10.25.

Figure 3.5

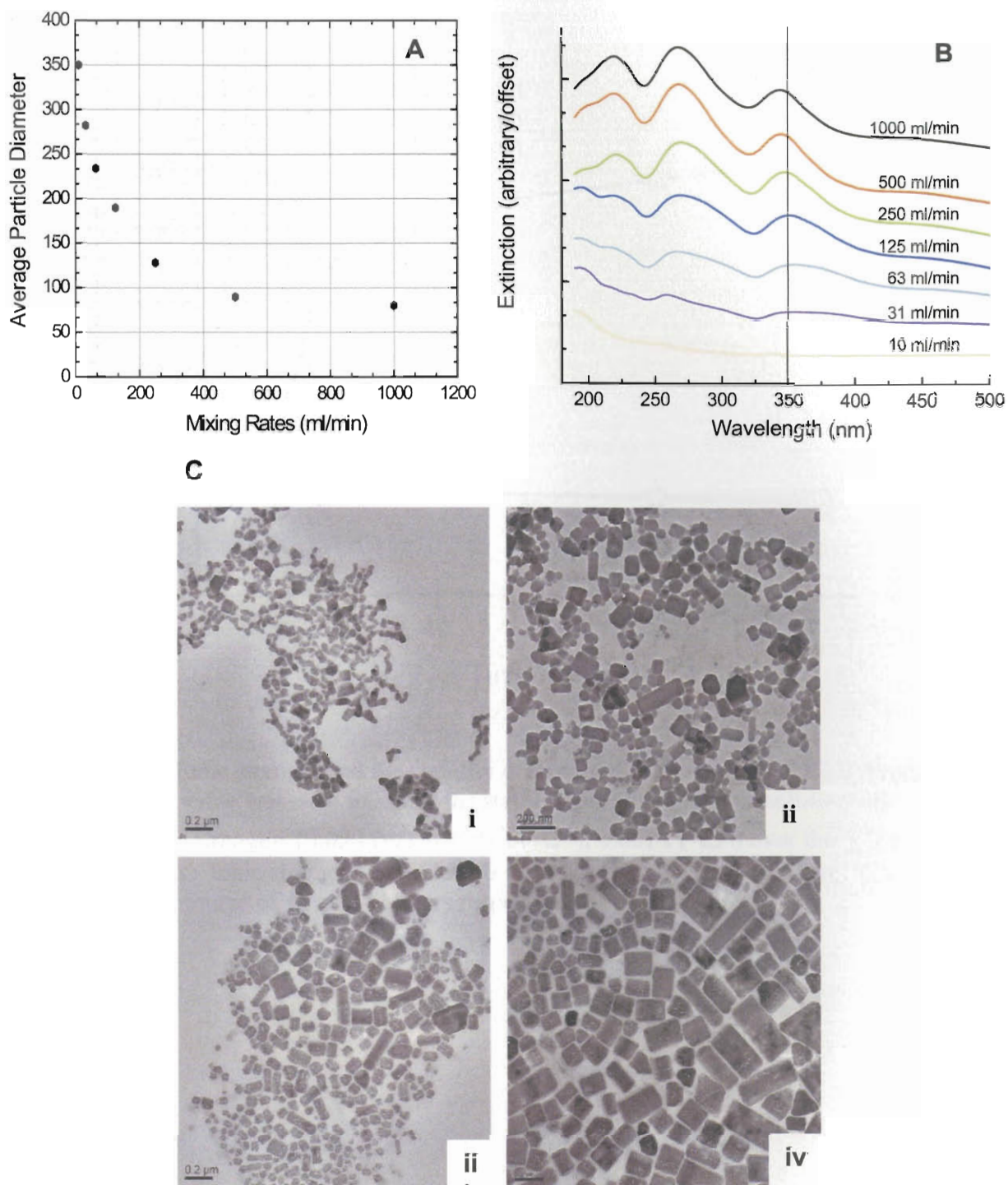


Figure 3.5 Effect of the rate of water addition during the synthesis of nano-C₆₀. **(A)** DLS average particle size value as a function of the rate of water addition during the formation process. **(B)** UV/Vis absorption spectrums of suspensions. Note the blue shift in the 330-350 nm region as the rate is increased. All spectra are offset with arbitrary adsorption units assigned. **(C)** Representative Dried TEM images of these nano-C₆₀ suspensions: **(i)** Prepared at 1000 ml/min. **(ii)** Prepared at 500 ml/min. **(iii)** Prepared at 250 ml/min. **(iv)** Prepared at 63 ml/min.

Figure 3.6

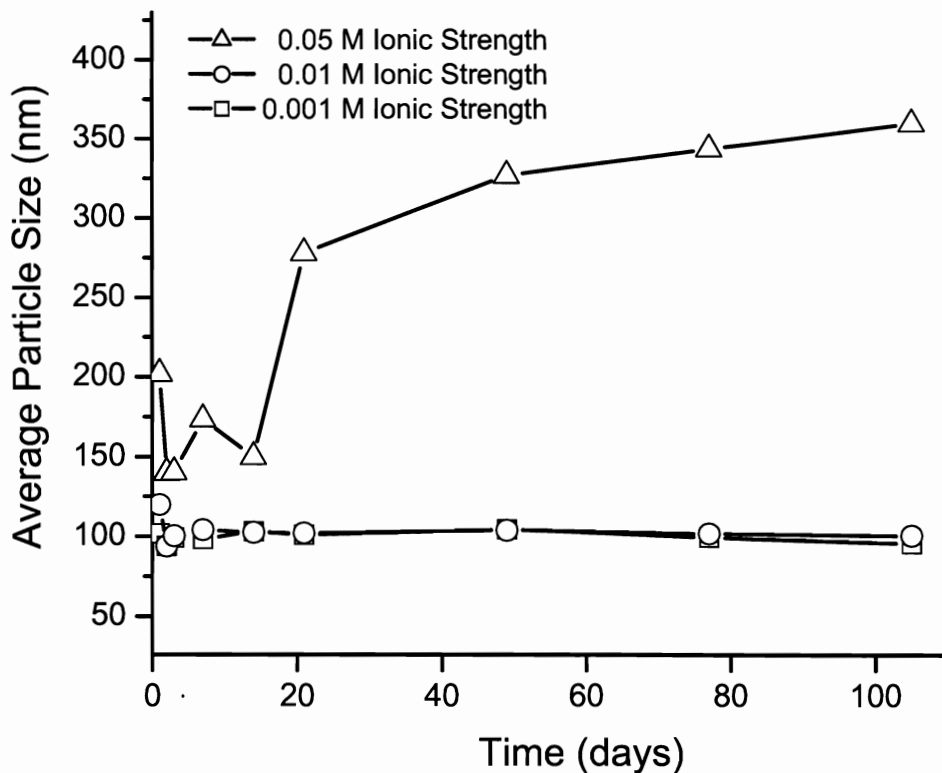


Figure 3.6 Ionic strength and the stability of nano-C₆₀ after synthesis. DLS Average particle size value was used to assess the stability of the particles in solutions of varying ionic strengths (0.05 I (-△-), 0.01 I (-○-), 0.001 I (-□-) over the course of fifteen weeks. Ionic strengths of 0.7 and 0.1 are not shown as nano-C₆₀ precipitated out over the course of 48 and 72 hours respectively.

Figure 3.7

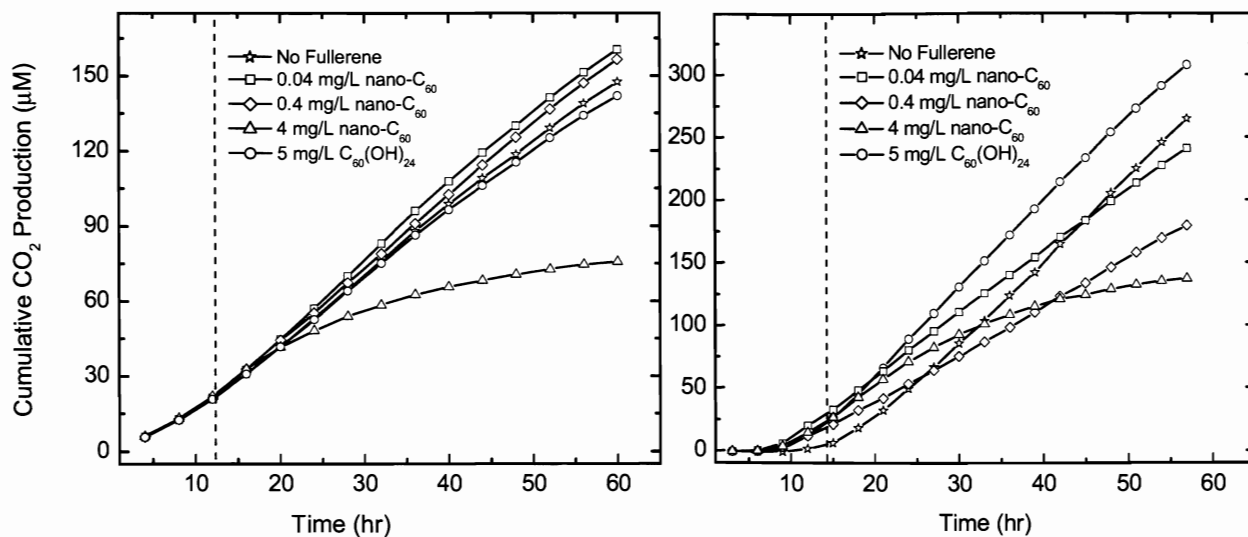


Figure 3.7 The response of Gram-negative *Escherichia coli* (A) and Gram-positive *Bacillus subtilis* (B) to nano-C₆₀ as measured by aerobic respiration rates. Nano-C₆₀ was administered to the cultures early in the exponential growth phase indicated by the dotted line. Respiration is shown as average (run in duplicate) production of CO₂ expressed as total accumulation, rates correspond to the slope.

Table 3.1

Media + Fullerene	<i>Escherichia coli</i>		<i>Bacillus subtilis</i>	
	Aerobic	Anaerobic	Aerobic	Anaerobic
MD (negative control)	+	+	+	+
MD + 0.04 mg/L nano-C ₆₀	+	+	+	+
MD + 0.4 mg/L nano-C ₆₀	-	-	-	-
MD + 4 mg/L nano-C ₆₀	-	-	-	-
MD + 5 mg/L C ₆₀ (OH) ₂₄	+	+	+	+
LB (negative control)	+	+	+	+
LB + 2.5 mg/L nano-C ₆₀	+	+	+	+

Table 1. Bacterial response to nano-C₆₀ under both aerobic and anaerobic conditions in different media. MD is minimal Davis media defined in the materials and methods, LB is Luria broth. Results shown as (+) indicate growth, (-) indicate no growth as measured by optical density at 600 nm.

*All results reported were the same with or without light present

3.B Supplemental Characterization

The physical and chemical characterization of these materials has been ongoing since the publication of the ES&T manuscript (3.A); additional findings along with key supporting evidence (supplemental) of previous findings are reported here (3.B). Specifically, observations described in this sub-chapter elucidate specific methodologies of analysis including total organic carbon (TOC), gravimetric analysis and a protocol development for an efficient organic solvent extraction for HPLC analyses. Additional chemical/physical information including powder and thin film x-ray diffraction; enhanced liquid ^{13}C NMR and mass spectroscopy (MALDI-TOF) are also presented. These data strongly support the previous hypotheses that said materials are crystalline in order and comprised of underivatized C_{60} .

Materials and Methods

Chemicals: C_{60} (99.9% purified through sublimation), ^{13}C enriched C_{60} (25% of carbon labeled, 99.5% pure) and $\text{C}_{60}(\text{OH})_{22-24}$ fullerol were purchased from the Materials Electronics Research Corporation (MER Corp., Tucson, AZ). All water used was ultra purified to $> 18.2 \Omega$ (Millipore Synergy system). All other reagents were reagent grade or higher.

Nano- C_{60} Preparation: Unless noted, nano- C_{60} was prepared as described in the previous section (3A) at pH 5, with water being added at approximately 500 ml/min. To ensure consistency, samples were taken from homogenized composites: 11 L (sterile) or 2 L ^{13}C (25%) enriched (for NMR analysis). To ensure the removal of residual, dissolved trace organics (THF or possible THF derivatives) $> 99.5 \%$ of the suspension water was

replaced (Ultrapure, 18.2 Ω) using a pressurized (20-30 psi) stir cell membrane unit (Amicon, 45 mm 10,000 NMWCO, at 20-30 psi, Millopore Corp) for all reactions and characterizations described. Residual THF (or any similar MW derivative) in water-replaced suspensions were verified to be below the detection limits (sub ppb) of GC-MS head space analysis: Agilent Model 6890N gas chromatograph (GC) equipped with a Teledyne Tekmar HT3 headspace autosampler and a 30 m by 0.25 mm OD DB-5ms column connected to an Agilent Model 5974 inert mass selective detector (MSD). The headspace autosampler was programmed to hold each sample at 70°C for a period of 30 min prior to transferring the headspace gas to the GC inlet.

Oxidizing Destabilization / Extraction / HPLC Concentration Determination: Based on the net negative surface charge demonstrated by ζ potential measurements, a matrix of oxidizing agents at variable pH values was employed to 1.) Gain understanding of the surface chemistry and 2.) Optimize the efficiency of the destabilization/extraction process into a non-polar phase (to be measured via HPLC). A 500 mL nano-C₆₀ aliquot was split into 5 sub-batches each (100 mL) then carefully adjusted to the pH values of 3, 5, 7, 9, and 11. Five oxidizing agents were chosen to represent a range of reduction potentials (Table 3B.1). Each oxidizing agent was investigated at all 5 pH values in addition a negative control (no oxidizing agent). Each reaction was stirred for 12 hours in sealed serum bottle with 5 mL of stock nano-C₆₀, 5 ml toluene and the stated amount of oxidizing agent. Samples were then stored at -20 C for three hours, freezing the aqueous portion. Toluene aliquots were taken for immediate HPLC analysis. Extraction times (*i.e.* mixing time before aqueous phase was frozen) were varied at 0.5, 3, 6 and 24 hours. HPLC was done as discussed in chapter 3A: High pressure liquid chromatography

(HPLC; Waters Millennium II system equipped with a diode array detector) analysis was performed on the toluene solutions. C₆₀ eluted at 5.6 minutes (4.6×250 mm Cosmosil PYE column, 1 mL/min toluene mobile phase) with characteristic molecular C₆₀ absorption peaks at 336, 407, 540, 595 nm observed.

Carbon Measurements: As mentioned in 3A, C₆₀ concentrations in water as nano-C₆₀ were measured using a Total Organic Carbon Analyzer (Shimadzu TOC-5050A, Columbia MD) equipped with a Non-Dispersive Infrared (NDIR) detector for the analysis of total, organic and inorganic carbon of soil and liquid samples. Samples were prepared by acidification (pH < 2) with dilute HCl and purged with N₂ (UHP) to remove inorganic carbon as CO₂. Triplicate measurements (25 µL injection volume) were performed for each sample. Carbon analysis was based on catalytic combustion of the sample at 680°C; resulting CO₂). Calibration was conducted with potassium hydrogen phthalate (KPH).

Gravimetric Concentration Determination: To ensure TOC and extraction/HPLC procedures were viable, verification of concentration was confirmed with a gravimetric analysis using a micro balance scale as mentioned in before (3A) (graciously provided by Dr. Maria Morandi, University of Texas, School of Public Health, Houston TX). Two 500 mL aliquots Nano-C₆₀ were taken as individual batches, never being mixed, for concentration analysis. 400 mL from each 500 mL aliquot was concentrated to 40 mL (10x fold) for analysis. In triplicate, using aluminum weigh boats, weighed before, 1 mL of each of aliquot was added and dried at approximately 100°C for ca. 48 hours and then weighed again. Final weights subtracted from the initial weigh boats gave mass per one mL which was compared to the extraction procedure mentioned previously.

Characterization

X-Ray Diffractometry: Thin film XRD data were collected on a Bruker AXS D8 powder X-ray diffractometer (Department of Geotechnical Engineering, ETH Zurich) using Cu-K-alpha radiation, incident- and diffracted beam Soller slits, automatic divergence slit and a 0.2 mm detector slit. Data were collected from 1 to $40^\circ 2\theta$ using a step size of $0.03^\circ 2\theta$ and a count time of 10 s per step. Sample solutions of the prepared material were analyzed as random (front loaded) mounts. Samples were prepared by simple pipetting (2-4 mL) the mixed suspension (25 mg/L C₆₀ as nano-C₆₀) onto a zero background silicon wafer slide. Oriented mounts were analyzed under ambient room conditions (temperature 23°C, relative humidity 50%) of fresh dried samples and after storing for up to 40 days.

Powder X-ray diffraction of the nano-C₆₀ crystals was performed with dried (<100°C) nano-C₆₀ (ca. 50 mg), poured into a 1 mm quartz capillary tube and packed by centrifugation (1 min., 1,000 g). The packed solid was approximately 3 cm in height, providing an area large enough for x-ray analysis. Crystallographic data was collected on an R-Axis IV++ image plate mounted on a Rigaku X-ray generator (Cu-K-alpha = 1.54 Å) (Department of Chemistry, Rice University taken by Joshua Faulkner). The Crystal Clear software package, 1.3.5SP1g, was used to measure *d*-spacings of the diffraction rings. The measurement was taken at room temperature while oscillating the sample 90° with a 30 minute exposure time and at a distance of 200 mm. The measured *d*-spacings were compared to a simulated pattern created by Carine version 3.1 software assuming a simple hexagonal unit cell parameters (space group=191, *a* = 9.54 Å, *c* = 10.06 Å) and

inserting a single carbon atom in positions where the C₆₀ would sit. This was sufficient enough to determine which reflection would appear. Only the clearly delineated peaks were indexed.

NMR: A 100 mg/L nano-C₆₀ suspension prepared with ¹³C enriched C₆₀ (25%) in D₂O (pH 5, 500 mL/min water addition) was analyzed using a 600 MHz NMR (Varian Inova) equipped with a carbon enhanced cold probe (Varian) at Rice University operated by Dr. Sean Moran. The experiment used a 30° ¹³C pulse, 2.36-s FID without proton decoupling, taking 78,373 complex points were collected over a sweep width of 33,209 Hz resulting in 1024 scans over 2 hr. 5 min (1-D). The FID was processed with 5 Hz of line broadening to further increase signal to noise ratio. The chemical shift scale of this sample, dissolved in D₂O, is relative to the trimethylsilyl group (TMS) defined as 0 ppm in (CH₃)₃Si-CD₂-CD₂-COONa dissolved in D₂O. Comparison of a carbon sensitivity standard between this instrument and the other NMR spectrometer used previously to acquire carbon spectra (Bruker 500 MHz spectrometer with carbon direct detect (inner coil) probe) shows that the new probe is at least 3 times more sensitive (as measured by signal to noise ratio) at lower scan numbers.

Mass Spectroscopy: Mass spectroscopic analyses of the materials (nano-C₆₀ and for reaction products described in later chapters) were accomplished using a laser desorption ionization (LDI) setup without and without an organic matrix (MALDI) at the Georgia Tech Department of Chemistry and Biochemistry Mass Spectroscopy facilities, under the guidance of David Bostwick. The instrument, Applied Biosystems 4700 Proteomics Analyzer, is a tandem time-of-flight (TOF/TOF) mass spectrometer that generates ions with or without matrix assistance (MA) through laser desorption ionization (LDI) with a

200 Hz laser. Samples were normally run under positive ion mode and when applicable, products from were analyzed in a sample matrix (CHCA – cyano-4-hydroxycinnamic acid) to increase sensitivity (for less polar products) (3B.5).

Results and Discussion

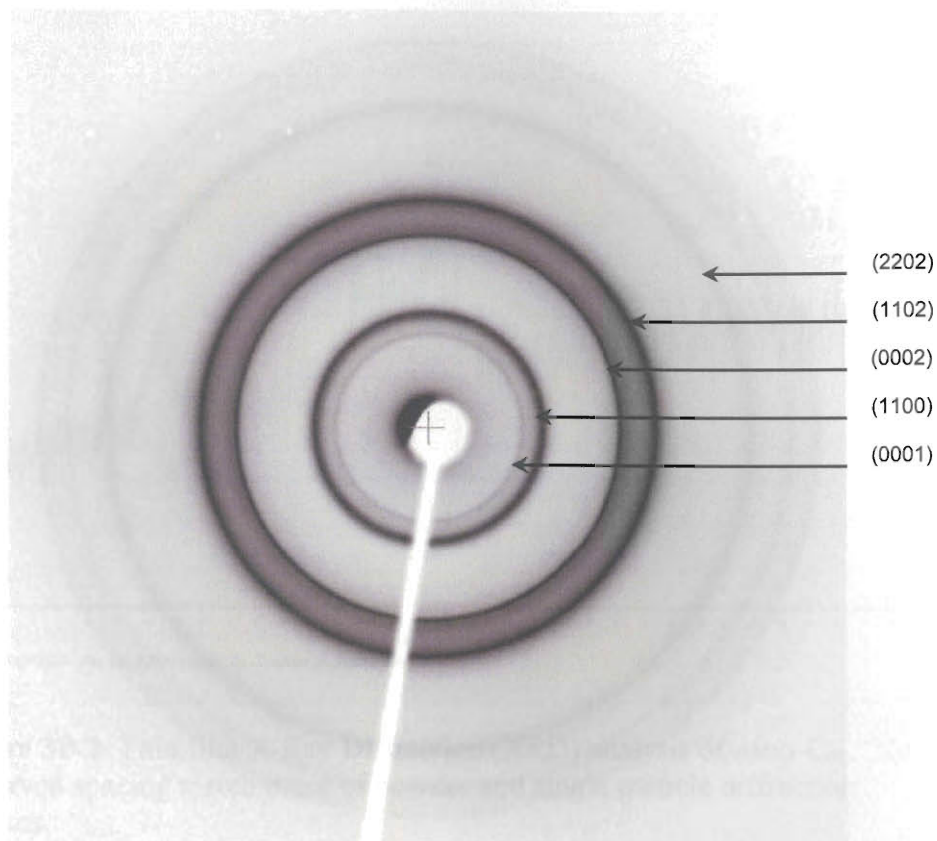
These supplemental findings, both molecular and bulk analyses of nano-C₆₀ suspensions using XRD, HPLC, ¹³C NMR and MS, strongly agree with findings in Chapter 3A. Specifically, bulk (Figure 3B.1) and thin film (Figure 3B.2) diffraction patterns (strong) confirm previous observations (single particle electron diffraction Figure 3A.3) that aggregates are crystalline. Furthermore, both indexing results confirm the previously suggested unit cell assignment of a simple hexagonal crystal structure. The measured d-spacings were compared to a simulated pattern created by Carine version 3.1 software assuming a simple hexagonal unit cell parameters (space group=191, a = 9.54 Å, c = 10.06 Å).

HPLC analysis was completed after nano-C₆₀ was briefly treated with a mild oxidizing agent (Figure 3B.3, Top) over a range of pH values. A number of (electron withdrawing potentials) oxidizing agents were found to destabilize aggregates allowing for extraction into an organic phase (toluene) and subsequent HPLC measurement. Particularly though ClO₄²⁻ seemed to be the most efficient at a pH range of 3-9, with pH values of 7-9 demonstrating virtually 100% recovery (4.8 mg/L). HPLC chromatographs comparing destabilized/extracted C₆₀ from water (using ClO₄⁻, pH 7) with a control solution of C₆₀ in toluene, never having been exposed to water, are virtually identical. A single peak was observed for each (*A*³³⁶) at 5.6 minutes which consistently represented ≥

98% of the total chromatograph (3B.3, Bottom), displaying characteristic, underivatized C₆₀ absorption UV/Vis abs at 336, 407, 540, 595 nm.

¹³C NMR liquid analysis (Figure 3B.5) observes a slightly shifted, single peak at 146 ppm (39 Hz wide at 50% intensity), further indicating *I_h* symmetry, supporting underivatized, neutral C₆₀ (¹³C NMR) as detailed and discussed in Chapter 3.A. When compared to previous liquid ¹³C NMR of nano-C₆₀, Figure 3B.5 has a ca. 3 times higher signal to noise ratio (*i.e.* more sensitive) over a much shorter time period (1/7th the time) as expected due to the Carbon Enhanced Cold Probe employed. Mass spectroscopy (MALDI TOF Positive ion mode) analysis of nano-C₆₀ suspended in water alone is in agreement with ¹³C NMR results, basically observing a single peak at 720 m/z (MW of underivatized C₆₀) (Figure 3B.5).

Figure 3B.1



<i>hkl</i>	Measured	Simulated
(0 0 1)	10.06 Å	10.06 Å
(1 -1 0),(1 0 0)	8.26 Å	8.26 Å
(0 0 2)	4.99 Å	5.03 Å
(1 0 2),(1 -1 2)	4.27 Å	4.30 Å
(2 0 2),(2 -2 2)	3.18 Å	3.19 Å

Figure 3B.1 Top: diffraction patterns of ca. 50 mg nano-C₆₀ (solid). Bottom: Tabulated measured and simulated values (Crystal Clear software package, 1.3.5SP1g). The simulated values were done by defining a simple hexagonal crystal structure with $a = 9.54 \text{ \AA}$ and $c = 10.06 \text{ \AA}$ using CaRine v 3.1 software.

Figure 3B.2

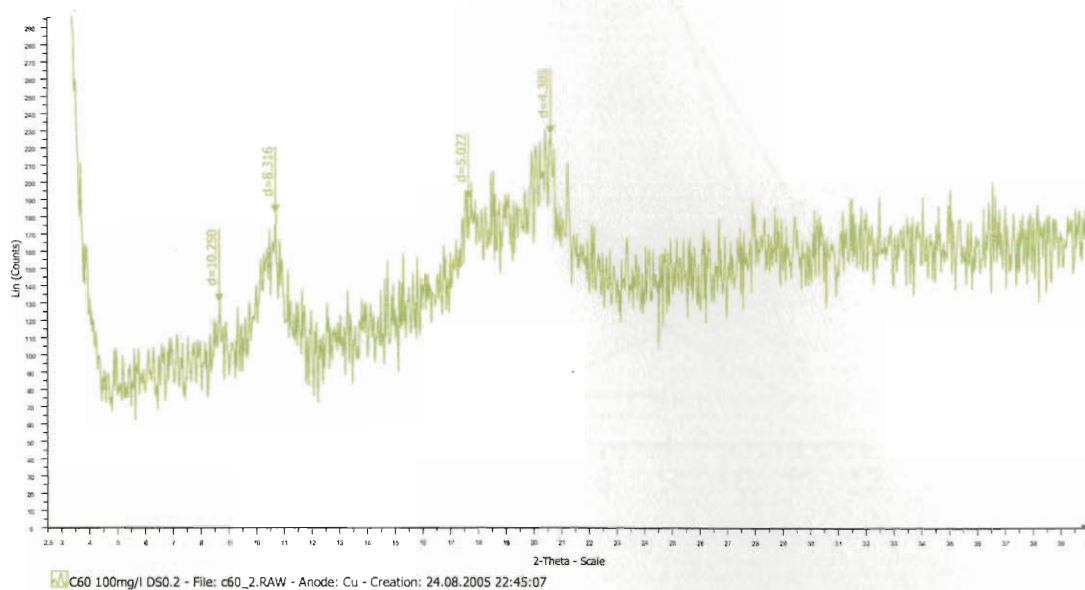


Figure 3B.2 Thin film X-Ray Diffraction (XRD) analysis of nano-C₆₀. Note: Observed spacing match those of powder and single particle diffraction patterns.

Figure 3B.3

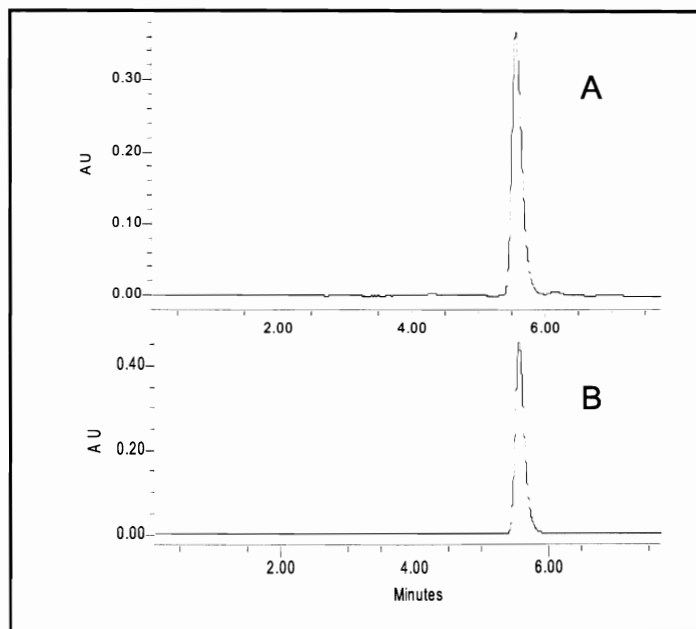
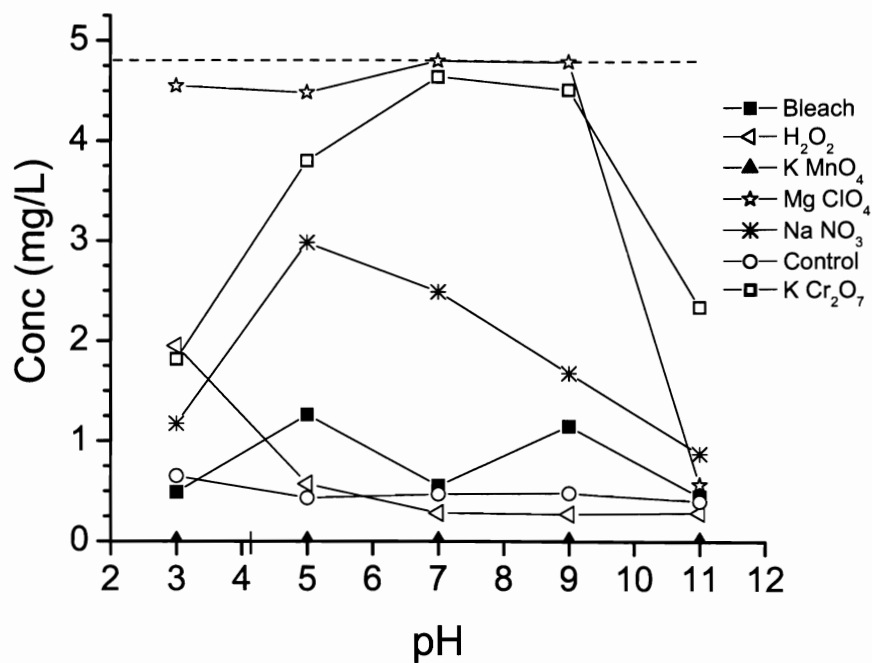


Figure 3B.3 Top: Oxidizing agent destabilization efficiency as measured by toluene layer concentration (two phase system). Dotted line represents the starting 4.8 mg/L C₆₀ in the aqueous phase. **Bottom:** C₆₀ toluene elution for both (A) Destabilized/extracted nano-C₆₀ (B) Directly dissolved C₆₀ as a control, at 5.6 minutes (4.6×250 mm Cosmosil PYE column, 1 mL/min, toluene mobile phase).

Figure 3B.4

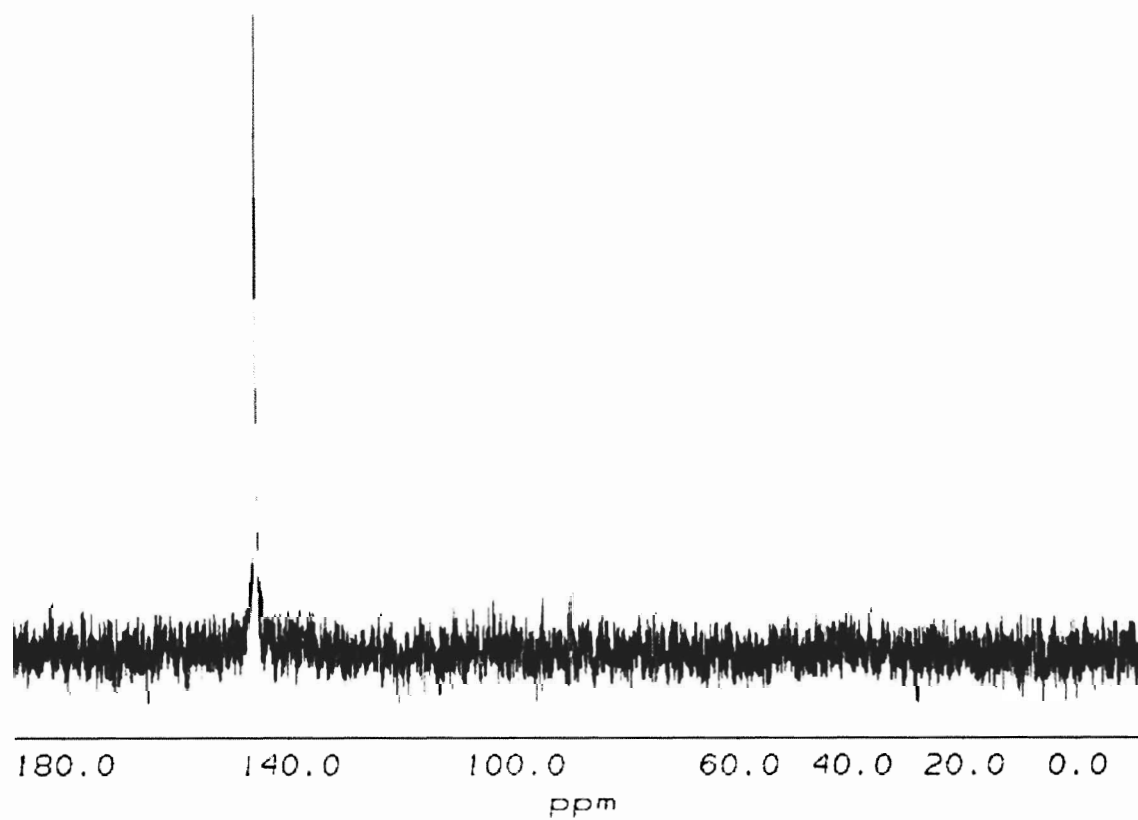


Figure 3B.4 ^{13}C NMR spectrum of nano- C_{60} in D_2O before $\text{C}_{60} = 100 \text{ mg/L}$ at 25% ^{13}C enriched

Figure 3B.5

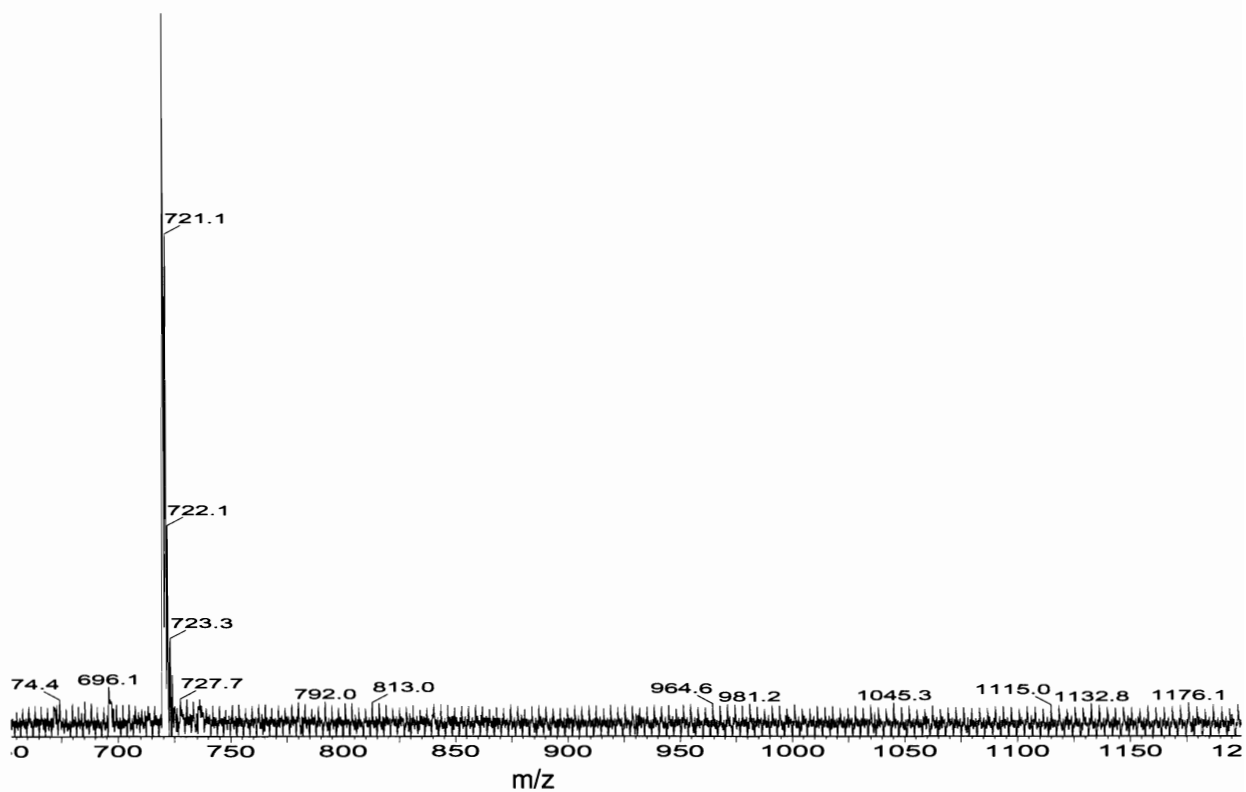


Figure 3B.5 LDI Mass Spectroscopy (positive ion mode) of nano-C₆₀ analyzed in water (100 mg/L) (no matrix assistance).

Table 3B.1

Oxidizing Agent	E ⁰ (acidic) (V)	Concentration
NO ₃ ⁻	0.94	0.1 M
ClO ₄ ⁻	1.19	0.1 M
Cr ₂ O ₇ ²⁻	1.33	0.1 M
MnO ₄ ⁻	1.51	0.1 M
ClO ⁻	1.63	0.5 % (as NaOCl)
H ₂ O ₂	1.77	3.0 % (V/V)

Table 3B.1 Oxidizing agents used to destabilize nano-C₆₀ for subsequent extraction into toluene. Each was observed over a range of pH values (3-11) and times.

Chapter 4

Ozonation of C₆₀ in Water

Introduction

Reactivity of C₆₀ in a variety of solvents has been widely studied (1-4), yet little information is available regarding C₆₀ reactivity in water as it is virtually insoluble (estimated C₆₀ solubility < 10⁻⁹ mg/L) (5-7). C₆₀ along with C₇₀ can be rendered 'available' in water however, through facile formation of aggregate suspensions from ~5 to 500 nm in diameter, depending on the synthesis protocol (8-11). Perhaps the simplest of these methods describes stable aggregate formation by adding pristine C₆₀ (as a solid powder) to water and mixed for an extended period of time (days to weeks) (12).

Aggregate formations have been well characterized both physically and chemically and determined to be comprised of underivatized fullerene, crystalline in order, and stabilized by a slight surface charge (8-10,13-15). This stabilization phenomenon permits suspended concentrations (5-200 mg/L) *ca.* 10-11 orders of magnitude above estimated aqueous solubility (16), allowing for fullerene interactions previously considered improbable (*e.g.* biological availability in an aqueous phase) (17-20).

C₆₀ aggregation in water was first observed via solvent exchange protocols such as those described by Scrivens *et al.*, beginning with toluene containing dissolved C₆₀, which was diluted into THF, further into acetone and finally into 150 mL of water whereby a fine mustard colored suspension was formed and remained after solvents were distilled (11). Other protocols varying intermediate solvent composition(s) and mixing procedures have been since described (8,10). Andrieysky *et al.*, observed a similar

aqueous suspension after sonicating C₆₀ dissolved in toluene overlaying water (9). Cheng *et al.* observed that by simply adding C₆₀ to room temperature D.I. water, at a high shear rate (rapidly stirred), water stable C₆₀ aggregates readily form which are similar those previously reported (12). As a function of the intermediate solvent(s) and mixing conditions, variable average aggregate sizes have been reported along the nano to micron scale with varying degrees of deviation and even polydispersed populations (8-10,12,16,21). UV-Vis spectra of the suspensions show characteristic C₆₀ absorbance, with a red shift and broad absorption bands, with additional broad absorption at approximately 400 - 500 nm, which has been suggested to arise from symmetry forbidden C₆₀-C₆₀ interactions, similar to what is observed in C₆₀ thin films (8-10,16,22,23). Other spectral evidence, particularly FTIR and ¹³C NMR outcomes, indicate that aggregation occurs without derivatization (13,24) which is supported by surface chemistry analyses suggesting a probable donor-acceptor complex charge source (9,13,21,25). Diffraction analyses indicate that aggregates can be crystalline in order, with a simple hexagonal unit cell assignment (Deguchi *et al.* THF method; SAED) (10,16). Due to the negative surface potentials (ζ potential ranging from ca. -9 mV to -40 mV depending), these aggregates do not readily appreciate back into a polar solvent (0.8 – 3.6 % extraction efficiency) and are quite stable (10,11,16,21,26). A number of identifying terms have been assigned C₆₀ suspensions based on preparation methods: nano-C₆₀, aqu/nano-C₆₀, SON/nano-C₆₀, THF/nano-C₆₀, TTA/nano-C₆₀ (19,21); C₆₀ dispersions (8,10); C₆₀ hydrosol, C₆₀ FWS (9,13,14); and nano-C₆₀ (16,17). For consistency, the term nano-C₆₀ is used throughout this document.

With a relatively high oxidation potential ($E_H^o = 2.07$ V), in organic solvents ozone readily oxidizes dissolved C_{60} (27-30), which can exhibit olefin like reactivity (1,3). Varying reactant concentrations, reaction time, temperatures and solvents; C_{60} - O_3 reaction kinetics and a number of products, as fullerene derivatives, have been described (27-30). Unlike other olefins though, steric constraints of the cage structure do not allow a typical Criegee's mechanism to occur (31). Based on empirical evidence along with AM1 and PM3 RHF calculations, under typical conditions O_3 attack occurs primarily along the [6,6] C-C double bond (part of the hexagon ring structure) resulting in a short lived ozonide $C_{60}O_3$ ([6,6]-closed primary ozonide, exothermically formed -280 kJ mol⁻¹) which dissociates (evolving O_2) via thermolysis (at room temperatures) through a first order reaction to form a [6,6]-closed epoxide $C_{60}O$ (29,31) or through low temperature photolysis, forming [5,6]-open $C_{60}O$ (C_{60} oxidoannulene) as Weisman *et al.*, first observed (27). Multiple oxygen adducts ($C_{60}O_x$) have been observed through such mechanisms as a function of O_3 availability and reaction time. As discussed by Malhorta *et al.*, higher oxide additions generally decrease solubility in polar solvents such as toluene, thus becoming unavailable for further reactions (28). Higher oxides have been reported at molar ratios upwards of 21:1 ($O_3:C_{60}$) resulting in ~ 21 oxygen's per C_{60} (28,32), but are usually reported at lower ratios 2 - 10:1 ($O_3:C_{60}$) depending on the reaction conditions (28,30,33). Specific molecular characterization of highly ozonated fullerenes is complex based on the sheer number and types of possible derivative structures. Nevertheless, a range of C_{60} ozonolysis products have been described in the literature, indicating that in addition to epoxide structures; carbonyl, ketone, epoxide and hydroxyl functionalities readily occur (28,34,35).

Work presented here further investigates a fullerene aggregate suspension, demonstrating direct reactivity with dissolved ozone in water. Findings indicate that C₆₀, in this form, is reactive with dissolved ozone as similarly observed in non-polar solvents such as toluene, resulting in high molecular weight, water soluble fullerene oxide(s). Specific semi-batch reaction kinetics empirically describe a mixed order reaction over a range of pH values (5.4-8.9) with and without *tert*-butanol (*t*-BuOH), a hydroxyl radical buffer to minimize potential radical chain side reactions. Product characterization results describe a highly oxidized cage (approximately 2:1 C:O) with mono- and di-oxygenated carbons. Spectral analyses suggest that both hydroxyl and carbonyl functional groups are present. Furthermore, these findings suggest that enhanced availability through stable aggregation may facilitate other aqueous fullerene chemistries previously considered prohibitive.

Materials and Methods

Nano-C₆₀: 250 ml individual batches of nano-C₆₀ were prepared with ultra-pure water with an unadjusted pH of ~5.0 (18.2 Ω) added to rapidly stirred C₆₀ saturated tetrahydrofuran (10 mg/L) as described elsewhere (10,16). After removing the THF by distillation, suspensions were filtering sterilized and combined into a sterile PVP container and stored in the dark providing a homogenous starting material. The 11.5 liter composite was determined to be 5.1 mg/L C₆₀ for the 11.5 liter batch (homogenized) and virtually identical with regard to particle size (90 nm average diameter) distribution and spectral analysis to suspensions described under these conditions previously (Chapter 3) (15). To ensure the removal of residual, dissolved organics (as THF or possible THF

derivatives), > 99.5 % of the suspension water was replaced (Ultrapure, 18.2 Ω) using a pressurized (20-30 psi) with a stir cell membrane unit (Amicon, 45 mm 10,000 NMWCO, at 20-30 psi, Millopore Corp.). Residual organics (as THF) in the water-replaced suspensions were verified to be below the detection limits (sub ppb) of a GC-MS head space analysis (Agilent Model 6890N GC equipped with a Teledyne Tekmar HT3 headspace auto sampler and a 30 m by 0.25 mm OD DB-5ms column connected to an Agilent Model 5974 inert mass selective detector).

Ozone Reactions: Stock solutions of dissolved ozone concentration ranging from 2.0 to 15 mg/L were prepared by bubbling gas ozone through ultra-pure (18.2 Ω) water at a pH 5 in a 500-mL gas-washing cylinder. Ozone gas was generated by a Wedeco Model GSO 10 ozone generator (Herford, Germany) from pure oxygen. Prior to contact with the stock solution, the ozone gas was washed through a 500 mL gas washing bottle containing a 10 mM phosphate buffer solution at pH 6. Dissolved ozone in water was measured by the indigo method described by Chiou *et al.* (36). Stock indigo solution stored in the dark and prepared no more than 1 week prior to experiments.

Semi-batch experiments, defined as an open system holding the ozone concentration constant (continuously bubbled) in the liquid phase, were performed, at pH of 5.6, 7.4 and 8.9 at $19.5 \pm 0.5^\circ\text{C}$, in the absence and presence of excess *tert*-butanol (*t*-BuOH), which acts to suppress the hydroxyl radical concentration ($k[t\text{-BuOH} + \cdot\text{OH}] = 5 \times 10^8 \text{ M}^{-1} \text{ s}^{-1}$) (37,38). Typical semi-batch reactions were prepared by first allowing buffered water to reach equilibrium concentration with diffused gas from the stock ozone solution. Nano-C₆₀ was added as a concentrate $\leq 10\%$ (or $\leq 20 \text{ mL}$) of the total reaction volume (200 mL) resulting in a 5-10 mg/L solution. 2 mL samples were taken at

appropriate time intervals with a disposable borosilicate pipette and the total sample volume was $\leq 10\%$ of reaction volume. Additional experiments were performed in batch, defined here as a closed system with set initial reactant concentrations. Batch reactions were performed using a custom built, multi-channel stopped-flow reactor developed to accurately measure the rate of binary reactions involving ozone (39). All batch systems were strongly buffered against hydroxyl radicals with 10 mM *t*-BuOH. For all semi-batch and batch experiments, ozone reactions were quenched at appropriate intervals with excess sodium thiosulfate (4:1 $\text{Na}_2\text{S}_2\text{O}_3 : \text{O}_3$) ($k[\text{Na}_2\text{S}_2\text{O}_3 + \text{O}_3] = 7.2 \times 10^7 \text{ M}^{-1} \text{ s}^{-1}$) (37) or stripped with N_2 (UHP) for ^{13}C NMR, MS (MALDI), XPS, ATR-IR and TOC analyses to avoid potential background interferences.

Characterization: Aggregate size and shape were analyzed by two primary methods as demonstrated previously (Chapter 3) (15): dynamic light scattering (DLS) using a ZetaPALS (Brookhaven Instruments Corporation) and transmission electron microscopy (TEM), which provided dimensional information. TEM images were prepared by evaporating 40 μL of concentrated suspension on a 400 mesh carbon coated copper grid and imaged with a JEOL FasTEM 2010 transmission electron microscope at 100 kV calibrated to an aluminum standard. All reported UV/Vis absorption spectra were taken within a range of 190 – 800 nm (Varian Cary 50 UV-Vis, at 0.5 nm intervals) at room temperature and corrected for the appropriate background. A 150 mg/L nano- C_{60} suspension prepared with ^{13}C enriched C_{60} (25%) in D_2O for ^{13}C NMR liquid analysis using a Varian Inova 600 MHz NMR equipped with a carbon-enhanced cold probe. The chemical shift scale of this sample in D_2O is relative to the trimethylsilyl (TMS) group defined as 0 ppm ($(\text{CH}_3)_3\text{Si-CD}_2\text{-CD}_2\text{-COONa}$ dissolved in D_2O). One-dimensional ^{13}C

and ^1H NMR experiments were performed on samples of nano- C_{60} (25% enriched with ^{13}C) and reaction products in water. Experiments were run with and without proton decoupling with similar results. X-ray Photo-electron spectroscopy (XPS) (PHI Quantera SXM Scanning X-ray Microprobe (TM) ULVAC-PHI) with an Al mono, 24.8 W x-ray source, 100.0 micron x-ray spot size at 45.0 degrees, (26.00 eV for 1 hour). Samples were prepared by first sputter coating a cleaned silicon substrate with Au for 2-10 min. at 100 mA. Concentrated liquid samples were pipetted (approx. 100 μL) and allow them to dry at least overnight at room temperature and pressure, dust free. Data are analyzed with PeakFit[®] to give peak position and relative peak areas. ATR-FTIR was taken with Thermo Nicolet Nexus 870 FTIR with Pike HATR equipped with Germanium (Ge) trough. Mass spectroscopic analyses (both nano- C_{60} and reaction products) via a laser desorption ionization (LDI) setup was done with and without an organic matrix (MALDI) using a tandem time-of-flight (TOF/TOF) mass spectrometer equipped with a 200Hz laser (Applied Biosystems 4700 Proteomics Analyzer). Aqueous samples were normally run under positive ion mode and when applicable, products from were temporarily dried and dissolved into an organic matrix (Cyano-4-hydroxycinnamic acid (CHCA)) for increased sensitivity towards less polar products. Total organic carbon (TOC) in water was determined taken with a Shimadzu TOC-5050A Total Carbon Analyzer (Shimadzu Scientific Instruments, Inc., Columbia, MD) equipped with non-dispersive infrared detector with catalytic combustion at 680°C.

Results and Discussion

Semi-Batch Reactions: Results of preliminary semi-batch reactions, shown in Figure 4.1A, indicate that C_{60} as a water stable aggregation (nano- C_{60}) is susceptible to

ozonolysis. Spectrum changes over time, particularly the loss of characteristic C_{60} absorbance peaks at 450, 340, 260 nm, indicate fundamental molecular alteration as a function of reaction time (or CT which is defined as $\text{mg-O}_3 \cdot \text{min} / \text{L (aq)}$). Parent C_{60} absorptions peaks below 400 have been calculated by others to correspond with allowed ${}^1T_{1u} \rightarrow {}^1A_g$ transitions (40). In line with UV-Vis observations, visually, the solution decreased in color intensity (yellow-orange) with increased reaction time, becoming clear with no apparent surface residues or precipitates observed. Under these conditions (pH 5.4), the degradation kinetics (Figure 4.1B), taken at 340 nm over time, did not follow either first-order or second-order kinetics, suggesting possible involvement of a more complex mechanism(s) and/or intermediates. For example, the accumulation of reaction intermediate such a molozonide as a cyclic adduct as $C_{60}(\text{O}_3)_n$, or even a dissociated ozonide ([6,6] or [5,6]), probably occur at different rates as a function of the degree of derivatization and position within aggregate (*i.e.* interior vs. surface) or in the bulk solution (*i.e.* soluble products) (28,29,31).

Parallel in procedure at an unbuffered pH of ~ 5 , semi-batch experiments detailed the aggregate change in shape, via TEM, and size, via DLS and TEM, as the reaction proceeded. Figures 4.2 presents converging lines of evidence, through DLS and TEM analyses, detailing a decrease in aggregate size as the reaction proceeds. TEM analyses demonstrates faceted aggregates as observed by others at $t=0$ (16,20) and a loss of aggregate size along with surface/edge integrity, which is particularly clear at the CT = 8 $\text{mg O}_3\text{-min/L}$, as a function of CT (Figure 4.2). Under prolonged ozonation, aggregate size was observed to be below the DLS detection limit of approximately 5 nm.

Semi-batch reactions at higher pH values of 6.8 and 8.9 with and without *t*-BuOH (37) were performed to understand the role of pH and hydroxyl radical as a potential reactant. Overall, slightly faster reaction rates (Figure 4.1B-D) were observed at higher pH values, both in the presence and absence of *t*-BuOH. We speculate this may be an artifact of product(s) partitioning behavior (*i.e.* protonation may influence derivative partitioning between the aggregate and solution). Furthermore, at pH 8.9, there is also a slight difference in reaction rates when *t*-BuOH is present (slower), indicating that a radical side chain reaction may be involved at higher pH values. This result is interesting, as it has been speculated that nano-C₆₀ should be susceptible to hydroxyl radical attack, especially in this case at a higher pH such as 8.9 where hydroxyl radical concentration should be a few orders of magnitude (38) higher than the lower pH values of 6.8 and 5.4. Conversely as discussed by *et al.*, C₆₀ may act as to quench produced radicals including ·OH (41). Typical TOC analysis of a completed reaction (semi-batch, CT > 200 mg O₃*min/L, at pH ~5, no buffer added) at pH 5.4 demonstrated high product recovery >85% (C/C) as soluble products which could passed through a 30,000 NMWL filter (~ 5-6 nm) (Amicon Ultra 15, Millipore Corp.). Specific reaction kinetics observed with aggregate populations may differ from other size distributions.

Batch Stoichiometry Results: In a closed system, ozone decay curves were determined for a pH 5.4 batch system (chosen to minimize ozone self decay) with and without nano-C₆₀ present. Direct comparison gave insight into ratios of O₃:C₆₀ consumed during the reaction. By knowing the initial concentration of nano-C₆₀ and a decay curve of O₃ under the given conditions, it is possible to back out the mass of O₃ consumed in the reaction with nano-C₆₀ after a set time. After approximately 30 min., it was estimated that

approximately 10 mg/L (270 μ M) ozone was consumed when 5 mg/L (10 μ M) C₆₀ was lost (27:1 molar ratio), which is close to the 26:1 mole ratio described through extrapolation by Anachkov, *et al.* as the maximum possible ozone consumed per molecule of C₆₀ (42). These calculations do not necessarily mean that a 27:1 stoichiometric ratio should be assumed for the reaction. It simply gives a normalized molar ratio of ozone consumed for all processes involved including direct C₆₀ oxidation and all other ozone decay processes that may be ‘promoted’ in the presence of C₆₀.

Product Analyses: A mass spectrum of parent compound without matrix assistance showed a single peak at 720 m/z (Figure 4A), consistent with previous finding that nano-C₆₀ is underivatized in nature (13,16). The product obtained after exposing nano-C₆₀ (semi-batch, CT > 200 mg O₃*min/L, at pH ~5, no buffer added) exhibited not only parent peak at 720 m/z but also multiple, less intense, peaks of 16-17 additional m/z units, indicative of probable addition of oxygen and or hydroxyl based functionalities (Figure 4B). Additional mass spectrum obtained with organic matrix assistance (Figure 4.3C) showed an increase in relative intensity in less polar, lower numbered oxide peaks. The occurrence of parent molecule and products with a small number (n = 1-5) of oxygen atoms under this extreme oxidizing condition might be an artifact due to stripping of functional groups during ionization (28,29,43). The presence of 720 m/z peak in the products is insightful however, as it suggests that 60 carbon cage structure remains intact throughout the ozonation.

¹³C NMR spectrum of ¹³C-labeled parent compound exhibited a single nano-C₆₀ peak at 146 ppm indicative of underivatized material with *I_h* symmetry (Figure 4) (15,44-46). After the reaction with ozone (semi-batch, CT > 200 mg O₃*min/L, at pH ~5, no

buffer added), the peak at 146 ppm is no longer observed. However, four new peaks were observed at 176, 168, 128 and 95 ppm, indicating high derivatization and loss of I_h parent symmetry (1,3). Product peak shifts suggest the presence of different oxygen moieties as carbonyl functionality at 176, vinyl ether carbon at 168, carbon-carbon cage bonding at 128 and carbon-oxygen at 95 ppm (as a hydroxyl or ketal functionality) (47,48). Furthermore, the low number of observed shifts in relation to the high number of functionality (C:O ratio) suggest symmetry of a repeating functional arrangement.

The ATR-IR spectrum of final products ((semi-batch, CT > 200 mg O₃*min/L, at pH ~5 (no buffer), final pH 3.4) suggested the presence of a number of oxygen functionalities (Figure 6). A broad OH absorption at 3400 cm⁻¹, C-OH in-plane bending at 1360cm⁻¹ and C-O stretching at 1315 cm⁻¹ collectively indicate existence of hydroxyl functionalities. A sharp and strong absorption at 1630 cm⁻¹ along with weaker shoulder at 1760-1770 cm⁻¹ suggested other forms of oxygen moieties, as similar peaks have been observed for other fullerene oxides including ozonated fullerenes and hemiketal fullerols. In particular, these peaks have been attributed to aryl ketones and ketones conjugated with double bonds by Cataldo (34) or as part of a hemiketal moiety (R-O-C-OH) by Xing *et al.* and Chiang *et al.* (34,47,49). Ether functionality could be responsible for the broad and weak band centered at 1110 cm⁻¹ (48). In any case, presently there are few absolute reports of IR functional identification of fullerene oxide groups, as the types of possible derivatives vary widely depending on oxidation conditions (34,47,50,51). For example, an IR spectrum for a commercial fullerene oxide prepared through substitution of a brominated C₆₀ at pH 3 (C₆₀(O)_x(OH)_y where x + y = ~22 (MER Corp., Tucson AZ)) having potentially similar hydroxyl and carbonyl moieties (52), is provided in Figure 6

for comparison. Therefore, the above interpretations should be taken as supporting evidence in combination with other techniques.

The XPS absorption spectrum of the product (nano-C₆₀ 150 mg/L, CT > 150 mg O₃-min/L, no buffer, final pH 3.4,) shown in Figure 7 provided further information on the nature of oxygen functionalities. In addition to C(1s) binding energy at 285.5 eV characteristic of underivatized carbon, two additional peaks appeared at higher energy levels were observed. As C₆₀ was the only carbon source in the suspension, additional peaks represented the carbons at different oxidation states, *i.e.* monoxygenated carbon (C-O) at 287.5 eV and dioxygenated carbon (O-C-O, C=O) at 298.7 eV (51).

Dioxygenated carbons have been observed in fullerene oxides particularly in hemiketal, and carbonyl forms by Chiang *et al.* (51, 2) and others (53). Spectrum deconvolution by a curve fitting indicates that the ratio between nonoxygenated and oxygenated carbons was *ca.* 31:29, suggesting an average derivative structure as C₆₀(O)_x(OH)_y where x + y = ~29. Among ~29 oxygenated carbons, approximately 11 carbons were monoxygenated, while the remaining 18 carbons were dioxygenated.

UV-Vis analysis of concentrated (50 mg/L) ozonated products (CT >150 mg O₃-min/L, final pH 3.4) shows a broad UV absorption increase as an inverse function of wavelength (Figure 4.5A). Similar spectra are observed for commercial fullerol (Figure 4.5B). Compared to nano-C₆₀ with 30 π bonds associated with hexagon ring structure (diatropic) (54), ozonated products appear to have relatively low extinction coefficients in the UV region. When the pH was varied for ozonated fullerenes, an increase in absorbance was observed at *ca.* 260 and 360 (pH 11.4), indicating that the derivative

structure is pH sensitive. In contrast, the commercial fullerol did not exhibit similar sensitivity.

Taken together, these results illustrate direct, facile C₆₀ ozonation in water over a range of pH values, resulting in a highly oxidized, molecular soluble derivative. Reaction kinetics appear to be slightly affected by the pH of solution and hydroxyl radical may become a reactant at higher pH values (pH 8.9). Initial ozonation reaction is hypothesized to proceed with preferentially along (hexagon) double bonds [6,6] first through the [6,6]-closed primary ozonide, which dissociates to a [6,6] epoxide which in water can be readily hydrolyzed, opening a range of possible functionalities and combinations. Final products appear to be molecularly soluble (< ~5 nm) and take on anionic forms, as the pH of the final solution is lower in pH as a function of the product concentration. Molecular characterization indicates the ozonated fullerenes in water maintain a carbon cage (720 MW skeleton) with a number of oxygen functionalities. ATR-IR, XPS, and NMR product results suggest a highly derivatized oxide (average ~29 oxygen additions), with a number of mono- and di-oxygenated carbons. Based on spectral analysis presented here in relation to other, high molecular weight fullerene oxides in the literature; multiple hemiketal arrangements as described by Chiang *et al.* (47,51), seem a likely situation upon hydrolysis of the epoxide. For clarity, Figure 4.8 has been provided illustrating a hemiketal fullerene scheme, taken with permission from Prof. Chiang. Such a symmetrical arrangement would be inline with observed FTIR and NMR spectra, along with providing an explanation for the pH sensitivity observed by UV-Vis and the anionic form.

In conclusion, direct C₆₀ reactivity in water has been demonstrated by way of aggregated clustering. As a reactant in water, aggregated fullerenes present an opportunity for chemistries previously considered prohibitory based on molecular solubility. Such aqueous based fullerene chemistries have the potential for green synthesis pathways which could prove widely applicable. However, aqueous reactivity takes on additional significance as inadvertent reactions (*e.g.* water treatment processes) resulting in soluble products, behaving different from the parent aggregate, must be considered

Acknowledgments

I would like to thank David Bostwick at the Georgia Tech Department of Chemistry and Biochemistry Mass Spectroscopy facilities MS analyses and Brandon Lafferty, Department of Plant and Soil Science at the University of Delaware, for ATR-IR analyses and insightful discussions. I would also like to acknowledge and thank the generous financial support of the US EPA (RD832526) and the National Science Foundation (EEC-0118007).

Figure 4.1

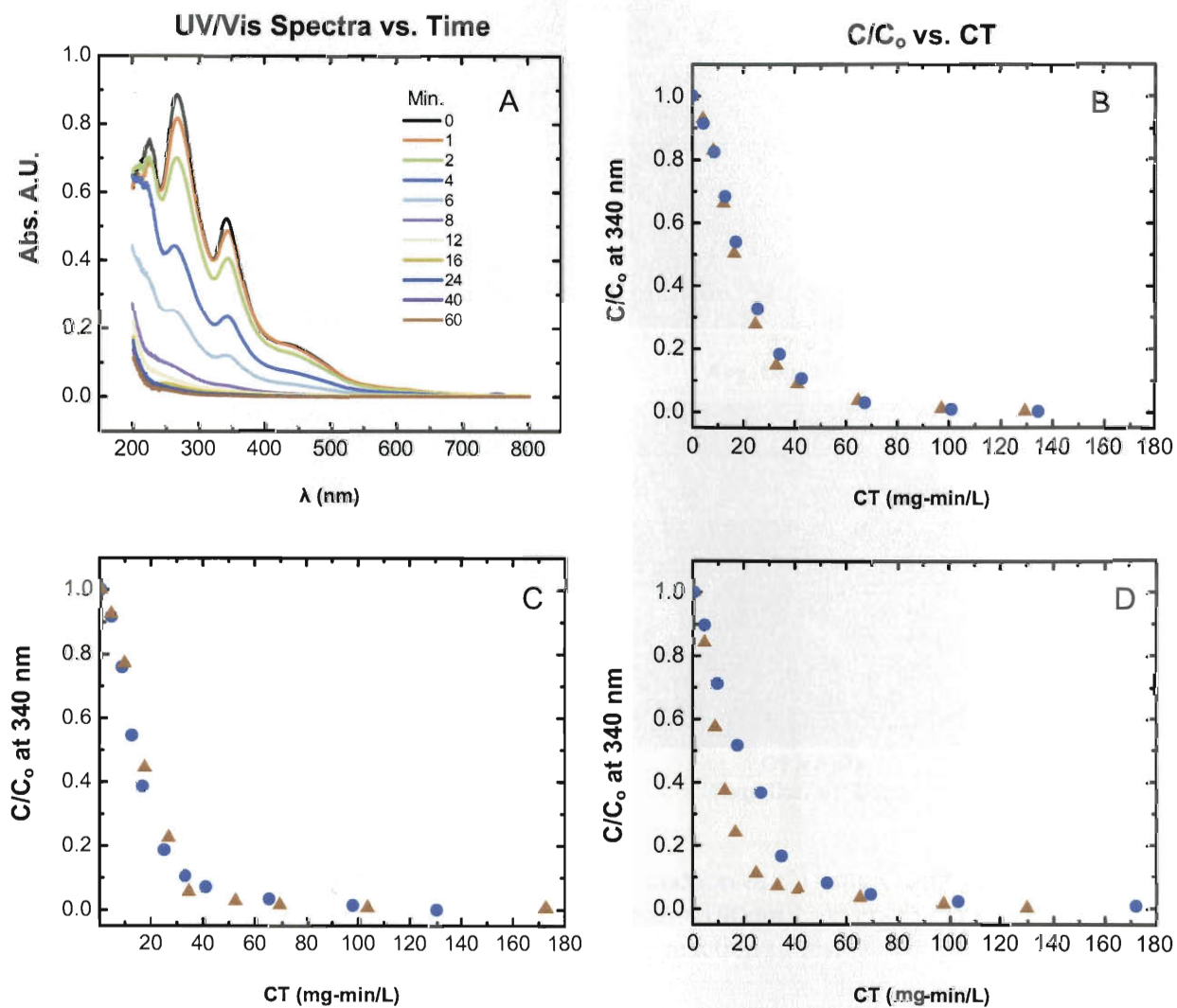


Figure 4.1 Semi-Batch nano-C₆₀ Ozonolysis Reactions. **A.)** nC₆₀ (5mg/L) spectra as a function of ozonation time in minutes (initial pH 6.8). **B.)** C/C₀ taken at 340 nm as a function of reaction time with a starting pH 5.4. **C.)** C/C₀ taken at 340 nm as a function of reaction time at pH 6.8. **D.)** C/C₀ taken at 340 nm as a function of reaction time at pH 8.9. For **B-D** with (●) and without (▲) 10 mM *t*-BuOH (hydroxyl radical suppression) corrected.

Figure 4.2

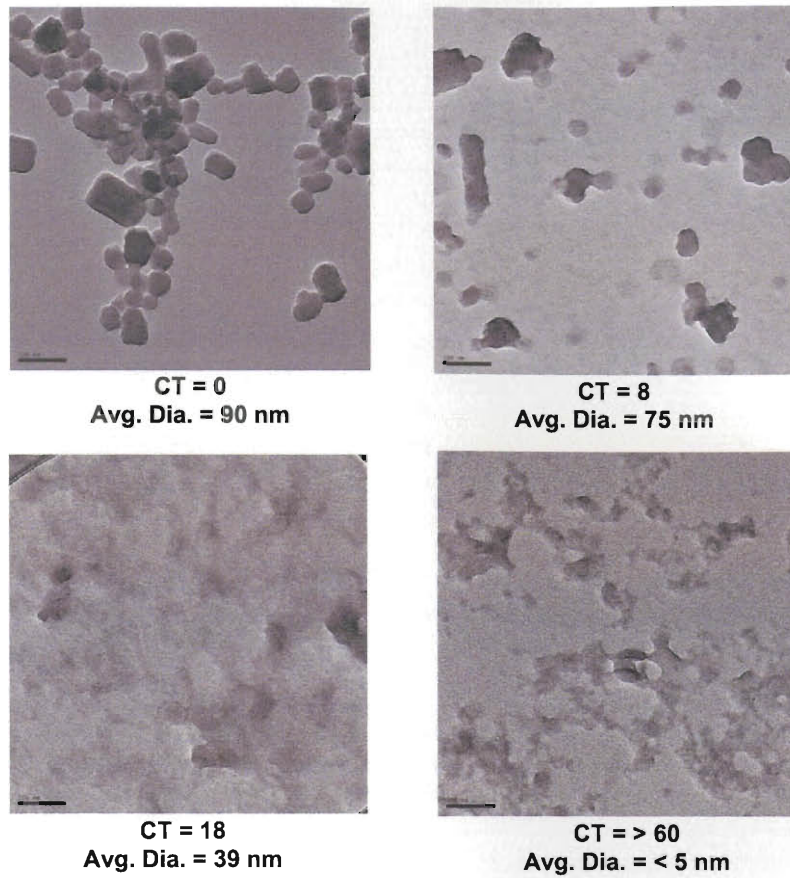


Figure 4.2 Aggregate Size and Shape as a function of CT (mg O₃-min/L). Transmission Electron Micrographs (scale bar = 100nm). Average diameter values represent DLS results taken at corresponding reaction times.

Figure 4.3

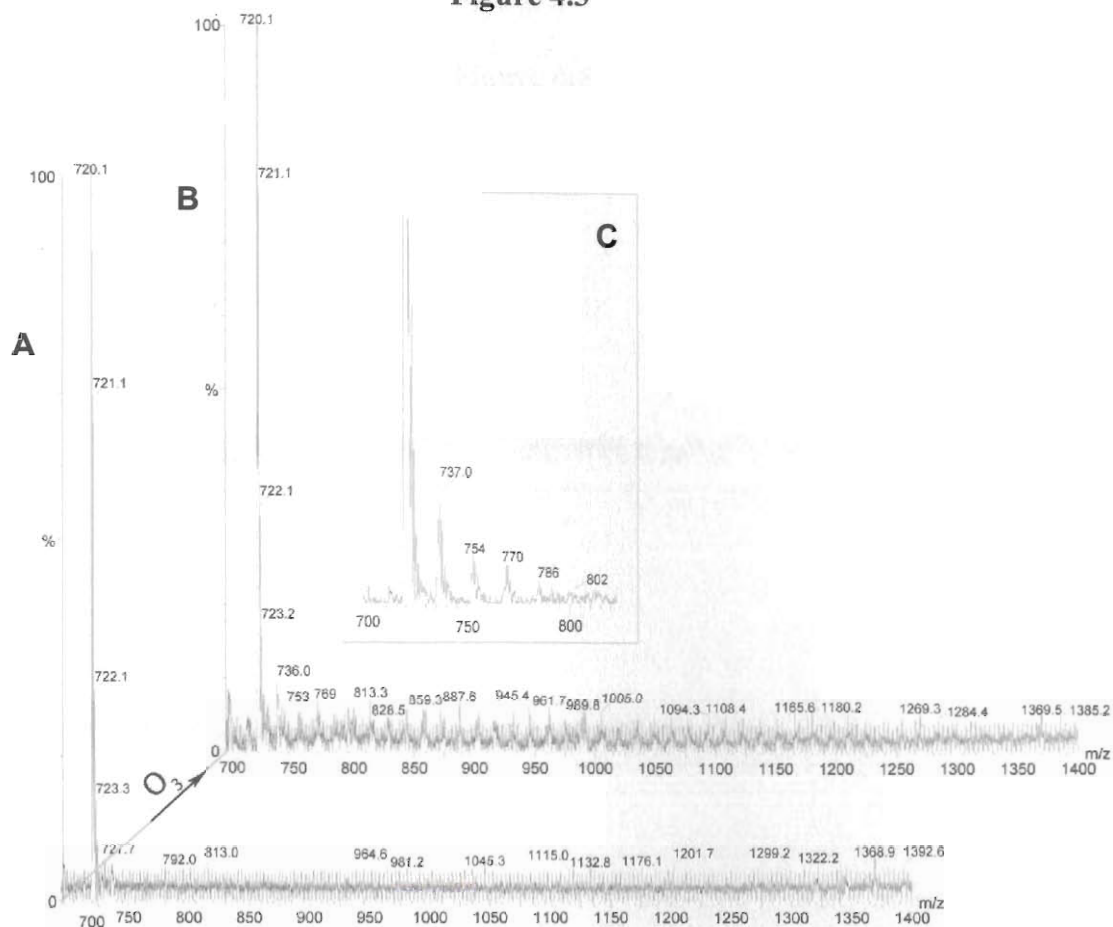


Figure 4.3 LDI Mass Spectroscopy Comparison (A) Parent nano-C₆₀ analyzed in water t = 0. (B) Product analysis measured in water after ozonation (Semi-Batch, CT = ≥ 200 min – mg O₃/L). (C) Matrix assisted (MALDI) product analysis: (CHCA – a Cyano-4-hydroxycinnamic acid).

Figure 4.4

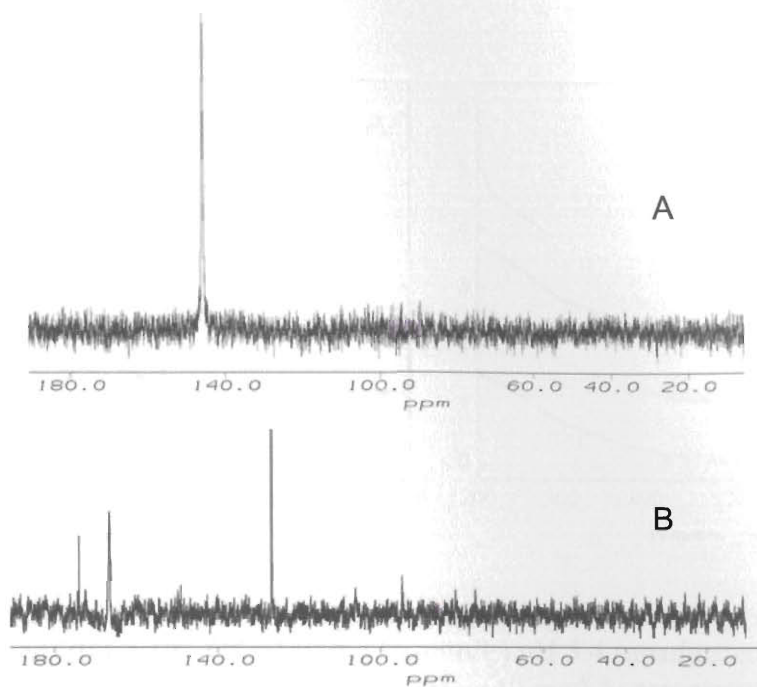


Figure 4.4 ^{13}C NMR analysis (A) spectrum of nano- C_{60} in water before ozonation ($\text{C}_{60} = 150 \text{ mg/L}$ as 25% ^{13}C n C_{60} (B) product(s) spectrum after 25% ^{13}C enriched nano- C_{60} reacted with ozone in water (CT value of $>150 \text{ mg O}_3 - \text{min/L}$, pH 5, C_0 nano- $\text{C}_{60} = 180 \text{ mg/L}$).

Figure 4.5

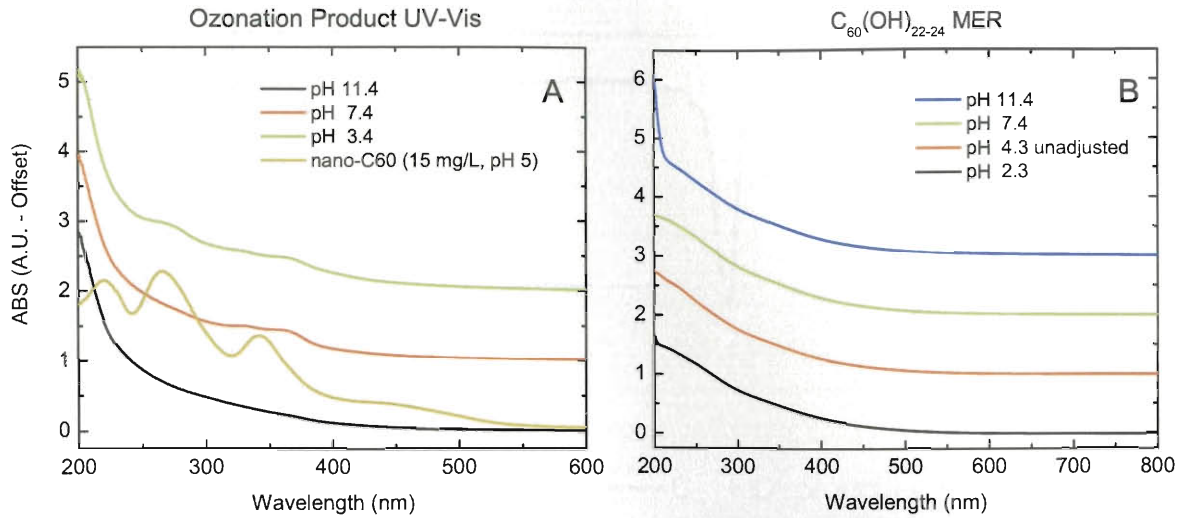


Figure 4.5 UV-Vis Product Analysis: **(A)** 100 mg/L nano-C₆₀ (99.5% H₂O exchanged) ((O₃ aq.) - CT >150 mg O₃-min/L) pH 3.4 (unadjusted) and adjusted at 7.4 and 11.4. **(B)** C₆₀(OH)₂₂₋₂₄ (MER Corp.) (40 mg/L) comparison pH adjusted to 2.3, 7.4, 11.4 and unadjusted at 4.6.

Figure 4.6

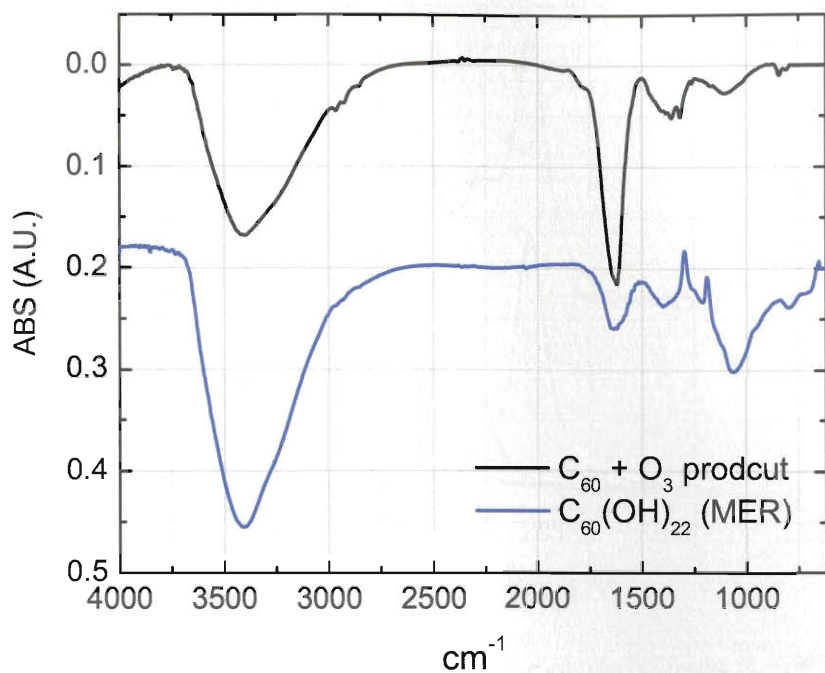
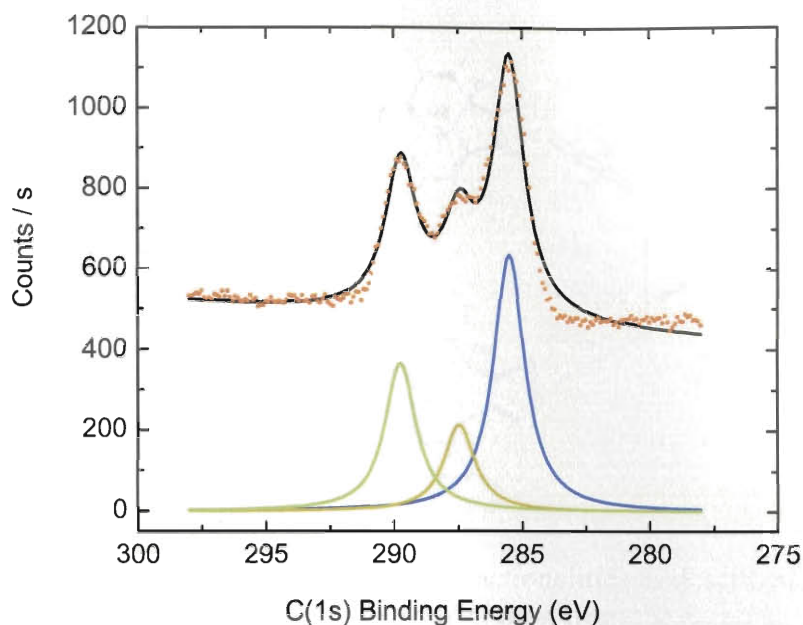


Figure 4.6 ATR-IR Product Comparison. **Top:** nano-C₆₀ ozonation product at pH 3.4, no adjustment. **Bottom:** C₆₀(OH)₂₂₋₂₄ (MER Corp.) 200 mg/L at pH 3.
Note: nano-C₆₀ parent at 180 mg/L; > 99.5% H₂O exchanged before ozonolysis (CT >150 mg O₃-min/L)

Figure 4.7



Peak	Position	Area	% C1s	Carbon- ID
1	285.50	1457.1	52%	<i>Pristine C₆₀</i>
2	287.45	489.75	18%	Mono-oxidized C
3	289.73	836.67	30%	Di-oxidized C

Figure 4.7 C(1s) X-Ray Photoelectron Speciation (XPS) spectra and curve-fitting analysis of ozonated products (CT >150 mg O₃-min/L). **Top:** Points represent C1s spectral data points taken. **Bottom:** Curve-fitting deconvolution expressed in relative intensity. **Table:** Identification and Integrated peak areas (relative intensities).

Figure 4.8

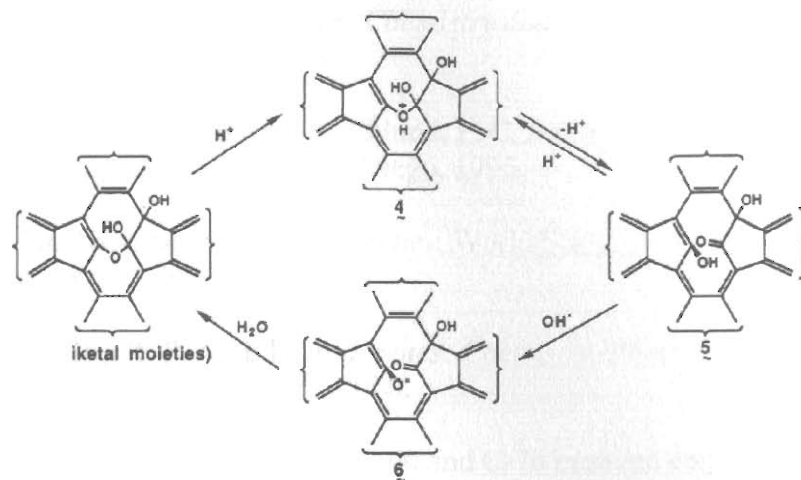


Figure 4.8 Fullerene hemiketal functionalities as described by Chiang *et al.* (47, 50). Image used with permission from the authors.

Literature Cited

1. Hirsch, A.; Brettreich, M. *Fullerenes: Chemistry and Reactions*; Wiley-VCH Verlag GmbH & Co.: Weinheim, 2005.
2. Dresselhaus, M. S.; Dresselhaus, G.; Eklund, P. C. *Science of Fullerenes and Carbon Nanotubes*; Academic Press: San Diego, 1996.
3. Taylor, R., Ed. *The Chemistry of Fullerenes*; World Scientific Publishing Co. Pte. Ltd.: Singapore, 1995; Vol. 4.
4. Kadish, K. M.; Ruoff, R. S., Eds. *Fullerenes: Chemistry, Physics, and Technology*; Wiley-Interscience: New York, 2000.
5. Heymann, D. Solubility of fullerenes C-60 and C-70 in seven normal alcohols and their deduced solubility in water. *Fullerene Science and Technology* **1996**, *4*, 509-515.
6. Heymann, D. Solubility of C-60 in alcohols and alkanes. *Carbon* **1996**, *34*, 627-631.
7. Ruoff, R. S.; Tse, D. S.; Malhotra, R.; Lorents, D. C. Solubility of C-60 in a Variety of Solvents. *J. Phys. Chem-Us* **1993**, *97*, 3379-3383.
8. Alargova, R. G.; Deguchi, S.; Tsujii, K. Stable Colloidal Dispersions of Fullerenes in Polar Organic Solvents. *J. Am. Chem. Soc.* **2001**, *123*, 10460-10467.
9. Andrievsky, G. V.; Kosevich, M. V.; Vovk, O. M.; Shelkovsky, V. S.; Vashchenko, L. A. On the Production of an Aqueous Colloidal Solution of Fullerenes. *J. Chem. Soc. Chem. Comm.* **1995**, 1281-1282.
10. Deguchi, S.; Alargova, R. G.; Tsujii, K. Stable Dispersions of Fullerenes, C60 and C70, in Water. Preparation and Characterization. *Langmuir* **2001**, *17*, 6013-6017.
11. Scrivens, W. A.; Tour, J. M. Synthesis of ¹⁴C-Labeled C₆₀, Its Suspension in Water, and Its Uptake by Human Keratinocytes. *J. Am. Chem. Soc.* **1994**, *116*, 4517-4518.
12. Cheng, X. K.; Kan, A. T.; Tomson, M. B. Naphthalene adsorption and desorption from Aqueous C-60 fullerene. *J. Chem. Eng. Data* **2004**, *49*, 675-683.
13. Andrievsky, G. V.; Klochkov, V. K.; Bordyuh, A. B.; Dovbeshko, G. I. Comparative analysis of two aqueous-colloidal solutions of C-60 fullerene with help of FTIR reflectance and UV-Vis spectroscopy. *Chem. Phys. Lett.* **2002**, *364*, 8-17.

14. Andrievsky, G. V.; Klochkov, V. K.; Karyakina, E. L.; McHedlov-Petrosyan, N. O. Studies of aqueous colloidal solutions of fullerene C-60 by electron microscopy. *Chem. Phys. Lett.* **1999**, *300*, 392-396.
15. Fortner, J. D.; Lyon, D. Y.; Sayes, C. M.; Boyd, A. M.; Falkner, J. C.; Hotze, E. M.; Alemany, L. B.; Tao, Y. J.; Guo, W.; Ausman, K. D.; Colvin, V. L.; Hughes, J. B. C60 in Water: Nanocrystal Formation and Biological Effects. *Environ. Sci. Technol.* **2005**, *39*, 4307-4316.
16. Fortner, J. D.; Lyon, D. Y.; Sayes, C. M.; Boyd, A. M.; Falkner, J. C.; Hotze, E. M.; Alemany, L. B.; Tao, Y. J.; Guo, W.; Ausman, K. D.; Colvin, V. L.; Hughes, J. B. C-60 in water: Nanocrystal formation and microbial response. *Environ. Sci. Technol.* **2005**, *39*, 4307-4316.
17. Sayes, C. M.; Fortner, J. D.; Guo, W.; Lyon, D.; Boyd, A. M.; Ausman, K. D.; Tao, Y. J.; Sitharaman, B.; Wilson, L. J.; Hughes, J. B.; West, J. L.; Colvin, V. L. The Differential Cytotoxicity of Water-Soluble Fullerenes. *Nanolett* **2004**, *4*, 1881-1887.
18. Oberdörster, E. Manufactured Nanomaterials (Fullerenes, C60) Induce Oxidative Stress in the Brain of Juvenile Largemouth Bass. *Environ. Health Persp.* **2004**, *112*, 1058-1062.
19. Lyon, D. Y.; Fortner, J. D.; Sayes, C. M.; Colvin, V. L.; Hughes, J. B. Bacterial Cell Association and Antimicrobial Activity of a C60 Water Suspension. *Environ. Toxicol. Chem.* **2005**, *24*, 2757-2762.
20. Lyon, D. Y.; Adams, L. K.; Falkner, J. C.; Alvarez, P. J. J. Antibacterial activity of fullerene water suspensions: Effects of preparation method and particle size. *Environ. Sci. Technol.* **2006**, *40*, 4360-4366.
21. Brant, J. A.; Labille, J.; Bottero, J.-Y.; Wiesner, M. R. Characterizing the Impact of Preparation Method on Fullerene Cluster Structure and Chemistry. *Langmuir* **2006**, *22*, 3878-3885.
22. Bensasson, R. V.; Bienvenue, E.; Dellinger, M.; Leach, S.; Seta, P. C60 in Model Biological-Systems - a Visible-Uv Absorption Study of Solvent-Dependent Parameters and Solute Aggregation. *J Phys Chem-Us* **1994**, *98*, 3492-3500.
23. Hungerbühler, H.; Guldi, D. M.; Asmus, K.-D. Incorporation of C60 into Artificial Membranes. *J. Am. Chem Soc.* **1993**, *115*, 3386-3387.
24. Fortner, J. D.; Zhang, C. L.; Spain, J. C.; Hughes, J. B. Soil column evaluation of factors controlling biodegradation of DNT in the vadose zone. *Environ. Sci. Technol.* **2003**, *37*, 3382-3391.

25. Brant, J.; Lecoanet, H.; Hotze, M.; Wiesner, M. Comparison of electrokinetic properties of colloidal fullerenes (n-C-60) formed using two procedures. *Environ. Sci. Technol.* **2005**, *39*, 6343-6351.
26. Mchedlov-Petrosyan, N. O.; Klochkov, V. K.; Andrievsky, G. V. Colloidal Dispersions of Fullerene C60 in water: Some Properties and Regularities of Coagulation by Electrolytes. *J. Chem. Soc. Faraday Trans.* **1997**, *93*, 4343-4346.
27. Weisman, R. B.; Heymann, D.; Bachilo, S. M. Synthesis and characterization of the "missing" oxide of C-60: [5,6]-open C60O. *J. Am. Chem. Soc.* **2001**, *123*, 9720-9721.
28. Malhotra, R.; Kumar, S.; Satyam, A. Ozonolysis of [60] Fullerene. *J. Chem. Soc. Chem. Commun.* **1994**, 1339-1340.
29. Heymann, D.; Bachilo, S. M.; Weisman, R. B.; Cataldo, F.; Fokkens, R. H.; Nibbering, N. M. M.; Vis, R. D.; Chibante, L. P. F. C60O3, a fullerene ozonide: Synthesis and dissociation to C60O and O2. *J. Am. Chem. Soc.* **2000**, *122*, 11473-11479.
30. Heymann, D. Ozonides and Oxides of C60 and C70: A Review. *Fullerene, Nanotubes, and Carbon Nanostructures* **2004**, *12*, 715-729.
31. Shang, Z.; Pan, Y.; Cai, Z.; Zhao, X.; Tang, A. An AM1 Study of the Reaction of Ozone with C60. *J. Phys. Chem. A* **2000**, *104*, 1915-1919.
32. Anachkov, M. P.; Cataldo, F.; Rakovsky, S. Ozone Reaction with C70 and C60 Fullerenes: The Effect of Temperature on Reaction Kinetics. *Fullerenes Nanotubes and Carbon Nanostructures* **2004**, *12*, 745-752.
33. Cataldo, F.; Heymann, D. A study of polymeric products formed by C-60 and C-70 fullerene ozonation. *Polym. Degrad. Stabil.* **2000**, *70*, 237-243.
34. Cataldo, F. Polymeric fullerene oxide (fullerene ozopolymers) produced by prolonged ozonation of C60 and C70 fullerenes. *Carbon* **2002**, *40*, 1457-1467.
35. Cataldo, F. Structural Analogies and Differences Between Graphite Oxide and C60 and C70 Polymeric Oxides (Fullerene Ozopolymers). *Fullerenes, Nanotubes, and Carbon Nanostructures* **2003**, *11*, 1-13.
36. Chiou, C. F.; Marinas, B. J.; Adams, J. Q. Modified Indigo Method for Gaseous and Aqueous Ozone Analysis. *Ozone Science and Engineering* **1995**, *17*, 329-344.
37. Buxton, G. V.; Greenstock, C. L.; Helman, W. P.; Boss, A. B. Critical Review of Rate Constants for reaction of hydrated electrons, hydrogen atoms and hydroxyl radicals in aqueous solution. *J. Phys. Chem. Ref. Data* **1988**, *17*, 2560-2564.

38. Staehelin, J.; Hoigne, J. Decomposition of Ozone in Water in the Presence of Organic Solutes Acting as Promoters and Inhibitors of Radical Chain Reactions. *Environ. Sci. Technol.* **1985**, *19*, 1206-1213.
39. Autho In *International Ozone Association - Pan American Group Regional Conference*: Windsor, Ontario, 2004.
40. Gasyna, Z.; Schatz, P. N.; Hare, J. P.; Dennis, T. J.; Kroto, H. W.; Taylor, R.; Walton, D. R. M. The Magnetic Circular-Dichroism and Absorption-Spectra of C₆₀ Isolated in Ar Matrices. *Chem Phys Lett* **1991**, *183*, 283-291.
41. McEwen, C. N.; McKay, R. G.; Larsen, B. S. C₆₀ as a radical sponge. *J. Am. Chem. Soc.* **1992**, *114*, 4412-4414.
42. Anachkov, M. P.; Cataldo, F.; Rakovsky, S. K. Reaction Kinetics of C₆₀ Fullerene Ozonation. *Fullerenes, Nanotubes, and Carbon Nanostructures* **2003**, *11*, 95-103.
43. Casavant, M. J.; Walters, D. A.; Schmidt, J. J.; Smalley, R. E. Neat macroscopic membranes of aligned carbon nanotubes. *J. Appl. Phys.* **2003**, *93*, 2153-2156.
44. Taylor, R.; Hare, J. P.; Abdul-Sada, A. a. K.; Kroto, H. Isolation, Separation and Characterisation of the Fullerenes C₆₀ and C₇₀: The Third Form of Carbon. *J. Chem. Soc., Chem Commun.* **1990**, 1423-1425.
45. Johnson, R. D.; Meijer, G.; Bethune, D. S. C₆₀ has icosahedral symmetry. *J. Am. Chem. Soc.* **1990**, *112*, 8983-8984.
46. Ajie, H.; Alvarez, M. M.; Anz, S. J.; Beck, R. D.; Diederich, F.; Fostiropoulos, K.; Huffman, D. R.; Kratschmer, W.; Rubin, Y.; Schriver, K. E.; Sensharma, D.; Whetten, R. L. Characterization of the Soluble All-Carbon Molecules C₆₀ and C₇₀. *J. Phys. Chem-Us* **1990**, *94*, 8630-8633.
47. Chiang, L. Y.; Upasani, R. B.; Swirezewski, J. W.; Soled, S. Evidence of Hemiketals Incorporated in the Structure of Fullerenols Derived from Aqueous Acid Chemistry. *J. Am. Chem. Soc.* **1993**, *115*, 5453-5457.
48. Silverstein, R. M.; Bassler, G. C.; Morrill, T. C. *Spectrometric Identification of Organic Compounds*; John Wiley & Sons: New York, 1981; Vol. 4.
49. Xing, G.; Zhang, J.; Zhao, Y.; Tang, J.; Zhang, B.; Gao, X.; Yuan, H.; Qu, L.; Cao, W.; Chai, Z.; Ibrahim, K.; Su, R. Influences of structural Properties on Stability of Fullerenols. *J. Phys. Chem. B.* **2004**, *108*, 11473-11479.
50. Chiang, L. Y.; Swirczewski, J. W.; Hsu, C. S.; Chowdhury, S. K.; Cameron, S.; Creegan, K. Multi-hydroxy Additions onto C₆₀ Fullerene Molecules. *J. Chem. Soc., Chem. Commun.* **1992**, *24*, 1791-1793.

51. Chiang, L. Y.; Wang, L.-Y.; Swirezewski, J. W.; Soled, S.; Cameron, S. Efficient Synthesis of Polyhydroxylated Fullerene Derivatives *via* Hydrolysis of Polycyclosulfated Precursors. *J. Org. Chem.* **1994**, *59*, 3960-3968.
52. Schneider, N. S.; Darwish, A. D.; Kroto, H. W.; Taylor, R.; Walton, D. R. M. Formation of Fullerols via Hydroboration of Fullerene-C₆₀. *J. Chem. Soc., Chem. Commun.* **1994**, *4*, 463-464.
53. Husebo, L.; Sitharaman, B.; Furukawa, K.; Kato, T.; Wilson, L. Fullerenols Revisited as Stable Radical Anions. *J. Am. Chem. Soc.* **2004**, *126*, 12055-12062.
54. Buhl, M.; Hirsch, A. Spherical Aromaticity of Fullerenes. *Chem. Rev.* **2001**, 1153.

Chapter 5

Association of Nano-C₆₀ with Clay Minerals

Introduction

Rapid industrial scale production, coupled with unique material properties, underpin rising concerns of engineered nano-scale materials inadvertently impacting the health and function of natural systems. Carbon based nano-scale materials such as fullerenes and nanotubes in particular, have been widely proposed for a variety of applications (1-15). Fundamentally understanding the behavior of these materials in natural matrixes is critical for accurate risk assessments and effective waste disposal management. Of particular interests are interactions with high-surface area, charged sub-surface materials such as clay minerals and even natural organic matter as they relate to the fate and transport processes along with low permeable barriers for waste containment. To date, information regarding interactions between fullerenes and fullerene derivatives with clay minerals has been limited, focusing on underivatized fullerenes in organic solvent and/or specific water soluble fullerene derivatives interacting with defined clay minerals (16,17). In addition, recent reports empirically described the transport of manufactured nanomaterials, including fullerenes, in flow through column systems with a glass beads matrix (18,19) and a basic transport study through a natural soil (20).

While molecular fullerenes are virtually insoluble in water (estimated C₆₀ solubility < 10⁻⁹ mg/L) (21-23), C₆₀ along with C₇₀ can be rendered 'available' in water however through facile formation of aggregate suspensions (~25-500 nm, depending on the synthesis protocol) as described by others (24-27). Perhaps the simplest of these methods describes stable aggregate formation by adding pristine C₆₀ (as a solid powder)

to water and mixed for an extended period of time (days to weeks) (28). Such formations have been well characterized both physically and chemically and determined to be comprised of underivatized fullerene, crystalline in order, and stabilized by a slight surface charge (24-26,29-31). This stabilization phenomenon permits suspended concentrations (5-200 mg/L) *ca.* 10-11 orders of magnitude above estimated aqueous solubility (32). For this work we choose a well characterized C₆₀ aggregate suspension prepared through a miscible solvent (THF) as described first by Deguchi *et al.* (26). With an average diameter of 90 nm, the term nano-C₆₀ is used throughout this chapter.

Herein, research is presented examining specific interactions of nano-C₆₀ with three defined mineral types in aqueous systems. Specifically, studies include nano-C₆₀ interactions with two ubiquitous clay mineral types, a smectite (Ca²⁺ bentonite Calcigel, Bavaria Germany; Sudchemie AG), a kaolinite (KGa-1, Georgia; CMS source clay), and a synthetically produced layered double hydroxide (LDH-Syntal[®] HSA 696; Süd-chemie AG). Results suggest that interactions with these materials are primarily a function of the available surface and edge charges of the materials in relation to the net negative surface charge of nano-C₆₀.

Materials and Methods

Nano-C₆₀: All nano-C₆₀ suspension were prepared according to the modified Deguchi method described by Fortner *et al.* (26,32) (Chapter 3) along with analytical procedures including UV-VIS, DLS, and TEM. For these studies, nano-C₆₀ was prepared with ultra pure water (> 18 Ω) at pH 5 mixed at 500 ml/min into C₆₀ saturated THF (Spectra analyzed, HPLC Grade, >99.99%, Fisher Scientific) unless otherwise noted. Suspended aggregates demonstrated an average diameter of 90 nm via DLS and confirmed through

TEM. Experiments were performed with no buffer (background pH 5 ± 0.3) to minimize ion interferences at the surface.

Clay Minerals: Previously characterized clay minerals chosen for this study included Montmorillonite: a swelling 2:1 Ca-Smectite high in specific surface area (SSA) and cation exchange capacity (CEC) (SSA $80 \text{ m}^2/\text{g}$, edge area $57 \text{ m}^2/\text{g}$, CEC $62 \text{ meq}/100\text{g}$); Georgia Kaolinite: as KGa-1, a well crystallized 1:1 kaolinite with a low specific surface area and cation exchange capacity (SSA $10.05 \pm 0.02 \text{ m}^2/\text{g}$, edge area *ca.* $2.7 \text{ m}^2/\text{g}$ (est. as 27% of SSA (33); CEC $3.0 \text{ meq}/100\text{g}$) (34-37); and Layered Double Hydroxide (LDH-Syntal[®] HSA 696; Süd-chemie AG), a synthetically produced, positively charged, clay like material with a high specific surface area (*ca.* $30\text{-}150 \text{ mg m}^2/\text{g}$), demonstrating an anionic exchange capacity (AEC). LDH charge arises from trivalent substitutions (M^{3+}) of divalent (M^{2+}) ions in the octahedral interstices of the hydroxide layers (38).

All clay minerals were prepared identically using differential centrifugation to separate the materials at a cut off at approximately $\sim 0.22 \mu\text{m}$ (220 nm). To do this, suspensions ($1 \text{ g} / 50 \text{ mL}$ ultra-pure water $>18 \Omega$) were dispersed in solution via ultrasonication (20 MHz) for 3 minutes and then centrifuged for 15 min at $5 \times 10^3 \text{ rpm}$ with the rotor break turned off. The overlying supernatant was removed and the clay pellet resuspended with ultra-pure water and centrifuged again, as described above. This procedure was repeated until the overlying supernatant was clear. If needed, clay suspensions were sonicated again after 3 centrifuge cycles to maintain a homogenized, dispersed suspension. Resuspended material, representing the large fraction of material ($>0.22 \mu\text{m}$), was then dried at 60°C , homogenized by hand via mortar and pestle, then

dispersed with methanol and passed through a 68 μm sieve. The material was then dried again at 60°C and homogenized again with a mortar and pestle.

Association Studies: Batch association studies examined, in suspension, the interaction between each of the three clay mineral types and nano-C₆₀. In triplicate, batch studies were carried out over a range suspended clay concentrations (0.5, 1.0, 5.0, 10, 25, 50, 250, 500 mg/L) keeping the nano-C₆₀ constant (4.6 mg/L). Stock solutions of size fractionated clays (>0.22 μm) in ultra-pure water were dispersed by ultra-sonication (20 MHz, 3 min) and then diluted into the nano-C₆₀ solution (9 mL). When needed, ultra-pure water was added to normalize the final volume (10 mL for all batch tests) and as a negative control (*i.e.* no clay present). Batch suspensions were mixed end over end for 20-24 hours. Samples from each mixed suspension were then filtered via a 0.2 μM syringe filter (25 mm Pall Life Sciences, Acrodisc Supor Membrane, a hydrophilic polyethersulfone filter) which separated the unassociated nano-C₆₀ (< 0.2 μM) from that which was associated with the excluded clay fraction (>0.2 μM). Filtrate was immediately analyzed at 340 nm to determine the ‘free’ nano-C₆₀ concentration. Controls included background spectral analyses of filtered and unfiltered, unassociated clay and nano-C₆₀ suspensions. No absorbance interference was observed from the clay fractions in any experiments.

Microscopy: Transmission electron microscopy (TEM) was utilized to qualitatively study nano-C₆₀ association with the minerals. TEM was performed as described previously by Fortner *et al.* (32). Batch association studies, prepared and equilibrated as described above with a 1:1 mass ratio (25 mg/L each) of clay : nano-C₆₀, were examined for two grid preparation methods. Grids were loaded as either a concentrated sample by

allowing 20 μL of suspension of sample, held by the surface tension of water, to dry for 12-18 hours, or as a dilute sample which was prepared by simply adding enough sample volume to gently flow off the grid and then allowed to dry. Dried sample grids were examined over a range of magnifications from 2,000 \times to 27,500 \times referenced an aluminum standard.

X-Ray Diffractometry: Thin film X-ray diffraction analyses were performed for clay - nano- C_{60} batch mixtures evaluating association as an intercalation phenomenon. XRD data were collected on a Bruker AXS D8 powder X-ray diffractometer using Cu-K-alpha radiation, incident- and diffracted beam Soller slits, automatic divergence slit and a 0.2 mm detector slit. Data were collected from 1 to 40 $^\circ$ 2θ using a step size of 0.03 $^\circ$ 2θ and a count time of 10 seconds per step. Sample solutions of the prepared clay material ($> 0.22 \mu\text{m}$, dispersed) were analyzed as random (front loaded) mounts. The other experiments were made with oriented clay mineral aggregates prepared and equilibrated in batch, as previously discussed, at different concentrations and clay- C_{60} ratios (1:1 and 0:1) in D.I. water. The sample was prepared by simple pipetting the mixed suspension onto a zero background silicon wafer slide. Oriented mounts were analyzed under ambient room conditions (temperature 23 $^\circ\text{C}$, relative humidity 50%) of fresh dried samples and after storing for up to 40 days (Ca-Smectite + nano- C_{60}).

Column Studies: One dimensional sand column experiments were designed to examine the effect of dilute clay mixtures ($\leq 10\%$ total mass) on the transport of nano- C_{60} suspensions. Columns were constructed of borosilicate glass columns (9 cm length x 0.9 cm i.d.) and fitted with glass wool plugs at the influent and effluent. A fine grained sand (Perth, Australia; particle size: median = 342 $\mu\text{m} \pm 139 \mu\text{m}$, $C_u = d_{60}/d_{10} = 1.8$; LA-950

Laser Scattering Particle Size Distribution Analyzer) was prepared by first removing associated carbonates in an acetic acid bath at $\sim 150^{\circ}\text{C}$, followed by ultra-pure water and dried at 100°C . Dry mixtures of sand and clay were prepared with the size fractioned ($>0.22\ \mu\text{m}$) clay minerals described previously by mixing the appropriate mass ratios of clay and prepared Australian sand homogenized (end over end mixing with 5 mm glass beads to enhance mixing). $3.0 \pm 0.1\ \text{g}$ of sand or sand-clay mixture was consistently packed in 1 cm lifts, with each lift's density being normalized via ten perpendicular taps with a glass stir rod. Solution influent was delivered through a 28 g stainless steel, sterile syringe needle fitted through a rubber stopper sealed in Teflon. Packed columns were saturated with ultra-pure water in an up-flow mode (0.1-0.2 ml/min, peristaltic pump) for at least 3 hours to remove residual gas from the system. After saturation, columns were reversed to a down-flow mode, minimizing sample dilution, and added a stock feed solution of 10 mg/L nano- C_{60} suspension for all experiments. Effluent samples were taken in at 1-20 minute intervals, depending on the experiment, and immediately analyzed for via UV-Vis spectral analysis. For all experiments, background sampling ensured that no absorbance interferences occurred. Each sand or sand-clay column experiment was done in triplicate with values averaged.

Results and Discussion

Taken together, results indicate that C_{60} , as a nano-scale aggregate (nano- C_{60}), in water does interact with clay minerals. Batch association studies, shown in Figure 5.1, demonstrate differential capacity of these mineral types to associate with nano- C_{60} . The synthetic LDH material, with a positive surface charge, clearly had the greatest capacity to associate with the negatively charged nano- C_{60} . Based on simple point estimations

from the (taken at 25 mg/L clay, linear range, Figure 5.1B), an association value was observed to approximated 175 g nano-C₆₀ per 1 kg of LDH (17.5% w/w). Ca-Smectite association was observed to also occur at an appreciable level: 37 g nano-C₆₀ per 1 kg smectite (taken at 25 mg/L clay, linear range, Figure 5.1B). These results are interesting in that smectite has a net negative surface charge, thus minor association might be expected. However, as discussed, smectite minerals can have positively charged edges and demonstrate the capacity to intercalate suspended materials, both of which may play a role in the observed association. Lowest in mass association, ca. 6.5 g nano-C₆₀ per 1 kg kaolinite (taken at 25 mg/L clay, linear range Figure 4.1B) was kaolinite (KGa-1) which like smectite, can acquire a positive edge charge, but is lower in total surface area including edge area with less intercalation tendency.

Transmission electron microscopy (TEM) imaging (Figures 5.2, 5.3 and 5.4), supports batch results, demonstrating nano-C₆₀ association with all clay minerals. Both kaolinite and smectite display enhanced association at the clay edges as hypothesized. In particular, the kaolinite hexagonal plates (Figure 5.2), with well defined edges, show nano-C₆₀ association not only along the edge but with a higher affinity toward broken edges corners, which are higher in positive charge density based on increased edge-to surface-area ratios. In comparison, nano-C₆₀ appears to readily associate with all available LDH surface area. In water, LDH alone appears to be a non-dense, loosely oriented flake and lath shaped material as observed in Figure 5.4 A, B. However in the presence of nano-C₆₀, the associated materials appear denser (based on transmittance) with few of the LDH features distinguishable (Figure 5.4 C, D). This phenomenon is

likely due to charge negation by the oppositely charged materials allowing for neutral or less charged surfaces to readily interact (classic electrostatics).

Diffraction experiments yielded information regarding the nature of association by looking for changes in mineral interlayer spacings in the presence of nano-C₆₀. Background X-ray diffraction analysis of concentrated nano-C₆₀, with no clay present, matches the previous electron and powder X-ray diffraction results, confirming a simple hexagonal unit cell (Chapter 3.B) (32). Batch association studies, done as previously described at a 1:1 mass ratio, were analyzed and overlaid with background clay diffraction patterns (Figure 5.2-5.4). XRD analyses of kaolinite- and LDH-clay mixtures did not show observable *d*-spacing shifts in the presence of nano-C₆₀, indicating no significant intercalation had occurred. However, in the presence of nano-C₆₀, smectite *d*-spacings differed, increasing along the *c* axis, which is common for interlayer intercalation (39), from a background *d*-spacing of 15.2 Å to a new value 18.5 Å. The difference in spacings (3-4 Å) however is considerably smaller than what would be expected even molecular intercalation of C₆₀ (*ca.* 9-10 Å). Such a difference may arise from partial intercalation at the interlayer edge, or as a result of an impurity.

Column experiments were designed to observe the effects of charged mineral surfaces on the movement of nano-C₆₀ through porous media. Figure 5.6 shows the varying effect of the three clay minerals tested on the breakthrough of nano-C₆₀ through sand media. Similar data was observed for both smectite and kaolinite. At 1% (w/w), smectite and kaolinite did not retard nano-C₆₀ when compared to a sand only matrix. However, at 10% smectite and kaolinite, nano-C₆₀ was retarded and displayed a breakthrough curve of lower slope than sand alone. As expected, LDH had an impact on

the transfer of nano-C₆₀. At concentrations of 0.1% w/w LDH, nano-C₆₀ breakthrough was twice that of other clays (1.0% w/w), at 1/10 the mass (factor of 20). At concentrations of 1% LDH, nano-C₆₀ was not observed to break through after 155 minutes, strengthening the previous conclusions regarding the high capacity of LDH to associate with nano-C₆₀. This study differed from others presented here in that the allowed contact time between materials was not hours to days, but seconds to minutes. Based on this difference in contact time and apparent differences in retardation and capacity between the anionic and cationic minerals to retain nano-C₆₀, association kinetics should be considered.

In summary, results presented here clearly indicate that C₆₀ as a water stable aggregate interacts with clay minerals. The degree of interaction was found to be a function of available surface charge in relation to the net negative surface charge of nano-C₆₀. Composition (*i.e.* positive or negative charge source) and percent fraction, as it relates to surface area, of clay materials should be considered in facilitated transport of aggregated nano-C₆₀ or even other similar carbon structures (higher fullerenes, nanotubes) through sub-surface media. Furthermore, these results are useful in proper waste management practices to contain (*e.g.* clay liners) nano-scale, charged aggregates.

Acknowledgments

I would like to thank Professor Alexander Puzrin at Institute of Geotechnical Engineering (IGT), Swiss Institute of Technology Zurich (ETHZ) for directly supporting this research and my time in Zurich. I would also like to thank Dr. Michael Plötze (IGT) and Dr.

Christian Solenthaler, Department of Materials (ETHZ) for various analyses (XRD and TEM, respectively) and insightful discussions.

Figure 5.1

Batch Association of nano-C₆₀ and Clay Minerals

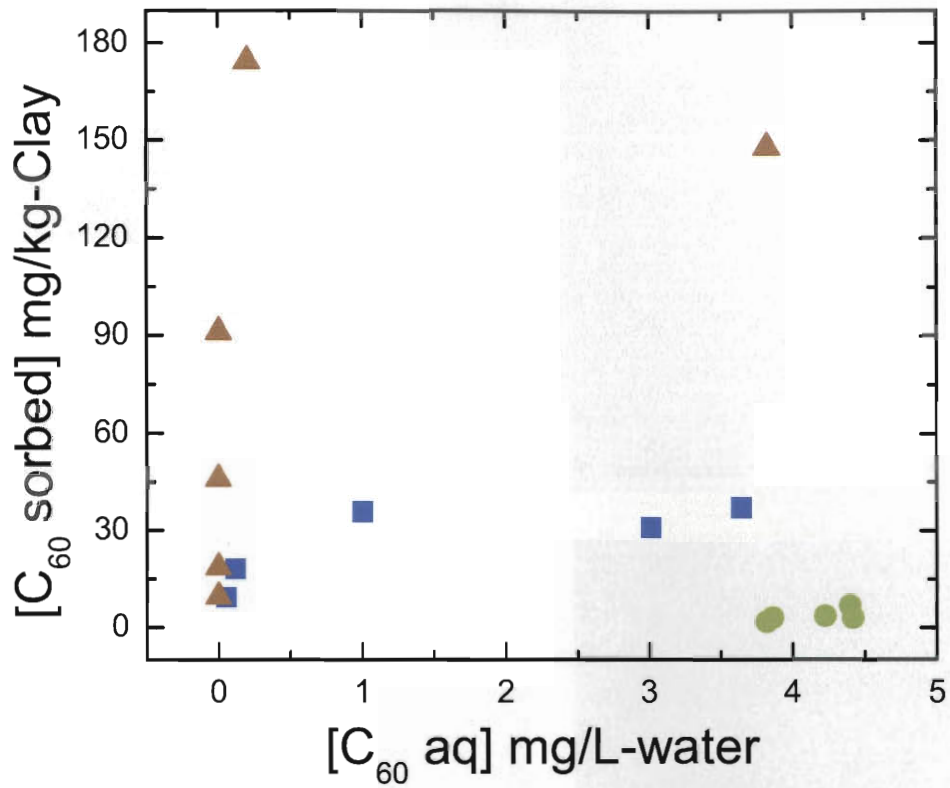


Figure 5.1 Batch association studies: ▲ LDH, ■ GaK-1, ● Smectite.

Figure 5.2

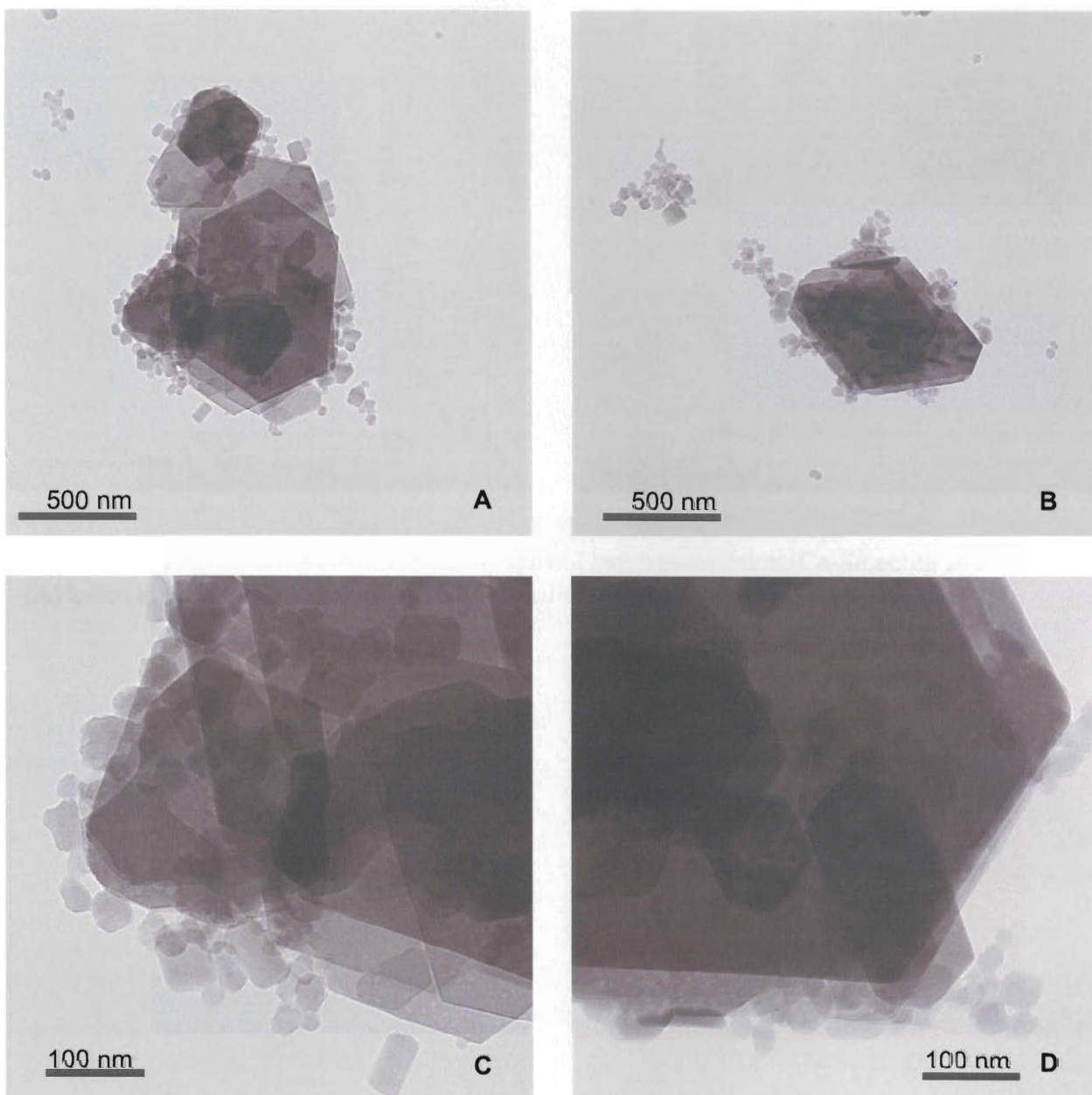


Figure 5.2 Transmission electron micrographs of batch association: KGa-1 and nano-C₆₀. Images (A) and (B) were taken at $\times 8800$ and images (C) and (D) at $\times 27500$. Smaller, faceted particles are nano-C₆₀.

Figure 5.3

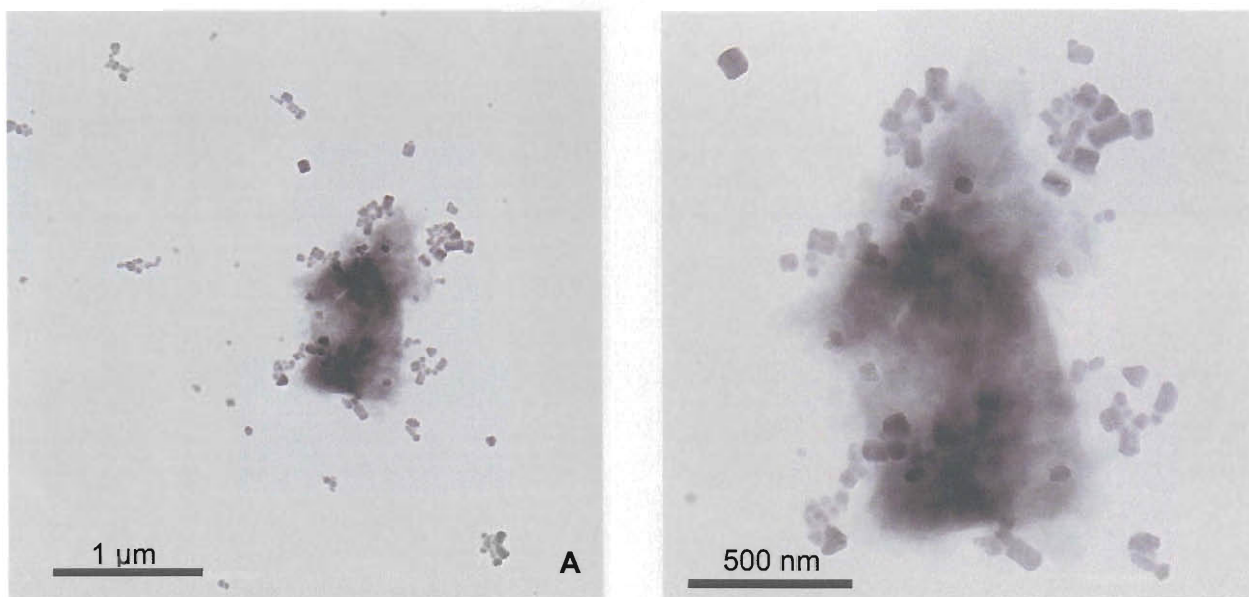


Figure 5.3 Transmission electron micrographs of batch association: Ca-Smectite and nano-C₆₀. (A) taken at ×5000 (B) Taken at ×11500. Smaller, faceted particles are nano-C₆₀

Figure 5.4

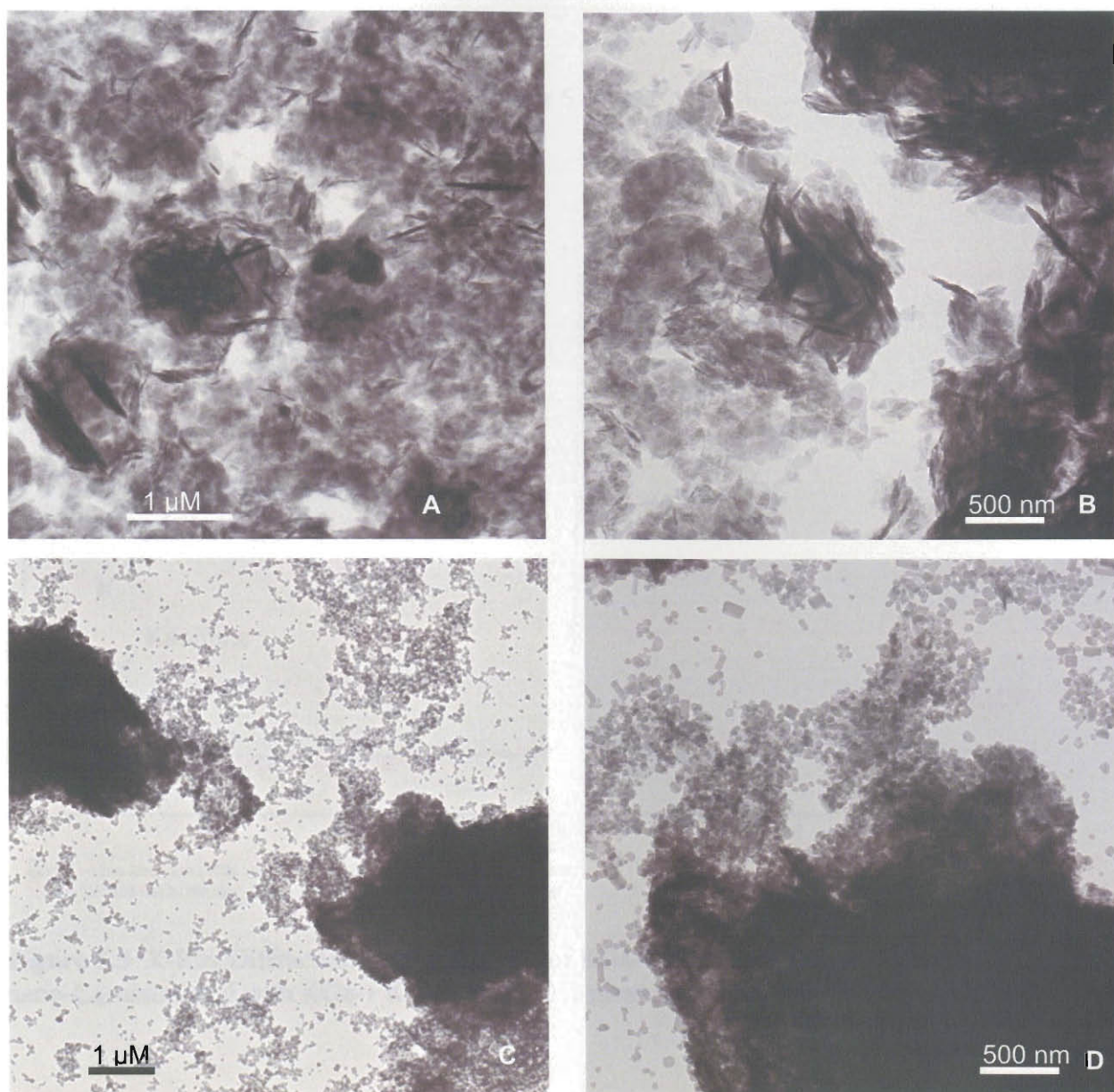


Figure 5.4 Transmission electron micrographs of batch association: LDH and LDH - nano-C₆₀. LDH (A) taken at ×3800 (B) Taken at ×6600 (C) taken at ×2750 (D) Taken at ×6600. Small, faceted particles in C and D are nano-C₆₀.

Figure 5

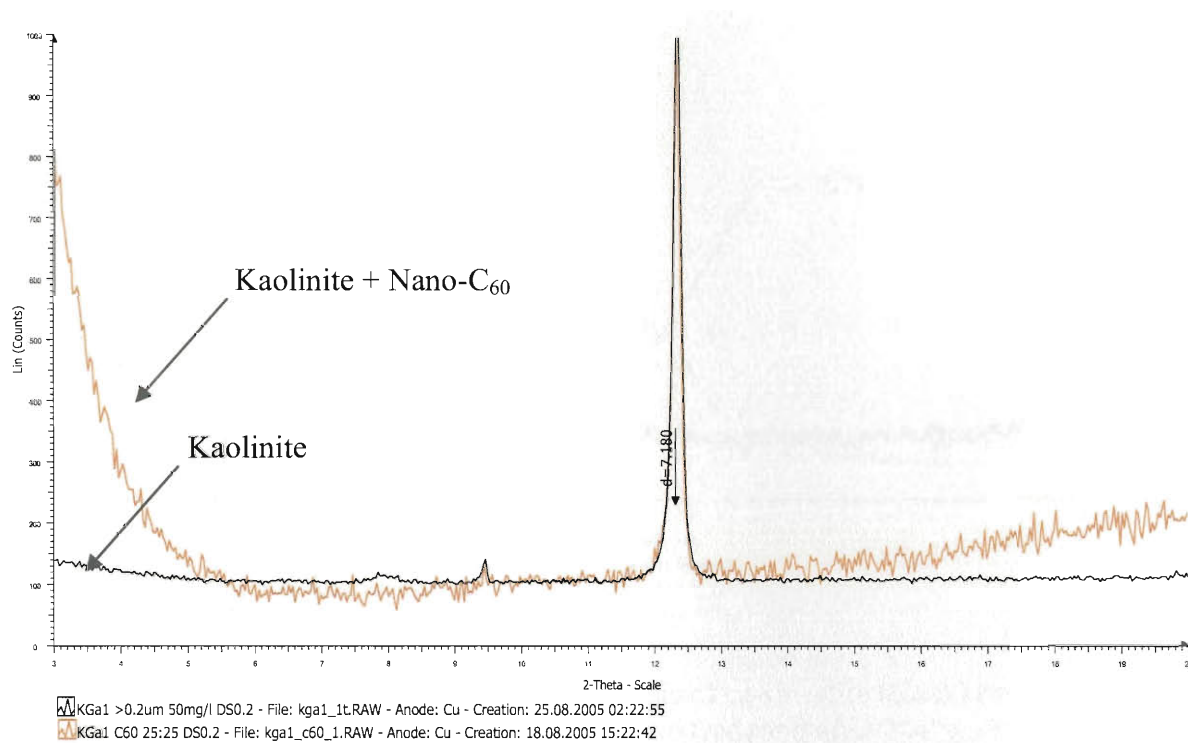


Figure 5.5 X-Ray Diffraction (XRD) analysis of KGa-1 kaolinite (black) baseline and nano-C₆₀ associated with KGa-1 Kaolinite at a 1:1 mass ratio (red).

Figure 5.6

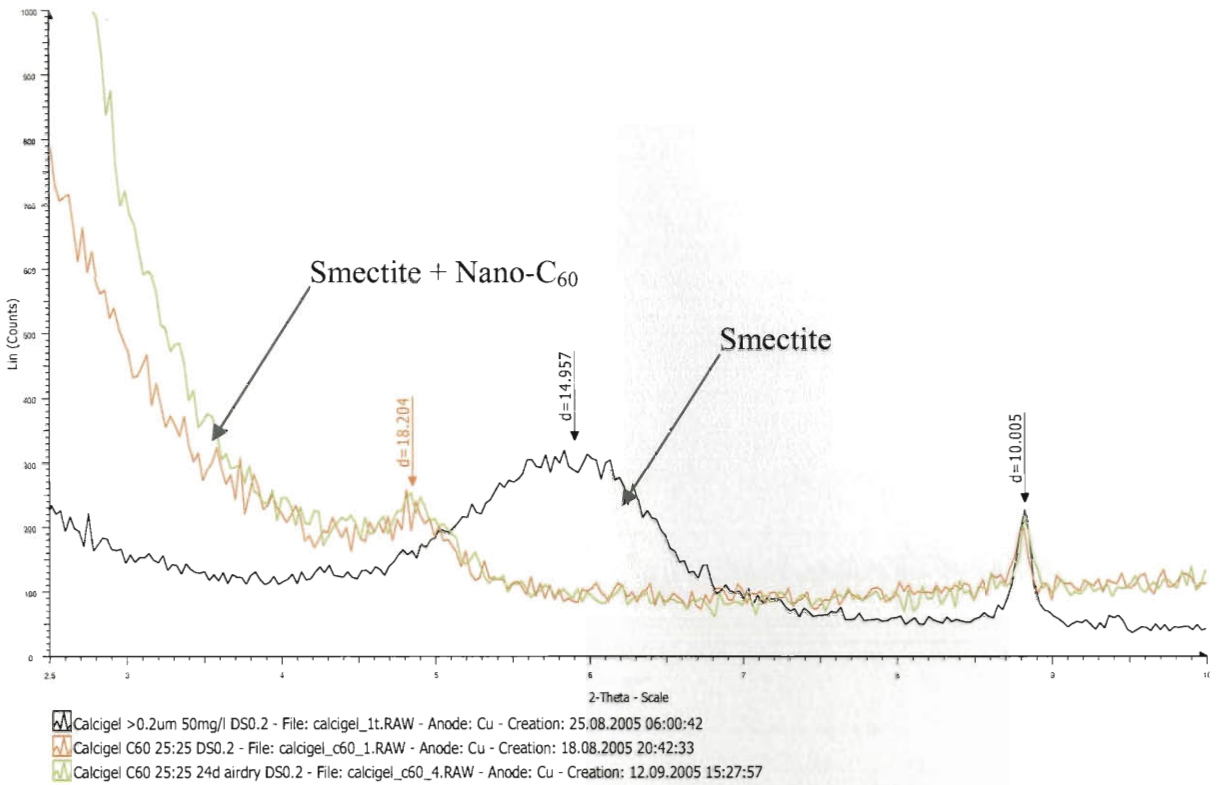


Figure 5.6 X-Ray Diffraction (XRD) analysis of ca-smectite (black) baseline and nano-C₆₀ associated with smectite at a 1:1 mass ratio (red) and after 24 days of being air dried (20°C) (green).

Figure 5.7

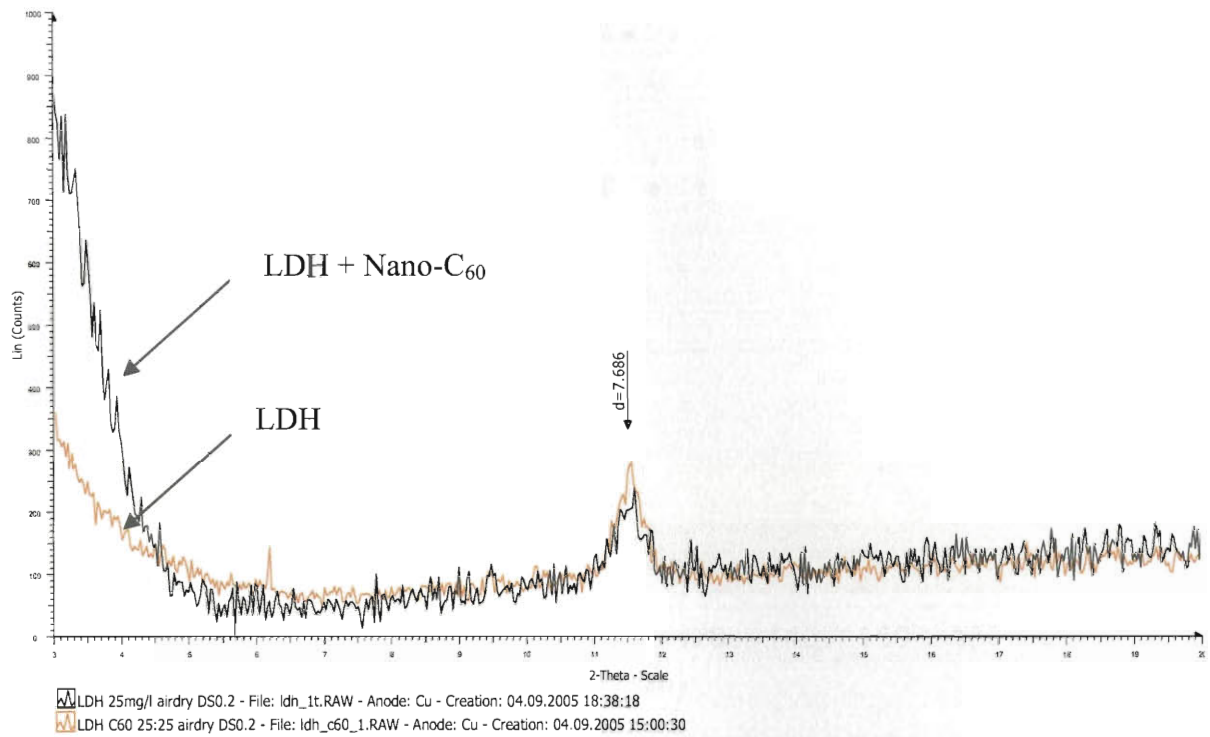


Figure 5.7 X-Ray Diffraction (XRD) analysis of LDH (black) baseline and nano-C₆₀ associated with LDH at a 1:1 mass ratio (red).

Figure 5.8

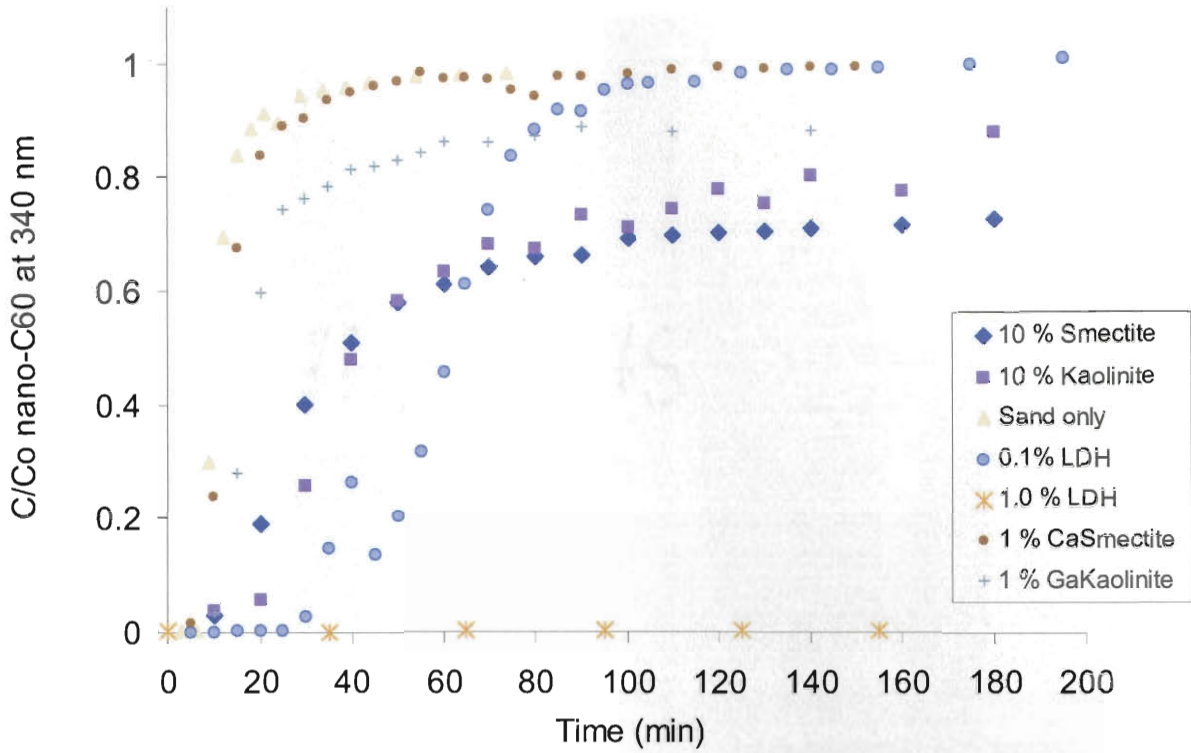


Figure 5.8 Nano-C₆₀ breakthrough experiments in 1-D sand and mixed sand-clay columns. Top to Bottom Break Through Curves (all % values are in w/w):

- ◆ 10 % Smectite – Sand Break Through
- 10 % Kaolinite - Sand Break Through
- ▲ 0 % Sand Only Break Through
- 0.1 % LDH - Sand Break Through
- * 1.0 % LDH - Sand Break Through
- 1.0 % Smectite – Sand Break Through
- + 1.0 % Kaolinite - Sand Break Through

Figure 5.9

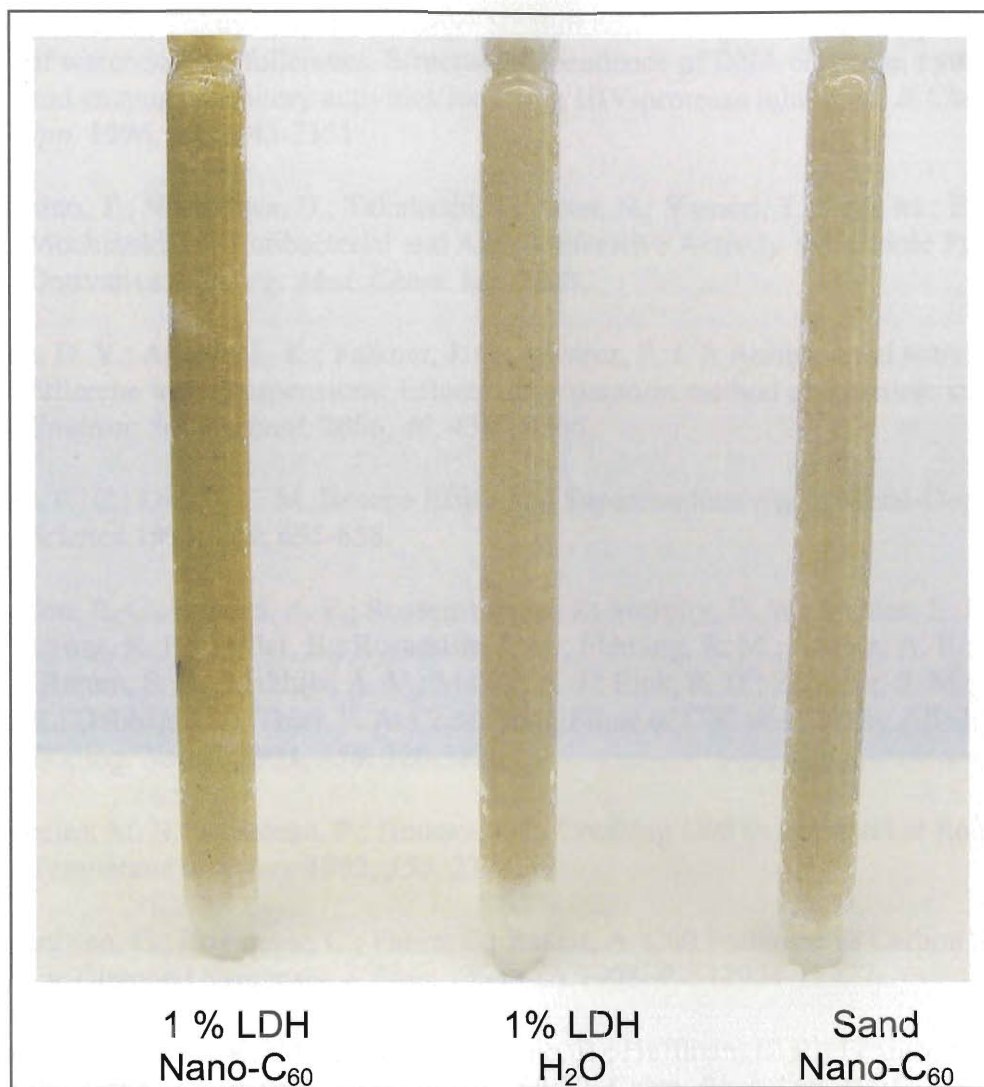


Figure 5.9 LDH association of nano-C₆₀ during 1-D column flow through experiment. **(A)** 1% (w/w) LDH-Sand at the completion of the flow through column experiment (155 minutes). **(B)** 1% (w/w) LDH-Sand with only water added. **(C)** Sand only with nano-C₆₀ at the completion of the flow through column experiment (75 minutes).

Literature Cited

1. Nakamura, E.; Tokuyama, H.; Yamago, S.; Shiraki, T.; Sugiura, Y. Biological activity of water-soluble fullerenes. Structural dependence of DNA cleavage, cytotoxicity, and enzyme inhibitory activities including HIV-protease inhibition. *B Chem. Soc. Jpn.* **1996**, *69*, 2143-2151.
2. Mashino, T.; Nishikawa, D.; Takahashi, K.; Usui, N.; Yamori, T.; Seki, M.; Endo, T.; Mochizuki, M. Antibacterial and Antiproliferative Activity of Cationic Fullerene Derivatives. *Bioorg. Med. Chem. Lett.* **2003**.
3. Lyon, D. Y.; Adams, L. K.; Falkner, J. C.; Alvarez, P. J. J. Antibacterial activity of fullerene water suspensions: Effects of preparation method and particle size. *L. Environ. Sci. Technol.* **2006**, *40*, 4360-4366.
4. Chen, C. C.; Lieber, C. M. Isotope Effect and Superconductivity in Metal-Doped C60. *Science* **1993**, *259*, 655-658.
5. Haddon, R. C.; Hebard, A. F.; Rosseinsky, M. J.; Murphy, D. W.; Duclos, S. J.; Lyons, K. B.; Miller, B.; Rosamilia, J. M.; Fleming, R. M.; Kortan, A. R.; Glarum, S. H.; Makhija, A. V.; Muller, A. J.; Eick, R. H.; Zahurak, S. M.; Tycko, R.; Dabbagh, G.; Thiel, F. A. Conducting Films of C60 and C70 by Alkali-Metal Doping. *Nature* **1991**, *350*, 320-322.
6. Regueiro, M. N.; Monceau, P.; Hodeau, J. L. Crushing C60 to Diamond at Room-Temperature. *Nature* **1992**, *355*, 237-239.
7. Bocquillon, G.; Bogicevic, C.; Fabre, C.; Rassat, A. C60 Fullerene as Carbon Source for Diamond Synthesis. *J. Phys. Chem-US* **1993**, *97*, 12924-12927.
8. Mort, J.; Okumura, K.; Machonkin, M.; Ziolo, R.; Huffman, D. R.; Ferguson, M. I. Photoconductivity in Solid Films of C60/70. *Chem. Phys. Lett.* **1991**, *186*, 281-283.
9. Tremblay, J. Mitsubishi Aims at a Breakthrough. *Chem. Eng. News* **2002**, *80*, 16-17.
10. Wharton, T.; Kini, V. U.; Mortis, R. A.; Wilson, L. J. New non-ionic, highly water-soluble derivatives of C-60 designed for biological compatibility. *Tetrahedron Lett.* **2001**, *42*, 5159-5162.
11. Iqbal, Z.; Baughman, R. H.; Ramakrishna, B. L.; Khare, S.; Murthy, N. S.; Bornemann, H. J.; Morris, D. E. Superconductivity at 45-K in Rb/Tl Codoped C60 and C60/C70 Mixtures. *Science* **1991**, *254*, 826-829.

12. Kelty, S. P.; Chen, C. C.; Lieber, C. M. Superconductivity at 30-K in Cesium-Doped C₆₀. *Nature* **1991**, *352*, 223-225.
13. Gupta, B. K.; Bhushan, B.; Capp, C.; Coe, J. V. Materials Characterization and Effect of Purity and Ion Implantation on the friction wear of Sublimed Fullerene Films. *J. Mat. Res.* **1994**, *9*, 2823.
14. Wang, Y. Photoconductivity of Fullerene Doped Polymers. *Nature* **1992**, *356*, 585-587.
15. Koruga, D.; Hameroff, S.; Withers, J.; Loufty, R.; Sundareshan, M. *Fullerene C60: History, Physics, Nanobiology, Nanotechnology*; Elsevier Science Publishers: Amsterdam, 1993.
16. Tseng, W.-Y.; Lin, J.-T.; Mou, C.-Y.; Cheng, S.; Liu, S.-B.; Chu, P. P.; Liu, H.-W. Incorporation of C₆₀ in Layered Double Hydroxide. *J. Am. Chem Soc.* **1996**, *118*, 4411-4418.
17. Mehrotra, V.; Giannelis, E. P.; Ziolo, R. F.; Rogalskyj, P. Intercalation of Ethylenediamine Functionalized Buckminsterfullerene in Mica-Type Silicates. *Chem. Mater.* **1992**, *4*, 20-22.
18. Lecoanet, H. F.; Bottero, J. Y.; Wiesner, M. R. Laboratory assessment of the mobility of nanomaterials in porous media. *Environ. Sci. Technol.* **2004**, *38*, 5164-5169.
19. Lecoanet, H. F.; Wiesner, M. R. Velocity Effects on Fullerene and Oxide Nanoparticle Deposition in Porous Media. *Environ. Sci. Technol.* **2004**, *38*, 4377-4382.
20. Cheng, X.; Kan, A. T.; Tomson, M. B. Study of C₆₀ transport in porous media and the effect of sorbed C₆₀ on naphthalene transport. *J. Mat. Res.* **2005**, *20*, 3244-3254.
21. Heymann, D. Solubility of fullerenes C-60 and C-70 in seven normal alcohols and their deduced solubility in water. *Fullerene Sci. Tech.* **1996**, *4*, 509-515.
22. Heymann, D. Solubility of C-60 in alcohols and alkanes. *Carbon* **1996**, *34*, 627-631.
23. Ruoff, R. S.; Tse, D. S.; Malhotra, R.; Lorents, D. C. Solubility of C-60 in a Variety of Solvents. *J. Phys. Chem.-Us* **1993**, *97*, 3379-3383.
24. Alargova, R. G.; Deguchi, S.; Tsujii, K. Stable Colloidal Dispersions of Fullerenes in Polar Organic Solvents. *J. Am. Chem. Soc.* **2001**, *123*, 10460-10467.

25. Andrievsky, G. V.; Kosevich, M. V.; Vovk, O. M.; Shelkovsky, V. S.; Vashchenko, L. A. On the Production of an Aqueous Colloidal Solution of Fullerenes. *J. Chem. Soc. Chem. Comm.* **1995**, 1281-1282.
26. Deguchi, S.; Alargova, R. G.; Tsujii, K. Stable Dispersions of Fullerenes, C60 and C70, in Water. Preparation and Characterization. *Langmuir* **2001**, *17*, 6013-6017.
27. Scrivens, W. A.; Tour, J. M. Synthesis of ¹⁴C-Labeled C₆₀, Its Suspension in Water, and Its Uptake by Human Keratinocytes. *J. Am. Chem. Soc.* **1994**, *116*, 4517-4518.
28. Cheng, X. K.; Kan, A. T.; Tomson, M. B. Naphthalene adsorption and desorption from Aqueous C-60 fullerene. *J. Chem. Eng. Data* **2004**, *49*, 675-683.
29. Andrievsky, G. V.; Klochkov, V. K.; Bordyuh, A. B.; Dovbeshko, G. I. Comparative analysis of two aqueous-colloidal solutions of C60 fullerene with help of FTIR reflectance and UV-Vis spectroscopy. *Chem. Phys. Lett.* **2002**, *364*, 8-17.
30. Andrievsky, G. V.; Klochkov, V. K.; Karyakina, E. L.; McHedlov-Petrossyan, N. O. Studies of aqueous colloidal solutions of fullerene C60 by electron microscopy. *Chem Phys Lett* **1999**, *300*, 392-396.
31. Fortner, J. D.; Lyon, D. Y.; Sayes, C. M.; Boyd, A. M.; Falkner, J. C.; Hotze, E. M.; Alemany, L. B.; Tao, Y. J.; Guo, W.; Ausman, K. D.; Colvin, V. L.; Hughes, J. B. C60 in Water: Nanocrystal Formation and Biological Effects. *Environ. Sci. Technol.* **2005**, *39*, 4307-4316.
32. Fortner, J. D.; Lyon, D. Y.; Sayes, C. M.; Boyd, A. M.; Falkner, J. C.; Hotze, E. M.; Alemany, L. B.; Tao, Y. J.; Guo, W.; Ausman, K. D.; Colvin, V. L.; Hughes, J. B. C60 in water: Nanocrystal formation and microbial response. *Environ. Sci. Technol.* **2005**, *39*, 4307-4316.
33. Buckmore, B. R.; Nagy, K. L.; Sandlin, P. E.; Crater, T. S. Quantifying surface areas of clays by atomic force microscopy. *Am. Mineral* **2002**, *87*, 780-783.
34. Borden, D.; Giese, R. F. Baseline studies of the clay mineral society source clays: Cation exchange capacity measurements by the ammonia-electrode method. *Clays Clay Min.* **2001**, *49*, 444-445.
35. Schroth, B. K.; Sposito, G. Surface Charge Properties of Kaolinite. *Clays Clay Miner.* **1997**, *45*, 85-91.
36. Zhou, Z.; Gunter, W. D. The Nature of the Surface Charge of Kaolinite. *Clays Clay Miner.* **1992**, *40*, 365-368.

37. Zbik, M.; Smart, R. S. C. Nanomorphology of Kaolinites: Comparitive SEM and AFM studies. *Clays Clay Miner.* **1998**, *46*, 153-160.
38. Pinnavaia, T. J., Ed. *Clay Catalyst: Opportunities for Use in Improving Environmental Quality*; CSIRO Publishing: Melbourne,, 1993.
39. Brindley, G. W.; , G. B., Eds. *Crystal Structures of Clay Minerals and their X-ray Identification*; Mineralogical Society London, 1980.

Chapter 6

Biological Interactions with Nano-C₆₀

Introduction

Research presented within this chapter evaluates the behavior of nano-C₆₀ upon exposure to selected fungal systems. Of interest are biochemical reactions that may occur including covalent derivatization to the cage structure, or transformation resulting in partial cage metabolites, and mineralization to CO₂. In addition, association processes of C₆₀ with cells including physical accumulation and sequestration are of interest.

For nano-C₆₀, biochemical transformation experiments were designed around two confounding factors: toxicity (common bacterial degradation pathways could not be considered *in vivo* based on recent toxicity observations (1,2)) and size (nano-C₆₀ aggregate size (ranging from ~5-500 nm; 90 nm for this report)). Based on this, manganese peroxidase, a cell free, non-specific oxidative enzyme (MnP, Jena Biosciences, GmbH, Germany) was chosen as a model system that had previously been shown to degrade amorphous low rank coal and lignin among a number of recalcitrant aromatic chemicals including trinitrotoluene (TNT) and a range of PAH's (3-6). The oxidizing radical mechanism of MnP is similar to other common non-specific, extracellular enzymatic systems such as Lignin Peroxidase (LiP) (7,8). In theory, the biologically catalyzed production of free radicals (as ·OH) associated with these enzymes is similar to abiotic, chemical based hydroxyl radical addition reactions with C₆₀ as observed by this lab (unpublished) and others (9).

While most cell cultures have demonstrated a toxicological response at low concentrations to nano-C₆₀ (2,10,11), a fungal contaminant discovered in an open

solution of nano-C₆₀ at Rice University was viable at relatively high concentrations of nano-C₆₀ (> 25 ppm) and tended to interact with the material. The fungus was isolated and identified by 18S rDNA. Cellular association of nano-C₆₀ in suspended cultures was investigated directly with spectral (UV-Vis, ¹³C NMR) and microscopy (TEM) analyses, along with carbon balance experiments.

Work presented in the chapter indicates that nano-C₆₀ can readily interact with certain biological systems without an acute toxic effect. Based on ¹³C NMR and TEM analyses, nano-C₆₀ was observed to accumulate outside the cell wall but within the extracellular matrix of an isolated ascomycete fungal culture. Respiration experiments suggest that C₆₀ is not utilized as a carbon source by this culture. Furthermore, cell free, peroxidase experiments did not observe a measurable transformation in nano-C₆₀.

Materials and Methods

Nano-C₆₀

Detailed protocols regarding the synthesis and standard characterization procedures, including UV-Vis, dynamic light scattering (DLS) and transmission electron microscopy (TEM) are provided by Fortner *et al.* (Chapter 3) (12). Individual batches for these studies were prepared with ultra-pure (>18 Ω) water with an unadjusted pH of ~5.0 (>18.0 Ω) added to rapidly stirred C₆₀ saturated THF at 500 mL/min. After distilling the THF, filtering sterilization, and characterization (DLS, UV-Vis), individual batches were homogenized and stored in PVP containers in the dark (12).

In vitro Enzymatic Studies

Enzyme assays were performed with a manganese peroxidase (MnP) (Jenna bioscience, Germany) purified from the ligninolytic, basidiomycete *Nematoloma frowardii*, as described elsewhere (3-6,13). This well characterized enzyme was chosen for its ability to degrade complex carbon macromolecules including lignin and low rank coal via non-specific radical ($\cdot\text{OH}$) oxidation. Assays were prepared with aqueous suspensions of nano-C₆₀ as described above (5.0 mg/L C₆₀, 90 nm average aggregate size) (12,14).

Kinetic studies were done with a NIR/UV/Vis spectrophotometer (Varian Cary 5000) at room temperature and corrected for the appropriate background, measuring absorption as a function of wavelength (200-900 nm, 0.5 nm intervals) with time (only 0 and 48 hour time points are shown). The degradation of humic acid, measured at 450 nm, acted as a positive control confirming enzyme activity (4). Negative controls consisted of heat denatured enzyme and no enzyme.

In vivo Studies

Discovered as a contaminate in an open aqueous system of nano-C₆₀, a fungal culture was isolated and stored on PDA plates at 4°C and suspended in 50% glycerol at -20°C for later studies and identification. Identification was done by AMODIA Bioservice GmbH (Braunschweig, Germany) based on 18S rDNA sequencing. Experiments included measurements of nano-C₆₀ fungal uptake; transmission electron microscopy (TEM) to discern physical and spatial dynamics of association; and NMR analysis of the nano-C₆₀ laden biomass to identify C₆₀ and possible derivatized and/or conjugated fullerenes. In addition, respirometry studies coupled with TOC measurements investigated fungal

growth in the presence of nano-C₆₀ with the goal of a carbon mass balance to assess possible C₆₀ metabolism.

Initial uptake studies consisted of simple nano-C₆₀ (suspended) measurements with and without (control) a fungal inoculum. Briefly, reactors containing C₆₀ suspensions were inoculated (ca. 1-2 mg) with isolated fungi from a refrigerated (4°C) slant (resting). Reactors were covered with aluminum foil and gently stirred at < 300 rpm. Aqueous samples (2 mL) were taken daily to monitor C₆₀ concentration (plotted as C/C₀) at 340 nm (filtered 0.45 μm, PES to remove biomass). Additional studies were conducted similarly but with nutrient amendment: adding (1:10 v/v) of stock (10×) = 0.70 g K₂HPO₄, 0.20 g KH₂PO₄; 1 g NH₄SO₄; 0.1g MgSO₄·7H₂O; 0.05 NaCl per 1L along with trace elements: 0.05 mg ZnCl₂, 0.05 MnCl₂·4H₂O, 0.05 mg H₃BO₃; 0.25 mg CoCl₂·6H₂O; 0.05 mg NiCl₂·6H₂O; 0.05 mg Na₃MoO₄·2H₂O per L. The carbon source is hypothesized to be residual THF or oxidized THF (probable 3,4-diol furan via NMR and MS analysis data not shown) in solution remaining from incomplete distillation as measured by TOC. In some instances, cultures were sacrificed for other analysis (NMR, TEM) once appreciable nano-C₆₀ association had occurred. Biomass was separated for NMR analyses via filtration through glass wool and then washed five times with 200 mL aliquots of ultra pure water with appropriate minimal mineral media previously described to avoid osmotic disturbances.

TEM micrographs of fungal association were taken at ETH Zurich, Institute for Applied Physics by Dr. Andres Kaech and Liliane Diener. Suspended samples were prepared via a cryo-immobilization, which involves a high pressure, low temperature solvent exchange process allowing for the fixation biological samples in a resin

(Epon/Araldite) as described by others (15), albeit slightly modified (specimens were not frozen in cellulose capillary tubes but directly in the aluminum specimen carriers with hexadecene as filler). The rapid drop in pressure and temperature (termed cryofixing) maintains a high level of integrity throughout the cell, allowing for a solvent exchange and eventual resin embedding of the sample that can then be cross sectioned (ca. 70 nm sections) via microtomy. Sections were stained with uranylacetate and lead citrate.

¹³C NMR studies were done at the Georgia Institute of Technology, School of Polymer, Textile & Fiber Engineering in collaboration with Dr. Johannes Leisen. Samples were prepared as follows: Solutions with nano-C₆₀, synthesized with both enriched ¹³C (25%) and with natural abundance ¹³C (~1%), and minimal nutrients were prepared as described above. Washed biomass with associated nano-C₆₀ (prepared as described above) was blotted semi dry on filter paper and loaded into a 4 mm ZrO₂ MAS NMR rotor. Solid phase ¹³C NMR was performed using a Bruker AMF 400 instrument equipped with a 9.4 T superconducting magnet and a 5 mm broad-band probe. ¹H-decoupling was used and the instrument was manually shimmed to achieve optimal peak shape. The spinning speed was 10 kHz and a simple Bloch decay pulse sequence was used with a $\pi/2$ pulse of 5 μ sec and an optimized pulse recycle delay of 5 seconds. Number of scans used in analyte detection was 13,368 and 14,295 for enriched and natural abundance samples, respectively. All chemical shift values are provided in reference to TMS.

All respirometry and TOC studies described were completed as described previously (16). Experiments were operated in 200 mL batch setup (in duplicate, 10 total) simultaneously as described previously for association experiments with source inoculum

(ca. 1-2 mg) and media amendment. As variables, four potential carbon sources were examined to delineate the carbon/energy source utilized by the fungal culture: 1.) Nano-C₆₀ stock solution taken after THF distillation containing 48.11 mg/L TOC (6.5 mg/L as nano-C₆₀ and 41.5 mg/L dissolved carbon, 0.02 μm cutoff); 2.) Dissolved carbon (41.5 mg/L TOC), filtrate from the nano-C₆₀ suspension that had passed through a 0.02 membrane (20 nm, Anodisc 47 mm, Whatman); 3.) Tetrahydrofuran (THF) at 100 mg/L (HPLC grade, Spectra Analyzed, Fisher Scientific); 4.) Water soluble fullerol (C₆₀(OH)₂₂₋₂₄, MER Corp.) at 88 mg/L TOC; 5.) Suspended nano-C₆₀ at 6.54 mg/L TOC separated > 0.02 nm (20 nm, Anodisc 47 mm, Whatman).

Results and Discussion

Results by from this work and others indicate that that C₆₀ as nano-C₆₀ suspended in water can interact with biological systems (1,2,10,11). However, results from enzymatic studies with MnP described here do not indicate a measurable change in parent material (underivatized C₆₀) as measured by C/C₀ at a characteristic fullerene peak (as a nano-scale aggregate at 340nm) over time (Figure 6.1). A positive control showed the degradation of humic acid at 450 nm confirming enzyme activity (Figure 6.2). MnP experiments were performed in triplicate and the entire experiment was done twice. These results, taken along with findings during ozonation experiments (Chapter 4), indicate that hydroxyl radical reaction kinetics with nano-C₆₀ in water are relatively slow, if possible at all. These observations suggest that as a colloidal suspension in water, the chemical reactivity of C₆₀ may differ from what is known for molecular C₆₀ dissolved in a non-polar solvent(s) and/or that reaction kinetics will differ based on surface to volume

ratios (compared to dissolved C₆₀ in non-polar solvents). Possible other nonspecific biochemical radical reactions that should be considered in future studies include nitration via radical nitrogen species such as ·NO₂ as observed by others (17-19) which has similarly been demonstrated to efficiently derivatize C₆₀ in abiotic scenarios (20,21).

A fungal contaminant, which was viable at relatively high concentrations of nano-C₆₀ (> 25 ppm), was isolated and identified by 18S rDNA analysis to be an ascomycete species, *Sagenomella verticillata*. Initial observations indicated uptake/association of nano-C₆₀ by the fungal biomass. In the presence of active fungal culture which required nutrient amendment, nano-C₆₀ was removed from suspension and increasingly associated with fungal biomass. Figure 6.3 presents the loss of nano-C₆₀ in the aqueous phase in the presence of the fungal culture over time. This fact was verified by UV-Vis analysis of suspended (unassociated) nano-C₆₀ at 340 nm (filtering the biomass at 0.45 μm) decreasing over time (Figure 6.3B). Visually, the yellow-orange color associated with the C₆₀ suspension decreased as fungal biomass increased when compared with a sterile suspension (Figure 6.3A). Fungal biomass was a dark-orange color when grown in the presence of C₆₀ (Figure 6.3A), where biomass grown without C₆₀ was white (not shown). Suspended C₆₀ remained stable in control reactors which were inoculated but did not receive nutrient addition (*i.e.* biomass growth slow, if at all) and fungal growth was not observed with media amendment only (C₆₀ suspension was not added) (Figure 6.3A).

Transmission electron microscopy (TEM) studies of this uptake process provided insight as to where the aggregates were associating (Figures 6.4 A-C). These images clearly demonstrate that the nano-C₆₀ associates outside of the cell wall but within an extra-cellular matrix as the cells were thoroughly washed before analysis. NMR studies

of the association phenomenon were performed in parallel to TEM studies using ^{13}C enriched (25% ^{13}C) nano- C_{60} in addition to natural abundance nano- C_{60} ($\sim 1\%$ ^{13}C) (Figure 6.5). Based on differential sensitivities, ^{13}C enriched material (top) allows for relatively easy comparison to the natural abundance associated material (bottom), highlighting with greater intensity those peaks associated with C_{60} shifts from other biological carbon shifts. Results support previous conclusions in that nano- C_{60} is associated with the fungal biomass as indicated by the strong shift centered at approximately 146 ppm in both the natural abundance and ^{13}C enriched samples. Associated ^{13}C enriched samples showed a considerable broadening in the parent peak (ca. 138-155 ppm) when compared to both the natural abundance and even other ^{13}C enriched nano- C_{60} ^{13}C NMR spectra (Chapters 3 and 4). Additionally, a broad shift 115-125 ppm region and two small shifts at approximately 43 and 40 ppm appear in the enriched sample both of which are minor (with regard to area) in comparison to the parent peak (146 centered). It remains unclear if these observations are in relation to a new bonding environment (*e.g.* conjugative, derivative, etc.) or even perhaps a change in aggregate structure (*e.g.* crystalline to amorphous).

Respirometry studies indicate that the fungi is using available dissolved organic carbon, as THF residual (oxidized THF as probable 3,4-diol furan), termed here simply as dissolved carbon, as the primary carbon and energy source and not C_{60} (Figure 6.6, 6.7). Mass balance calculations indicate that an appreciable portion of the total TOC is being utilized and even mineralized (47% of total TOC) (Figure 6.7). However when the dissolved portion of the TOC is separating via filtration (20 nm cutoff, Anodisc 47 mm, Whatman) from the suspended nano- C_{60} portion, CO_2 production is shown to be

dependant on the dissolved organic carbon (42% of total TOC as CO₂, visual growth) and not the suspended nano-C₆₀ (-1.6% of total TOC, no visual growth). In addition, THF (HPLC grade, Spectra Analyzed, Fisher Scientific) and water soluble, hydroxylated fullerenes (fullerol as C₆₀(OH)₂₂₋₂₄, MER Corp.) were similarly tested as potential carbon sources (at similar concentrations) with media amendment and fungus inoculum (Figures 6.6, 6.7). Results based on CO₂ production and visual growth estimates indicate that the fungus is not capable of mineralizing either of material. This strengthens the conclusion that the original dissolved carbon source is not C₆₀ or simply THF but rather a THF derivative (oxidized).

Figure 6.1

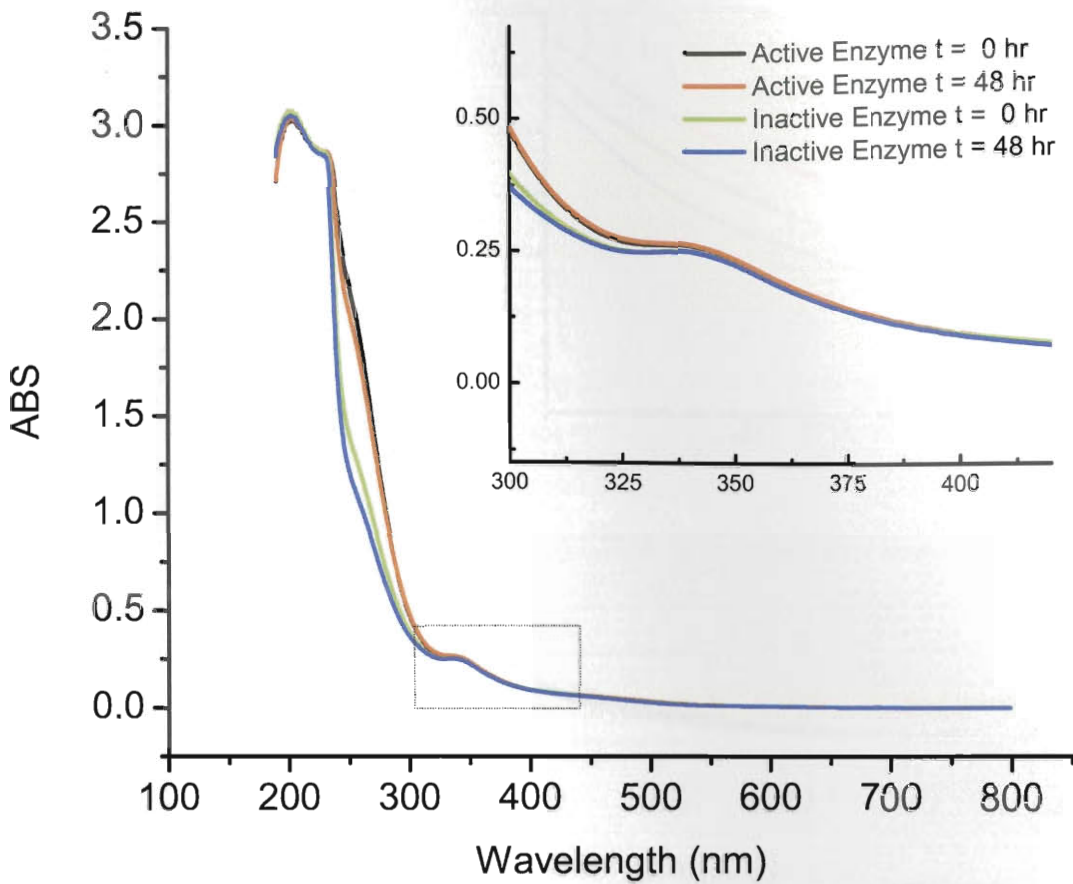


Figure 6.1 UV-Vis analyses of the MnP activity with nano-C₆₀ over 48 hours. Negative control includes denatured enzymes over the same time.

Figure 6.2

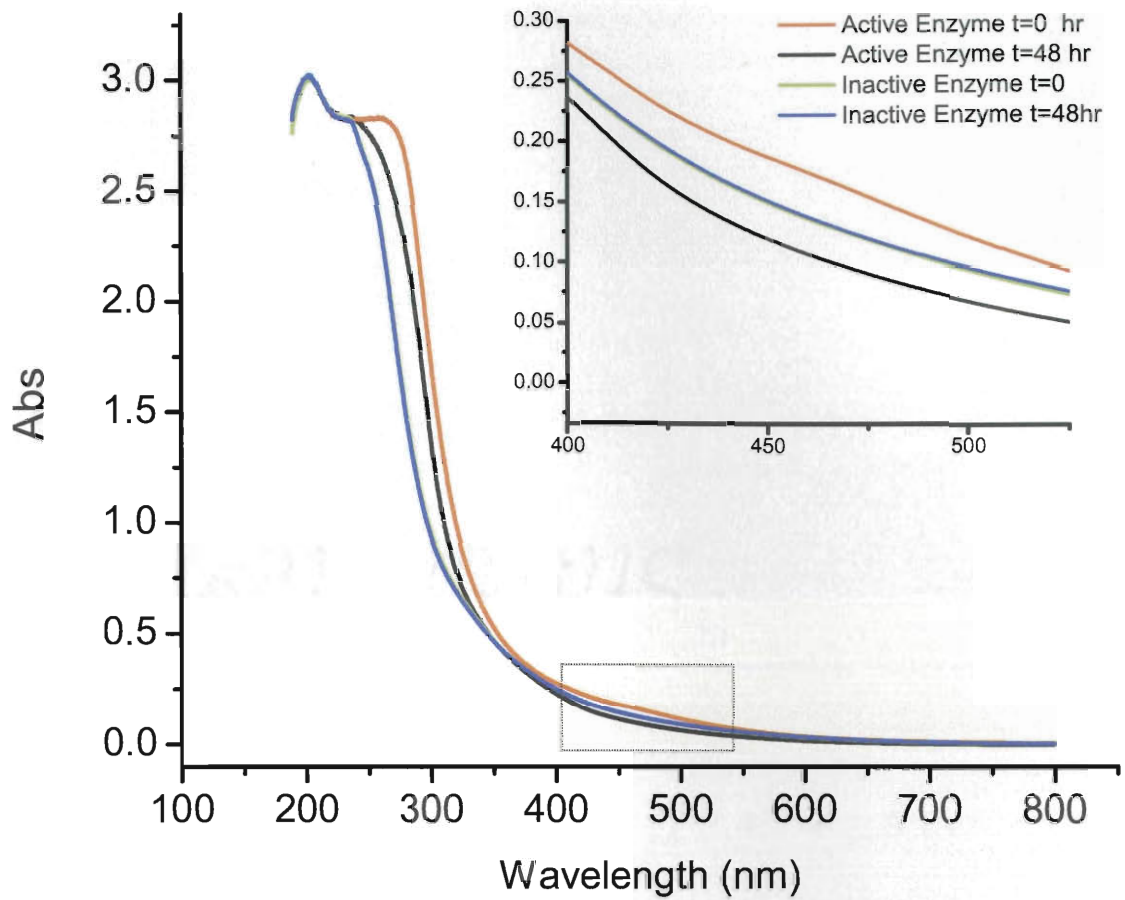


Figure 6.2 UV-Vis analyses of the MnP positive control: degradation of humic acid as measured at 450 nm over 48 hours. Negative control includes denatured enzymes.

Figure 6.3

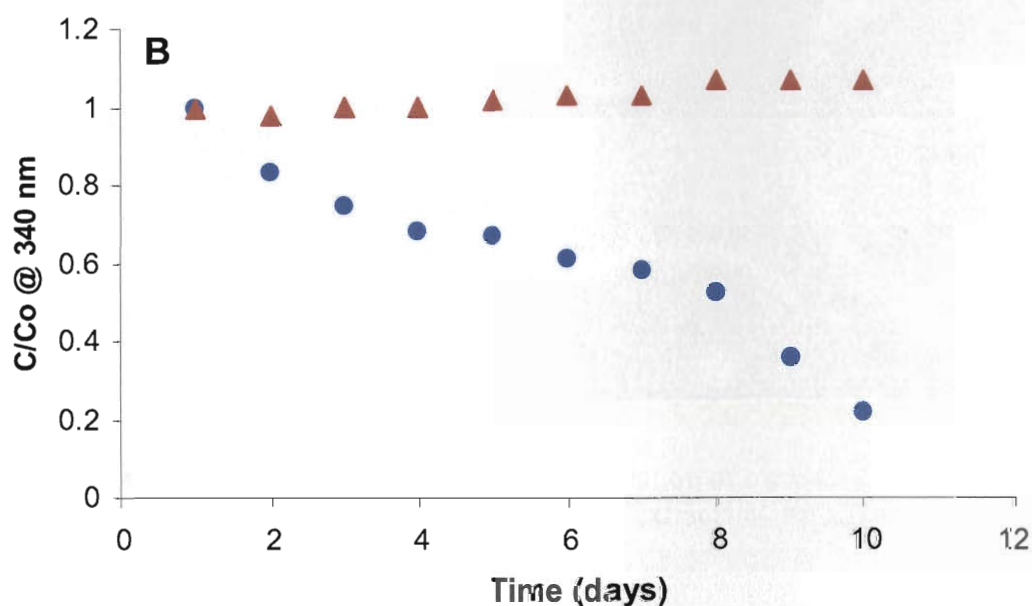
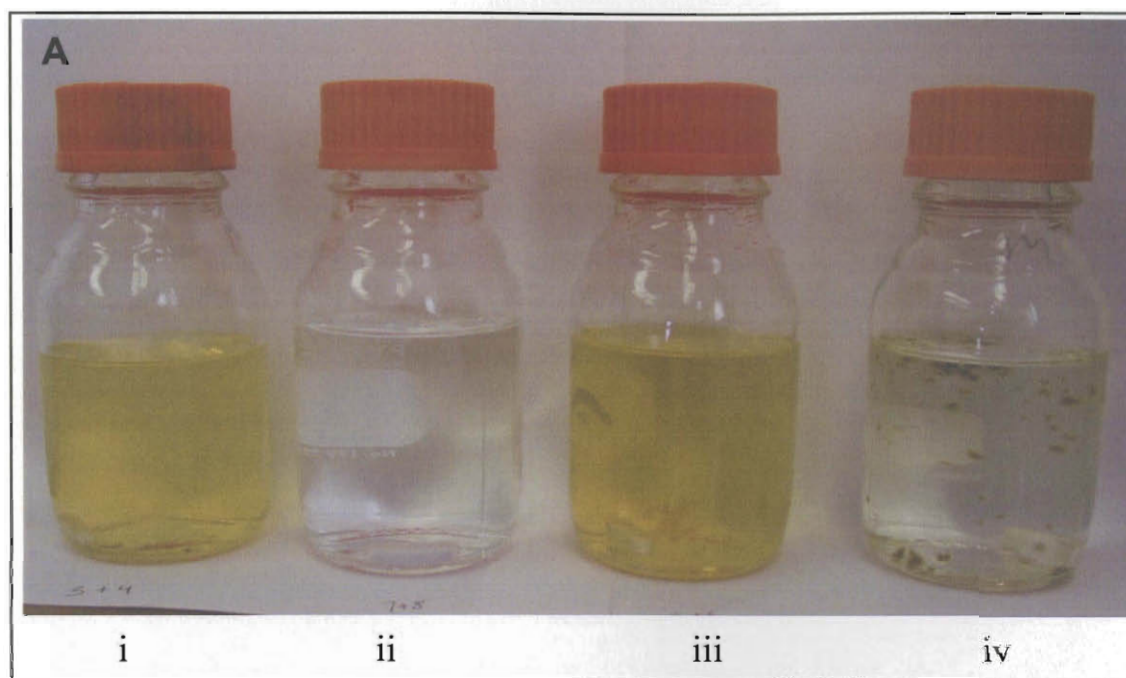


Figure 6.3 (A) Visual observations of fungal association: From left to right **i)** Nano- C_{60} in solution with media amendment and no fungal inoculum. **ii)** Media amendment with inoculum but no nano- C_{60} or any dissolved carbon. **iii)** Nano- C_{60} with inoculum but no media amendment. **iv)** Nano- C_{60} with mineral amendment and fungal inoculum. **(B)** Typical loss of nano- C_{60} absorbance at 340 nm over 10 days with fungal inoculum ($>5 \text{ mg}$) and media amendment (●) and without inoculum (▲).

Figure 6.4 A



Figure 6.4 A TEM micrograph of fungal association of nano-C₆₀. Nano-C₆₀ appears to associate outside of the cell wall but within the extracellular matrix.

Figure 6.4 B

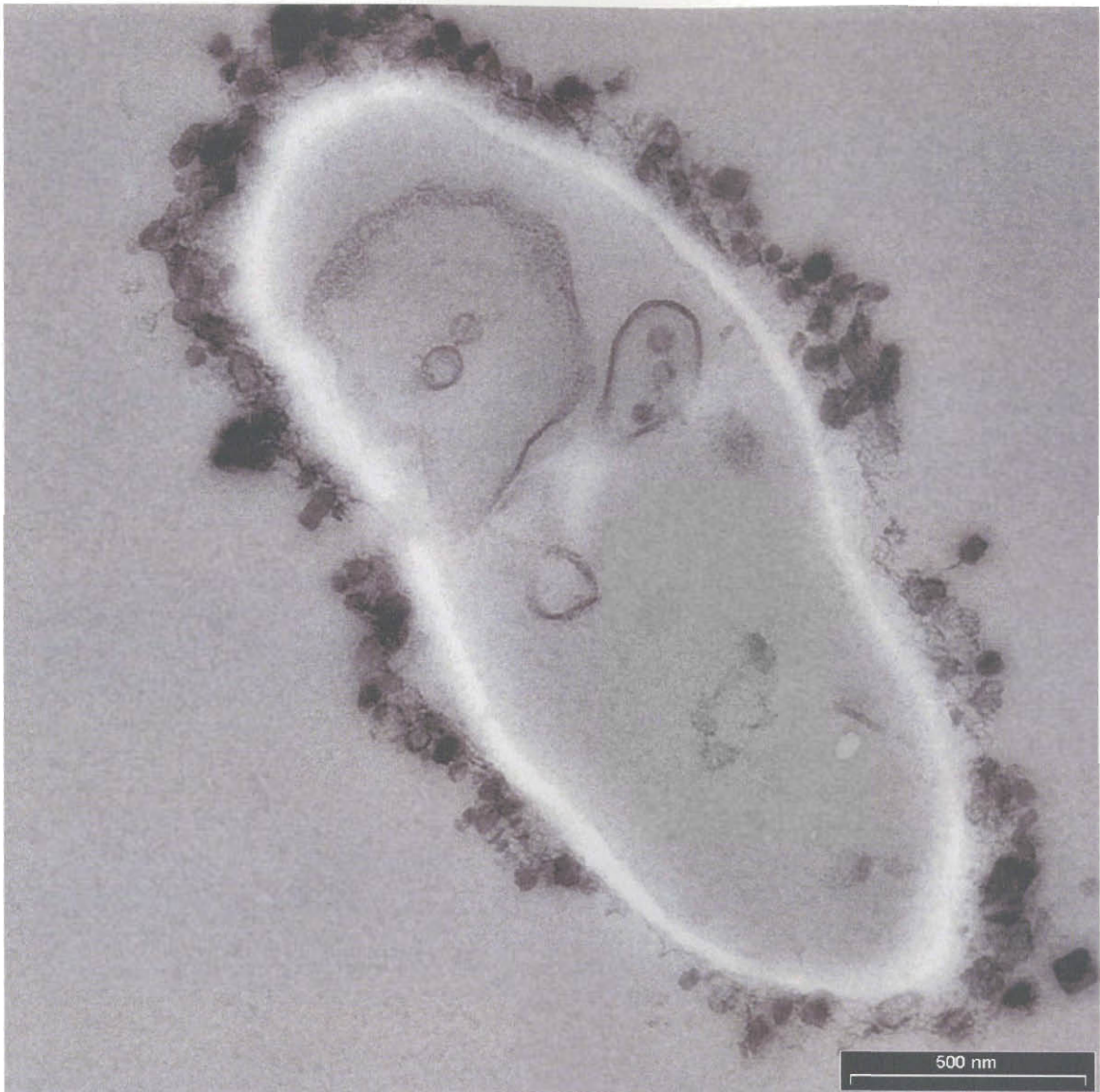


Figure 6.4 B TEM micrograph of fungal association with nano-C₆₀. Nano-C₆₀ appears to associate outside of the cell wall but within the extracellular matrix.

Figure 6.4 C

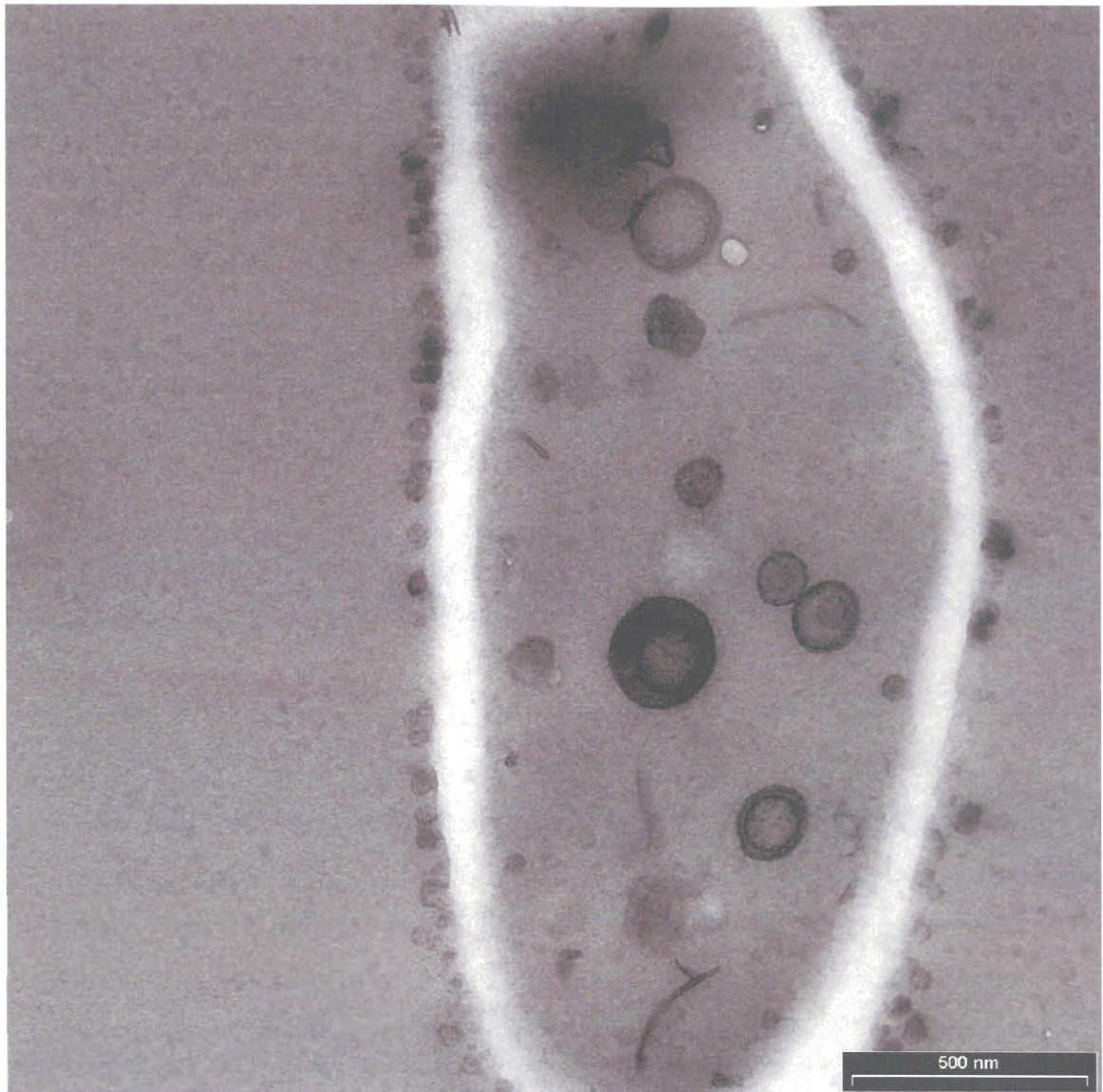


Figure 6.4 C TEM micrograph of fungal association with nano-C₆₀. C₆₀ appears to associate outside of the cell wall but within the extracellular matrix.

Figure 6.5

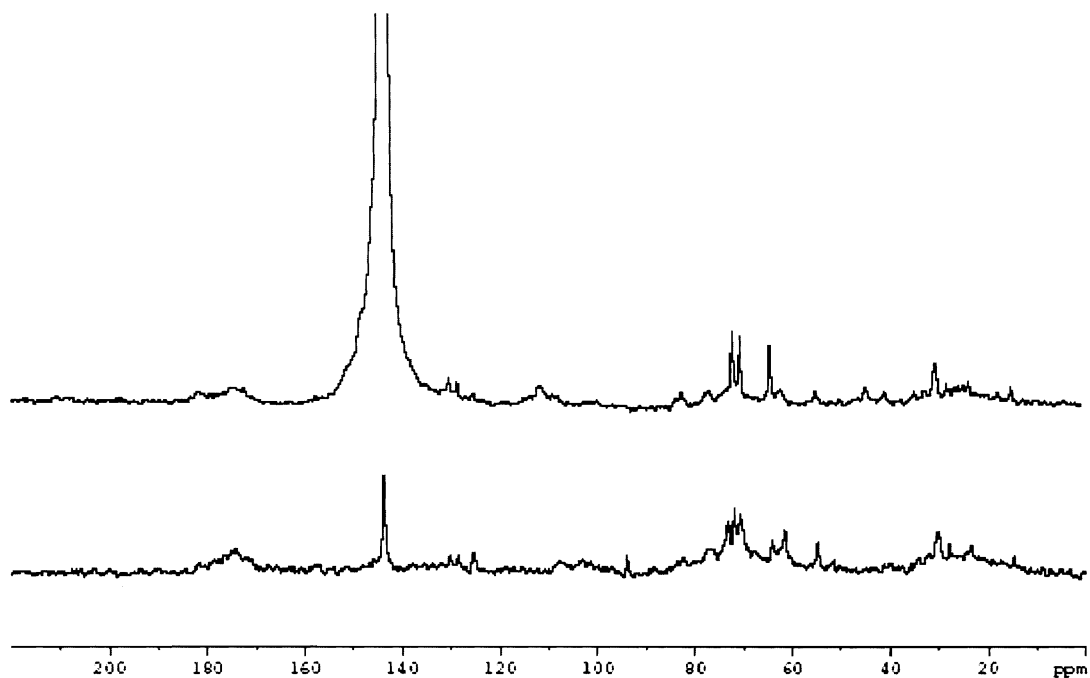


Figure 6.5: Solid-state ^{13}C -NMR analysis of nano- C_{60} fungal association. Directly, C_{60} can be identified by characteristic shift at approximately $\sim 143\text{-}146$ ppm shift from TMS. **Top:** ^{13}C Enriched ($\sim 25\%$) nano- C_{60} associated with fungal biomass. **Bottom:** Natural abundance ($\sim 1\%$ ^{13}C) nano- C_{60} associated with fungal biomass.

Figure 6.6

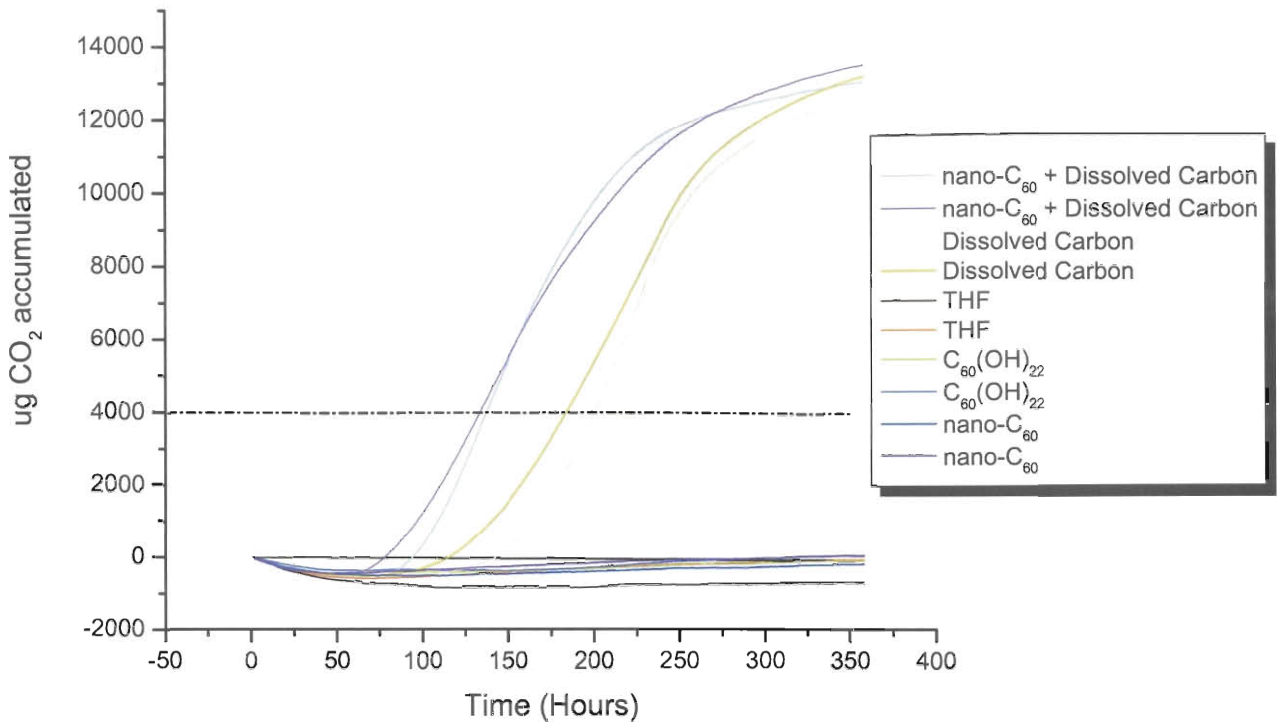


Figure 6.6 CO₂ (as Accumulation) from Fungal Metabolism:

From top to bottom:

Nano-C₆₀ and dissolved carbon (**nano-C₆₀ + Dissolved Carbon**)

Dissolved Carbon with no nano-C₆₀ (< 20 nm filtered) (**Dissolved Carbon**)

THF as the only Carbon and energy source (**THF**)

Hydroxylated C₆₀(OH)₂₂₋₂₄ as the only C and energy source (**C₆₀(OH)₂₂₋₂₄**)

Nano-C₆₀ separated from all other dissolved carbon (> 20 nm filtered) (**nano-C₆₀**).

*All experiments were done simultaneously with minimal media as described previously.

** The dashed line represents the theoretical amount of CO₂ if only C₆₀ in solution was completely mineralized.

Figure 6.7

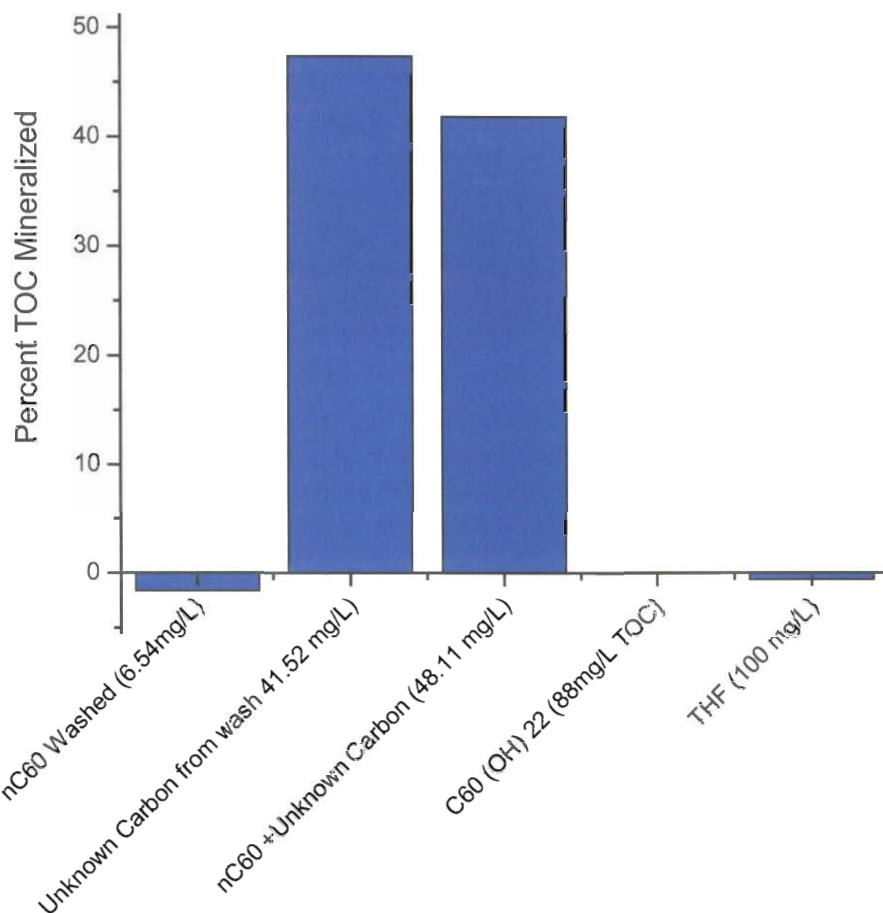


Figure 6.7 Percent of TOC Mineralized from Respirometry Studies:

From left to right:

Nano-C₆₀ separated from other dissolved carbon (>20 nm) (**nano-C₆₀**)

Dissolved carbon with no nano-C₆₀ (< 20 nm) (**Dissolved Carbon**)

Both nano-C₆₀ and dissolved carbon (**nano-C₆₀ + Dissolved Carbon**)

Hydroxylated C₆₀(OH)₂₂₋₂₄ as the only Carbon and energy source (**C₆₀(OH)₂₂₋₂₄**)

THF as the only Carbon and energy source (**THF**).

*All experiments were done simultaneously with minimal media as described previously.

Literature Cited

1. Lyon, D. Y.; Adams, L. K.; Falkner, J. C.; Alvarez, P. J. J. Antibacterial activity of fullerene water suspensions: Effects of preparation method and particle size. *L. Environ Sci Technol* **2006**, *40*, 4360-4366.
2. Lyon, D. Y.; Fortner, J. D.; Sayes, C. M.; Colvin, V. L.; Hughes, J. B. Bacterial Cell Association and Antimicrobial Activity of a C60 Water Suspension. *Environmental Toxicology and Chemistry* **2005**, *24*, 2757-2762.
3. Hofrichter, M.; Fritsche, W. Depolymerization of low rank coal by extracellular fungal enzyme systems. I. Screening for low-rank-coal depolymerizing activities. *Appl. Microbiol. Biotechnol.* **1996**, *46*, 220-225.
4. Hofrichter, M.; Fritsche, W. Depolymerization of low-rank coal by extracellular fungal enzyme systems. III. In vitro depolymerization of coal humic acids by a crude preparation of manganese peroxidase from white-rot fungus *Nematoloma forwardii* b19. *Appl. Microbiol. Biotechnol.* **1997**, *47*, 566-571.
5. Hofrichter, M.; Fritsche, W. Depolymerization of low-rank coal by extracellular fungal enzyme systems .II. The ligninolytic enzymes of the coal-humic-acid-depolymerizing fungus *Nematoloma frowardii* b19. *Appl Microbiol Biot* **1997**, *47*, 419-424.
6. Hofrichter, M.; Scheibner, K.; Schneegab, I.; Fritsche, W. Enzymatic Combustion of Aromatic and Aliphatic Compounds by Manganese Peroxidase from *Nematoloma frowardii*. *Applied and Environmental Microbiology* **1998**, *64*, 399-404.
7. Tien, M.; Kirk, T. K. Lignin Peroxidase of *Phanerocheate chrysosporium*. *Methods of Enzymology* **1988**, *161*, 238-249.
8. Tien, M.; Kirk, T. K. Lignin-degrading enzyme from hymenomycete *Phanerocheate chrysosporium*. *Science* **1983**, *221*, 661-663.
9. Chiang, L. Y.; Bhonsle, J. B.; Wang, L.; Shu, S. F.; Chang, T. M.; Hwu, J. R. Efficient One-Flask Synthesis of Water-Soluble [60]Fullerenols. *Tetrahedron* **1996**, *52*, 4963-4972.
10. Fortner, J. D.; Lyon, D. Y.; Sayes, C. M.; Boyd, A. M.; Falkner, J. C.; Hotze, E. M.; Alemany, L. B.; Tao, Y. J.; Guo, W.; Ausman, K. D.; Colvin, V. L.; Hughes, J. B. C60 in Water: Nanocrystal Formation and Biological Effects. *Environ. Sci. Technol.* **2005**, *39*, 4307-4316.
11. Sayes, C. M.; Fortner, J. D.; Guo, W.; Lyon, D.; Boyd, A. M.; Ausman, K. D.; Tao, Y. J.; Sitharaman, B.; Wilson, L. J.; Hughes, J. B.; West, J. L.; Colvin, V. L. The

- Differential Cytotoxicity of Water-Soluble Fullerenes. *Nanolett* **2004**, *4*, 1881-1887.
12. Fortner, J. D.; Lyon, D. Y.; Sayes, C. M.; Boyd, A. M.; Falkner, J. C.; Hotze, E. M.; Alemany, L. B.; Tao, Y. J.; Guo, W.; Ausman, K. D.; Colvin, V. L.; Hughes, J. B. C-60 in water: Nanocrystal formation and microbial response. *Environ Sci Technol* **2005**, *39*, 4307-4316.
 13. Hofrichter, M.; Scheibner, K.; Schneegab, I.; Ziegenhagen, D.; Fritsche, W. Mineralization of synthetic humic substances by manganese peroxidase from the white-rot fungi *Nematoloma frowardii*. *Appl Microbiol Biot* **1998**, *49*, 584-588.
 14. Alargova, R. G.; Deguchi, S.; Tsujii, K. Stable Colloidal Dispersions of Fullerenes in Polar Organic Solvents. *J. Am. Chem. Soc.* **2001**, *123*, 10460-10467.
 15. Hohenberg, H.; Mannweiler, K.; Muller, M. High-Pressure Freezing of Cell Suspensions in Cellulose Capillary Tubes. *Journal of Microscopy* **1994**, *175*, 34-43.
 16. Fortner, J. D.; Zhang, C. L.; Spain, J. C.; Hughes, J. B. Soil column evaluation of factors controlling biodegradation of DNT in the vadose zone. *Environ Sci Technol* **2003**, *37*, 3382-3391.
 17. Nishino, S. F.; Spain, J. C. Biodegradation of 3-Nitrotyrosine by Burkholderia sp. Strain JS165 and Variovorax paradoxus JS171. *Appl Environ Microbiol* **2006**, *72*, 1040-1044.
 18. Kers, J. A.; Wach, M. J.; Krasnoff, S. B.; Widom, J.; Cameron, K. D.; Bukhalid, R. A.; Gibson, D. M.; Crane, B. R.; Loria, R. Nitration of a peptide phytotoxin by bacterial nitric oxide synthase. *Nature* **2004**, *429*, 79-82.
 19. Buddha, M. R.; Tao, T.; Parry, R. J.; Crane, B. R. Regioselective nitration of tryptophan by a complex between bacterial nitric-oxide synthase and tryptophanyl-tRNA synthetase. *J Biol Chem* **2004**, *279*, 49567-49570.
 20. Chiang, L. Y.; Upasani, R. B.; Swirezewski, J. W. Versatile Nitronium Chemistry for C60 Fullerene Functionalization. *J. Am. Chem. Soc.* **1992**, *114*, 10154-10157.
 21. Wang, N.-X. Review on the Nitration of [60]Fullerene. *Propellants, Explosives, Pyrotechnics* **2001**, *26*, 109-111.

Chapter 7

Conclusions

Research presented within this thesis expands what is currently known about fullerenes in aqueous systems as suspended aggregates. Organized by focus, summarized findings include:

Characterization

- Nano-C₆₀ is an ordered, crystalline structure comprised of underivatized C₆₀.
 - ¹³C NMR spectrum of suspended nano-C₆₀ demonstrates a single shift at 146 ppm, characteristic of underivatized C₆₀ (*I_h* symmetry).
 - A single peak at 720 is observed for nano-C₆₀ analyzed by LDI mass spectroscopy.
 - Mild oxidizing agents can destabilize nano-C₆₀, increasing extraction efficiencies into a non-polar phase.
 - ClO₄⁻ was found to be the most efficient nano-C₆₀ destabilizing agent (94-101% recovery of C₆₀ into toluene).
 - Faceted structures observed via TEM along with diffraction analyses indicate a crystalline structure.
 - Based on diffraction patterns, *d*-spacing calculations suggest a simple hexagonal unit cell.
- The size and stability of these materials are affected by conditions of formation which include the rate of water addition and solution pH.

- In line with the aggregation mechanism suggested by Alargova, *et al.* (2001), aggregate size is correlated to the Δ solution polarity (*i.e.* as the rate of water addition was slowed to the THF solution, aggregate size increased).
- Aggregation was observed over a range of pH values (5-9), with no effect on aggregate size.
 - pH values outside this range, do not appear to have an impact on aggregate size; a lower value (3.75) gives rise to larger aggregates, a higher pH value (10.25) produces smaller aggregates.
- After formation, aggregate stability can be a function of ionic strength.
 - Ionic strengths ranging from 0.001 – 0.01 *I* do not affect the aggregate size or stability over 110 days.
 - At 0.05 *I* aggregation clustering is observed (*i.e.* average diameter increased) but remained as a stable over 110 days. At higher ionic strengths (>0.1 *I*), aggregate precipitation out of solution is observed.

Reactivity

- C₆₀, as nano-C₆₀, is susceptible to ozonation in water over a range of pH values (5.6-8.9).
 - Loss of characteristic UV peaks (260, 340 nm) is observed during ozonation.
 - The total reaction proceeds with variable rate constants.
 - A large number of reactions and partitioning scenarios to consider.
 - A higher solution pH (8.9) may increase the rate of ozonolysis.
- Aggregate size and integrity are a function of ozone contact time.
 - Final products (≥ 150 CT (mg O₃-min/L)) are less than 5 nm in diameter.

- Reaction products are water soluble, molecular fullerene oxides ($C_{60}(O)_y(OH)_x$, $y + x \sim 29$).
 - A 60 carbon skeleton remains in the product structure.
 - A mixture of mono- and di-oxygenated carbons (18%, 30% respectively) are present
 - Functional groups include, hydroxyl and carbonyl groups
 - A hemiketal arrangement is suggested as observed by other highly oxidized fullerenes.
 - Product solubility in water is increased by a factor of 10^{11-12} compared to parent C_{60} .
 - Carbonyl dipole(s) and acidic protons from hydroxyl groups increase solubility in water.
 - pH decreases with an increase in product concentration.

Mineral Surface Interactions

- Nano- C_{60} interactions with mineral surfaces were observed to be a function of available surface area and charge.
 - Based on opposite surface charges, nano- C_{60} readily associates with positively charged LDH.
 - Association with other minerals surfaces (net negatively charged) appeared to be a function of surface area and/or positive edge charges.

Biological System Interactions

- Cell free enzyme studies with a well characterized manganese peroxidase (MnP) did not transform C_{60} , as suspended nano- C_{60} , within detection limits.
- Facile fungal (*Sagenomella verticillata*.) association of nano- C_{60} *in vivo* was observed at the fungal cell wall.
 - ^{13}C NMR analysis confirmed C_{60} association.

- Widening of the parent peak centered at 146, a broad shift at 115-125 ppm region and two small shifts at approximately 43 and 40 ppm shift may be associated with new bonding environments (*i.e.* conjugation or derivatization).
- Respirometry studies coupled with TOC measurements suggest that C₆₀ (as nano-C₆₀) is not metabolized by this fungus.
 - Fungal growth is supported by residual THF oxide.
- Nano-C₆₀ can be inhibitory to common Gram positive and Gram negative bacteria cultures (*B. subtilis* and *E. coli* respectively).
 - Nano-C₆₀ inhibited growth at 0.4 mg/L in both cultures and decreased cellular respiration at 4.0 (*E. coli*) and 0.4 mg/L (*B. subtilis*).

In summary, this work demonstrates that C₆₀, as a model engineered carbon nanomaterial, can behave differently in aqueous matrixes than what is expected based on classic estimation parameters. Stabilization of fullerene aggregates in water opens to a number of transport, reactive and interaction scenarios which are otherwise improbable. While a limited number of studies were presented in this work, these results do provide answers to fundamental questions regarding composition and reactivity along with demonstrating direct interactions with mineral surfaces and biological systems. In addition, it is expected that these developed methodologies will be widely applicable in future studies of C₆₀ and similar materials. Taken together, this body of work contributes to the ongoing dialogue regarding the safe and effective handling of engineered nanomaterials, particularly carbon based, which are widely expected to grow in application in the future.

Chapter 8:

Engineering Significance

This work demonstrates that the environmental fate, distribution, reactivity and biological risk associated with this important class of engineered nanomaterial will require a model which addresses not only the properties of bulk C₆₀, but that of the aggregate form generated in aqueous media. Currently, most engineered nanomaterials, including C₆₀, are handled and disposed according to guidelines established for their bulk counterparts; these guidelines may need to be revisited. Proactive characterization of the environmental chemistry and associated ecological risk of engineered nanomaterials, before their use is widespread, ensures an environmentally sustainable and socially beneficial nanotechnology industry.

Chapter 9:

Future Work Recommendations

Based upon work presented in previous chapters, it is recommended that three areas of research regarding nano-C₆₀ research are continued. These areas hold promise into fundamental reactivity, formation and biological behavior(s) of these materials in water.

Reduction Reactions in Water

Fullerenes are generally considered to be electron deficient and due the HOMO-LUMO gap in the electronic structure are easily reduced as discussed previously (1,2). Such a reduction, forming a negatively charged fulleride, has been widely documented with C₆₀ⁿ⁻ (n = 1-6) (3-5) in various solvents with supporting electrolytes, with C₆₀¹⁻ observed in degassed water (6). Compared to oxidation reactions, reduction reactions with neutral fullerenes should occur more readily. Along these lines, recommended future research includes model abiotic reactions with well characterized, relevant reducing chemistries such as zero valent iron (ZVI), palladium, Al-Ni alloy, tin, zinc powder or sodium hydrosulfite (2,6,7). Additionally, such reactions will shed light on the potential for the biotic (microbial) reduction of fullerenes, either directly by anaerobic bacteria (probable extracellular processes) or indirectly by reducing compounds produced by such bacteria (8-13).

Surface Charge Source

As touched on briefly in the literature review, the surface charge mechanism is still not well understood. Additional work is recommended to produce empirical evidence of such a charge source which may prove useful not only in C₆₀ aggregated systems in polar

solvents, but other fullerene and perhaps carbon nanotubes - polar solvent interactions. Specifically, I would suggest expanding what is known regarding the aggregation process in other polar solvents as Alargova *et al.* (14) first demonstrated in 2001, with the goal of correlating the fullerene surface charge with solvent properties (*e.g.* Lewis base). Further studies of the destabilization/charge negation by mild oxidizing agents as discussed in Chapter 3 may also shed light on the nature of the surface.

Fungal Interactions

While Chapter 6 provided interesting observation regarding a tolerant fungal system to nano-C₆₀, further studies are needed to quantify the uptake process along with specific test designed to maximize any C₆₀ biochemical bonding (if any). Additional sensitivity for the later would provide insight into the potential of C₆₀ in the biological carbon cycle, which to date has been largely unobserved. Specifically, additional ¹³C NMR studies are recommended using enriched C₆₀ with longer reaction times under optima fungal growth conditions (*i.e.* additional carbon source). ¹⁴C labeled C₆₀, if available, could increase *in situ* analyses, specifically with regard to soluble products.

Literature Cited

1. Weaver, J. H.; Martins, J. L.; Komeda, T.; Chen, Y.; Ohno, T. R.; Kroll, G. H.; Troullier, N.; Haufler, R. E.; Smalley, R. E. Electronic-Structure of Solid C₆₀ - Experiment and Theory. *Phys. Rev. Lett.* 1991, *66*, 1741-1744.
2. Hirsch, A.; Brettreich, M. *Fullerenes: Chemistry and Reactions*; Wiley-VCH Verlag GmbH & Co.: Weinheim, 2005.
3. Stinchcombe, J.; Penicaud, A.; Bhyrappa, P.; Boyd, P. D. W.; Reed, C. A. Buckminsterfulleride(1-) Salts - Synthesis, Epr, and the Jahn-Teller Distortion of C-60-. *J. Am. Chem. Soc.* 1993, *115*, 5212-5217.
4. Heath, G. A.; Mcgrady, J. E.; Martin, R. L. Characterization of the Uv, Visible and near-ir Spectra of the Fulleride Anions C-60(1-), C-60(2-) and C-60(3-), and Theoretical-Analysis of the Spectra of C-60(1+), C-60(0), C-60(1-), C-60(2-) and C-60(3-) by Self-Consistent Field-X-Alpha-Scattered-Wave (Scf-X-Alpha-Sw) Calculations. *J. Chem. Soc. Chem. Comm.* 1992, 1272-1274.
5. Mcglashen, M. L.; Blackwood, M. E.; Spiro, T. G. Resonance Raman Spectroelectrochemistry of the C₆₀ Radical-Anion. *J. Am. Chem. Soc.* 1993, *115*, 2074-2075.
6. Wei, X.; Wu, M.; Qi, L.; Xu, Z. Selective solution-phase generation and oxidation reaction of C₆₀⁻ (n=1,2) and formation of an aqueous colloidal solution of C₆₀. *J. Chem. Soc. Perkin Trans. 2* 1997, 1389-1393.
7. Dresselhaus, M. S.; Dresselhaus, G.; Eklund, P. C. *Science of Fullerenes and Carbon Nanotubes*; Academic Press: San Diego, 1996.
8. Amonette, J. E.; Workman, D. J.; Kennedy, D. W.; Fruchter, J. S.; Gorby, Y. A. Dechlorination of carbon tetrachloride by Fe(II) associated with goethite. *Environ. Sci. Technol.* 2000, *34*, 4606-4613.
9. Fredrickson, J. K.; Zachara, J. M.; Kennedy, D. W.; Duff, M. C.; Gorby, Y. A.; Li, S. M. W.; Krupka, K. M. Reduction of U(VI) in goethite (alpha-FeOOH) suspensions by a dissimilatory metal-reducing bacterium. *Geochim. Cosmochim. Ac* 2000, *64*, 3085-3098.
10. McCormick, M. L.; Bouwer, E. J.; Adriaens, P. Carbon tetrachloride transformation in a model iron-reducing culture: Relative kinetics of biotic and abiotic reactions. *Environ. Sci. Technol.* 2002, *36*, 403-410.
11. Klausen, J.; Trober, S. P.; Haderlein, S. B.; Schwarzenbach, R. P. Reduction of Substituted Nitrobenzenes by Fe(Ii) in Aqueous Mineral Suspensions. *Environ. Sci. Technol.* 1995, *29*, 2396-2404.

12. Hofstetter, T. B.; Heijman, C. G.; Haderlein, S. B.; Holliger, C.; Schwarzenbach, R. P. Complete reduction of TNT and other (poly)nitroaromatic compounds under iron reducing subsurface conditions. *Environ. Sci. Technol.* 1999, *33*, 1479-1487.
13. Weber, K. A.; Picardal, F. W.; Roden, E. E. Microbially catalyzed nitrate-dependent oxidation of biogenic solid-phase Fe(II) compounds. *Environ. Sci. Technol.* 2001, *35*, 1644-1650.